8-2014

Theoretical investigation of the quantum-confined Stark effect

Christopher Jon Blanton
Syracuse University

ABSTRACT

The two main objectives of this dissertation are the systematic development of explicitly correlated electron-hole wave function based methods and the application of these methods to chemical systems with an emphasis on nanoparticles. The understanding of the basic physics of excited electronic states is an important consideration when developing new methods and applications. In this dissertation, excited electronic states were studied using the electron-hole quasiparticle representation. Theoretical treatment of electronic excitation in large quantum dots and nanoparticles is challenging because of the large number of electrons in the system. The quasiparticle representation provides an alternative representation that can partially alleviate the computational bottleneck associated with investigating these systems. However, in this representation, the effects of electron-hole correlation must be understood in order to accurately describe the system's optical and electronic properties.

The electron-hole wave function consists of two separate mathematical components which are the explicitly correlated part of the wave function and the reference wave function which is operated on by the explicitly correlated operator. This dissertation presents theoretical development of both of these components. In the first part, a systematic formulation for deriving the explicitly correlated form of the electron-hole wave function was performed. Towards that goal, the electron-hole correlation length was defined using the electron-hole cumulant. The construction of explicitly correlated wave function was improved by the introduction of the electron-hole correlation length which was determined using the electron-hole cumulant. The electron-hole correlation length allowed the determination of parameters in the explicitly correlated operator without the performance of energy minimizations. In the second part, the electron-hole reference wave function was improved by combining full configuration electron-hole wave function with the explicitly correlated operator. The developed methods were used to investigate the quantum-confined Stark effect (QCSE) and the effect of pH on the optical properties of quantum dots. The effect

of applied electric fields on nanoparticles is known as the quantum-conned Stark effect. In this dissertation, the effect of both homogeneous and inhomogeneous electric fields on the optical and electronic properties of quantum dots was investigated. The effect of electric fields on the optical and electronic properties of a GaAs quantum dot was determined by combining the variational polaron transformation with the explicitly correlated electron-hole wave function. The presence of charged ligands also influenced the optical properties of quantum dot and this effect is known as the ligand-induced quantum-confined Stark effect. In this dissertation, the effect of pH on the optical properties of functionalized quantum dots were investigated by first calculating the charged states of the surface ligands at a given pH and then performing electron-hole explicitly correlated wave function based calculations in the electrostatic field generated by the charged ligands.

Theoretical methods developed in this dissertation have impacted the field of computational nanoscience by reducing the computational bottleneck to investigate nanoparticles and by providing novel avenues for improving accuracy of existing methods.

Theoretical investigation of quantum-confined Stark effect in nanoparticles

by

Christopher J. Blanton

B.S., Francis Marion University, 2004

M.Phil., Syracuse University, 2011

Dissertation

Submitted in partial fulfillment of the requirements for the degree of

Doctor of Philosophy in Chemistry

Syracuse University

August 2014

Acknowledgments

First and foremost I'd like to thank my advisor, Professor Arindam Chakraborty for all the opportunities he has given me. He has always been the advisor I have needed. Without his many efforts and understanding, I could have never completed this endeavor. He has always been there with the right combination of intriguing ideas and support. I admire his mastery and integration of concepts and ideas from many fields.

I must thank Jen Elward for her support and help. Jen was always a friend, colleague, and an excellent researcher. She was always willing to have many wonderful conversations and discussions. The year that we were the only two members of the group will never happen again and I'm glad that I got to share it with you.

I would also to thank Mike Bayne, Ben Ellis, and Jeremy Scher. Mike Bayne has been a constant companion and a wonderful friend. Ben Ellis always brought both interesting work and a great sense of humor to the lab. Jeremy is a great guy and I wish him well (since it looks like he's taking over some of my work). I could not have had better colleagues in the group. Each of you has been a great colleague and I look forward to watching your careers grow with great interest. Each of you is going to touch the stars.

I wish to thank my parents, Johnny and Karen Blanton, for their support. I wish to also to thank my grandparents, Norwood and Ingrid Blanton, for their support. I must also thank my brother, Brian Blanton, who was always willing to talk with me and keep me grounded. My Uncle Chuck Floyd who was always there when I needed a place to crash on the long drives from Syracuse, NY to Nichols, SC. I must also think all of my extended family, who have always been supportive and proud of me. They all knew this day would come even when I thought it wouldn't.

Table of Contents

List of Figures

List of Tables

Chapter 1: Introduction

Accurate calculation of the properties of large excited electronic systems is an inherently difficult and expensive undertaking under current methods. However, the need to perform highly accurate calculations of the optical and electronic properties of large systems is a necessary and required tool. There are many tools for approaching these problems. Quantum dots are a particularly interesting class of nanopaticles that have become popular for many applications. Many aspects of quantum dots have been (and are being) explored, but this work focuses on the effect that electric fields have on the optical and electronic properties; that is, the quantum confined Stark effect. The quantum confined Stark effect is explored in cases where the applied electric field is homogeneous (chapter 3) and where the field is generated by discrete atomic charges (chapter 4), in the example of a set of charged ligands on the surface of a quantum dot. The methods that have been used in this work are explicitly correlated methods. In the pursuit of better explicitly correlated methods, the effects of correlation were studied by means of a newly defined method called the electron-hole correlation length. This method is the subject of chapter 3.

The organization of the rest of the introduction chapter is a brief summary of important components of quantum mechanics (section 1.1), electronic structure theory (section 1.2), and excited electronic systems (section 1.3), Then, the particular type of system (quantum dots) that has been used in the work will be discussed with emphasis on the applications that peek interest,

in section 1.4. Finally, the organization of the remainder of this work will be given in section 1.5.

1.1 Quantum mechanics

Chemistry is inherently a quantum mechanical science. While many aspects of chemistry have been successful treated using various models, it is necessary to face the dragon of quantum mechanics in order to improve the picture of physical reality. While a full treatment of quantum mechanics is beyond the scope of this work, a brief treatment of the most important parts of the discipline is necessary. There are a number of important works which give the many aspects of quantum mechanics,[3, 4, 5, 6] so only a brief review will be given in this chapter.

1.1.1 Postulates of quantum mechanics

Quantum mechanics is build upon a number of postulates.[3, 4, 5, 7] These postulates are the basis for every quantum system. It is a most amazing realization that the findings based on these postulates have given such a wonderful and accurate picture of the world. The far-reaching consequences of these postulates is the complete study of quantum mechanics. However, the postulates will be briefly stated and described.

Postulate 1. *The state of a quantum mechanical system at time t and set of coordinates x is described by a wave function* $|\Psi(x,t\rangle$. *The wave function is the complete set of all information about a quantum mechanical system. The wave function is complex and the complex conjugate is* $\langle\Psi(x,t)|$. *The probability of finding a particle at in the region* $[x,x+\mathrm{d}x]$ *at time t is given by*

$$p(x,t) = \Psi(x,t)^{*}\Psi(x,t)\mathrm{d}x. \tag{1.1}$$

An important consequence is that

$$\langle \Psi(x,t)|\Psi(x,t)\rangle = \int_{-\infty}^{+\infty} \Psi(x,t)^* \Psi(x,t) \mathrm{d}x = 1. \tag{1.2}$$

Postulate 2. *For every measurable quantity, there is a linear operator. Two of the most important operators are the position operator x and the momentum operator* $p_x = -i\hbar \frac{\mathrm{d}}{\mathrm{d}x}$.

Postulate 3. *The only possible values for a given measurement of a quantity are the eigenvalues of the operator.*

Postulate 4. *The time evolution of the quantum system is given by the time-dependent Schrödinger equation*

$$i\hbar \frac{\partial}{\partial t} \Psi(x,t) = H\Psi(x,t), \tag{1.3}$$

where H is the Hamiltonian (energy) operator.

Postulate 5. *A particle must obey the correct statistics for its particle-type. Interchange of two fermions must be antisymmetric*

$$\Psi(x_1,x_2) = -\Psi(x_2,x_1) \tag{1.4}$$

and bosons must be symmetric to interchange of coordinate

$$\psi(x_1,x_2) = \Psi(x_1,x_2). \tag{1.5}$$

1.1.2 Time-independent Schrödinger equation

The key equation in the study of quantum systems is the Schrödinger equation,[3, 4, 8, 9, 10] which is

$$H|\Psi\rangle = E|\Psi\rangle, \tag{1.6}$$

where H is the Hamiltonian (energy) operator, Ψ is the wave function for the system, and E is the energy of the system. This is the key equation in most applications. With the exception of a few cases (for example: hydrogen atom, harmonic oscillator, particle-in-a-box), the time-independent Schrödinger equation is unsolvable.[3, 11]

1.1.3 Approximation methods

In the majority of quantum mechanical problem, the exact solution to the Schrödinger equation is unknown. However, there are methods to develop approximate solutions to the Schrödinger equation. Two of the most useful methods are the variational and the perturbational methods. Variational methods use the requirement that the a quantum mechanical system energy must be bounded from below in the ground state. Perturbational methods begin with the case of either an exactly solved system or one in which the system has been approximately solved to high degree of accuracy and builds a solution from that system. Each method has strengths and weakness which lend each method to particular types of problems. In this section, the methods will be briefly described.

1.1.3.1 Variational method

The variational method is a key tool in quantum mechanics. For any exact system, the energy is given by

$$H|\Psi_0\rangle = E_0|\Psi_0\rangle, \tag{1.7}$$

where $|\Psi_0\rangle$ is the exact wave function. For a trial wave function Ψ_T,[3, 6]

$$E[\Psi_T] = \frac{\langle\Psi_T|H|\Psi_T\rangle}{\langle\Psi_T|\Psi_T\rangle}, \tag{1.8}$$

that $E \leq E_0$ and the equality only holds if $\Psi_T = \Psi_0$.[3, 11] The proof of the variational principle is found in many texts.[3, 6, 12] The key advantage to variational methods is that the one may chose a wide set of trial wave functions and search for the minimum energy wave function. The key disadvantage is that, without additional constraints, is the variational method only allows for the determination of the ground state since only the ground state is bounded from below without further restraints being imposed.[6]

1.1.3.2 Perturbational method

Perturbation theory is a highly useful approximation method in quantum mechanics.[3, 6, 11] In perturbational methods, the system is divided into components to which the true answer (or a very good approximation) is known and a perturbation which is relatively small, that is

$$H|\Psi_i\rangle = (H_0 + V)|\Psi\rangle = E_i|\Psi_i\rangle \tag{1.9}$$

where $H_0|\psi_n\rangle = E_n|\psi_n\rangle$, V is the perturbation, and $|\Psi_i\rangle$ is the exact wave function. Introduction of a parameter λ gives the energy and the wave function as the series

$$E_i = E_i^{(0)} + \lambda E_i^{(1)} + \lambda^2 E_i^{(2)} + \cdots, \tag{1.10}$$

$$|\Psi_i\rangle = |\psi_i\rangle + \lambda|\psi_i^{(1)}\rangle + \lambda^2|\psi_i^{(2)}\rangle + \cdots. \tag{1.11}$$

The full derivation can be found in many excellent textbooks.[3, 6, 11] The key results are the first energy corrections which are[6]

$$E_i^{(0)} = \langle\psi_i|H_0|\psi_i\rangle, \tag{1.12}$$

$$E_i^{(0)} = \langle\psi_i|V|\psi_i\rangle. \tag{1.13}$$

In this regime, a solution may be approximately be determined. The key advantage of perturbational methods is that excited all states are determined simultaneously. The key disadvantage to perturbational methods is the energy is only guaranteed to converge in the limit of the infinite expansion.[3, 6, 11, 12]

1.2 Electronic structure theory

Quantum chemistry concerns itself with the electronic properties of molecules. Molecules consist of atoms which contain nuclei and electrons. There are a number of very helpful textbooks;[6, 9, 11, 12, 13, 14, 15, 16, 17] therefore, the key concepts and results necessary for this work will be briefly described here.

The organization for this section is as follows. In this subsection 1.2.1, the molecular Hamil-

tonian will be presented. With the molecular Hamiltonian in hand, the Born-Oppenheimer approximation will be described in subsection 1.2.2. The antisymmetry of electrons will be discussed in subsection 1.2.3. Then, the Hartree-Fock method will be briefly described in subsection 1.2.4. Next, the problem of electron correlation will be presented in subsection 1.2.5 . The conceptually simplest solution to the electron correlation problem will be presented briefly in subsection 3.2.1. Finally, the alternative quantum mechanical method of density functional theory (DFT) will be briefly described.

1.2.1 Molecular Hamiltonian

The basic Hamiltonian operator for a molecular system in the absence of external fields can be written as[10]

$$H = T_{\mathrm{N}} + V_{\mathrm{NN}} + T_{\mathrm{e}} + V_{\mathrm{ee}} + V_{\mathrm{Ne}}, \tag{1.14}$$

where the T_{N} is the nuclear kinetic energy operator, V_{NN} is the nuclear-nuclear interaction operator, T_{e} is the electronic kinetic energy operator, V_{ee} is the electron-electron interaction operator, and V_{Ne} is the nuclear-electron interaction operator. The nuclear kinetic energy term is

$$T_{\mathrm{N}} = \sum_{A=1}^{N_A} -\frac{\hbar^2}{2M_{\mathrm{A}}}\nabla_A^2, \tag{1.15}$$

where A is the index for the nucleus, N_A is the total number of nucleus, and M_A is the mass of the nucleus A. The nuclear-nuclear interaction operator is

$$V_{\mathrm{NN}} = \sum_{A=1}^{N_A} \sum_{B<A}^{N_A} \frac{Z_A Z_B}{4\pi\varepsilon_0 |\mathbf{R}_A - \mathbf{R}_B|}, \tag{1.16}$$

where Z_A is the charge on nucleus A, Z_B is the charge on nucleus B, ε_0 is the permittivity of free space, $\mathbf{R}_A$ is the position of nucleus A, and $\mathbf{R}_A$ is the position of nucleus B. The electronic kinetic operator is

$$T_{\mathrm{e}} = \sum_{i=1}^{N_{\mathrm{e}}} -\frac{\hbar^2}{2m_{\mathrm{e}}} \nabla_i^2, \tag{1.17}$$

where i is the index for electron i, N_{e} is the total number of electrons, and m_{e} is the mass of the electron. The electron-electron interaction operator is

$$V_{\mathrm{ee}} = \sum_{i=1}^{N_{\mathrm{e}}} \sum_{j>i}^{N_{\mathrm{e}}} \frac{q_{\mathrm{e}} q_{\mathrm{e}}}{4\pi\varepsilon_0 |\mathbf{r}_i - \mathbf{r}_j|}, \tag{1.18}$$

where $\mathbf{r}_i$ is the coordinate of the electron i, $\mathbf{r}_j$ is the coordinate of the electron j, and q_{e} is the charge on the electron. The nuclear-electron interaction operator is

$$V_{\mathrm{Ne}} = \sum_{A=1}^{N_A} \sum_{i=1}^{N_{\mathrm{e}}} \frac{Z_A q_{\mathrm{e}}}{4\pi\varepsilon_0 |\mathbf{R}_A - \mathbf{r}_i|}. \tag{1.19}$$

The molecular Hamiltonian for general systems in the absence of applied fields has been described. The solution of the molecular Hamiltonian is the key to understanding molecular systems.

1.2.1.1 Atomic units

In the majority of this work, atomic units are used. In the atomic unit system, the values for the mass of the free electron (m_0), elementary charge e, the reduced Plank's constant $\hbar = \frac{h}{2\pi}$, and value of $\frac{1}{4\pi\varepsilon_0}$ (ε_0 is the permittivity of free space) are all set to 1.[10] The charge on the electron in atomic units is $q_e = -1$. This choice reduces the clutter of the many equations and decouples the results of the calculations from any particular value of many physical constants (which may be refined over time).

1.2.2 Born-Oppenheimer Approximation

The molecular Hamiltonian is still an imposing equation. In order to perform many calculations, approximations are usually made. The first approximation that is typically made is the Born-Oppenheimer approximation, which seeks to separate the electronic and nuclear motions.[10, 12, 16, 17] The electrons and nuclei are only coupled by the attractive nuclear-electronic Coulomb interaction.On a qualitative level, the large difference in the mass of the nucleus (the lightest nucleus is a single proton, which has mass $1836m_0$) leads to the separation of the molecular wave function into an electronic and nuclear wave function. In the Born-Oppenheimer approximation, the molecular wave function is separated into a nuclear and electronic component wave function; that is,

$$|\Psi(\mathrm{R},\mathbf{r})\rangle = |\Psi_{\mathrm{N}}(\mathbf{R})\psi(\mathbf{r},\mathbf{R})\rangle, \tag{1.20}$$

where Ψ_N is the nuclear wave function and ψ is the electronic wave function.[10] As a consequence of the Born-Oppenheimer approximation, the molecular Hamiltonian can be separated as

$$H|\Psi(\mathrm{R},\mathbf{r})\rangle = H|\Psi_N(\mathbf{R})\psi(\mathbf{r},\mathbf{R})\rangle \tag{1.21}$$

$$= (T_N + V_{NN} + T_e + V_{ee} + V_{Ne})|\Psi_N(\mathbf{R})\psi(\mathbf{r},\mathbf{R})\rangle \tag{1.22}$$

$$= H_N|\Psi(\mathbf{R})\rangle + H_e|\psi(\mathbf{r},\mathbf{R})\rangle \tag{1.23}$$

The electronic Hamiltonian is

$$H_e = T_e + V_{ee} + V_{Ne}, \tag{1.24}$$

which means

$$H_e|\psi(\mathbf{r},\mathbf{R})\rangle = E_e(\mathbf{R})|\psi(\mathbf{r},\mathbf{R})\rangle, \tag{1.25}$$

the electronic energy depends parametrically on the coordinates of the nuclei.[10, 11, 12, 14, 16] The nuclear Hamiltonian which contains only the terms which have explicit dependence on the nuclear coordinates and is[10, 11, 12, 14, 16]

$$H_N = T_N + T_{NN} + E_e(\mathbf{R}). \tag{1.26}$$

1.2.3 Antisymmetry of electrons

A key physical requirement of the any electron-containing wave function is that it must satisfy the antisymmetry of fermions (since electrons are fermions); that is,[3, 6, 12, 14, 16, 17]

$$\Psi(\mathbf{x}_1, \mathbf{x}_2, \ldots, \mathbf{x}_i, \ldots, \mathbf{x}_j, \ldots, \mathbf{x}_N) = -\Psi(\mathbf{x}_1, \mathbf{x}_2, \ldots, \mathbf{x}_j, \ldots, \mathbf{x}_i, \ldots, \mathbf{x}_N), \tag{1.27}$$

where Ψ is a N-electron wave function and $\mathbf{x}$ is an electronic coordinate containing both spatial and spin coordinates. Any electron-containing wave function that does not satisfy this requirement may give unphysical results. This is the more rigorous statement of the Pauli exclusion principle.[3, 10, 11, 12, 16]

1.2.4 Hatree-Fock method

The Hartree-Fock method is a cornerstone in modern electronic structure theory. The Hartree-Fock method is the variational search for the single Slater determinant that yields the lowest energy.[12, 14, 16, 17, 18]

1.2.4.1 Slater determinant

The choice for the wave function in the Hartree-Fock method is the single Slater determinant.[12, 14, 16, 17, 18] The Slater determinant was chosen because the Slater determinant is a relatively simple construction that guarantees the antisymmetric of the electrons and the building blocks are

relatively simple one-electron wave functions.[11] The Slater determinant is written as

$$\Phi(\mathbf{x}_1,\mathbf{x}_2,\ldots,\mathbf{x}_N) = \frac{1}{\sqrt{N!}} \begin{vmatrix} \chi_1(\mathbf{x}_1) & \chi_2(\mathbf{x}_1) & \chi_3(\mathbf{x}_3) & \cdots & \chi_N(\mathbf{x}_1) \\ \chi_1(\mathbf{x}_2) & \chi_2(\mathbf{x}_2) & \chi_3(\mathbf{x}_2) & \cdots & \chi_N(\mathbf{x}_2) \\ \vdots & \ddots & \ldots & \ddots & \vdots \\ \chi_1(\mathbf{x}_N) & \chi_2(\mathbf{x}_N) & \chi_3(\mathbf{x}_N) & \cdots & \chi_N(\mathbf{x}_N) \end{vmatrix} \tag{1.28}$$

$$= |\mathbf{x}_1\mathbf{x}_2\cdots\mathbf{x}_N\rangle, \tag{1.29}$$

where $\chi_1(\mathbf{x}_1)$ are molecular orbitals that are one-electron wave functions. Molecular orbitals (also called spin orbitals) consist of a spatial component and a spin component,

$$\chi(\mathbf{x}) = \begin{cases} \psi(\mathbf{r})\alpha(\omega) \\ \quad \text{or} \quad \\ \psi(\mathbf{r})\beta(\omega) \end{cases}, \tag{1.30}$$

where $\psi(\mathbf{r})$ is the spatial orbital, $\mathbf{r}$ is the spatial coordinate of the electron, $\alpha(\omega)$ is a possible spin function, $\beta(\omega)$ is a possible spin function, and ω is the spin coordinate of the electron.

In Eq. (1.29), a shorthand method for writing the Slater determinant is shown. The key advantage of using the Slater determinant is that the choice gives an antisymmetric wave function, since interchange of any two rows or two columns gives the negative of the initial arrangement. Furthermore, the Slater determinant enforces the condition that no two electrons can occupy the same set of quantum numbers at any time, since duplicate columns or duplicate rows will cause the determinant to vanish.

The Hartree-Fock method finds the best single Slater determinant for a given system. In the

next section, the highlights of the method will be described. Further details may be found in many references.[9, 11, 12, 14, 16, 18, 19]

1.2.4.2 Energy expression for a single Slater determinant

The energy expression for a single Slater determinant is[9, 11, 14, 16, 18, 19]

$$E[\Phi] = \sum_{i=1}^{N} \langle i|h(1)|i\rangle + \frac{1}{2}\sum_{i,j=1}^{N} (\langle ij|ij\rangle - \langle ij|ji\rangle), \tag{1.31}$$

where

$$h(1) = -\frac{\hbar^2}{2m_1}\nabla_1^2 + \sum_{A=1}^{N_{\text{atom}}} \frac{Z_A q_e}{r_{1A}}, \tag{1.32}$$

$$\langle i|h(1)|i\rangle = \int_{-\infty}^{+\infty} \mathrm{d}\mathbf{x}_1 \chi_i^*(\mathbf{x}_1) h(1) \chi_i(\mathbf{x}_1), \tag{1.33}$$

and

$$\langle ij|ij\rangle = \int_{-\infty}^{+\infty} \mathrm{d}\mathbf{x}_1 \mathrm{d}\mathbf{x}_2 \chi_i(\mathbf{x}_1)^* \chi_j(\mathbf{x}_2)^* \frac{1}{r_{12}} \chi_i(\mathbf{x}_1)\chi_j(\mathbf{x}_2). \tag{1.34}$$

The second integral in Eq. (1.31) is the Coulomb integral and the third integral is the exchange integral.

1.2.4.3 Coulomb and exchange operators

The presence of the two-body terms in Eq. (1.31) complicates what would be a one-electron Schrödinger equation of the spin orbital states in the field of the nuclei[18]

$$h(1)|\chi_a(1)\rangle = \varepsilon_i|\chi_a(1)\rangle, \tag{1.35}$$

where ε_a is the energy of ath energy level. In order to rewrite Eq. (1.31) as a one-electron form, the Coulomb operator (from the Coulomb portion of the two body integrals) is defined as[18]

$$J_b(1) = \int_{-\infty}^{+\infty} \mathrm{d}\mathbf{x}_2 |\chi_b(2)|^2 r_{12}^{-1}, \tag{1.36}$$

and the exchange operator (from the exchange portion of the two-body integrals) is[18]

$$K_b(1)\chi_1(1) = \left[\int_{-\infty}^{+\infty} \mathrm{d}\mathbf{x}_2 \chi_b^*(2) r_{12}^2 \chi_1(2)\right] \chi_b(1). \tag{1.37}$$

Using Eq. (1.36) and (1.37), Eq. (1.31) can be written as the single-electron eigenvalue problem[18]

$$\left[h(1) + \sum_{b\neq a} J_b(1) - \sum_{b\neq a} K_b(1)\right] \chi_a(1) = \varepsilon_a chi_a(1). \tag{1.38}$$

With the Coulomb and exchange operators defined, the Fock operator may now be defined.

1.2.4.4 Fock operator

In (1.38), the bracket term appears to be different for every spin orbital χ because of the restriction on the summation $b \neq a$; however,[18]

$$[J_a(1) - K_a(1)]|\chi_a(1) = 0. \tag{1.39}$$

The restriction on the summation can then be removed to give the operator

$$f(1) = h(1) + \sum_b J_b(1) - K_b(1), \tag{1.40}$$

which is called the Fock operator.[18] The Hartree-Fock equations are now

$$f|\chi_a\rangle = \varepsilon_a|\chi_a\rangle, \tag{1.41}$$

and the second and third term in Eq. (1.40) are usually combined and called the Hartree-Fock potential[18]

$$v^{\mathrm{HF}}(1) = \sum_b J_b(1) - K_b(1). \tag{1.42}$$

The Fock operator is then written as

$$f(1) = h(1) + v^{\mathrm{HF}}(1). \tag{1.43}$$

1.2.4.5 Energy minimization

The process by which the Hartree-Fock equations (Eq. (1.40)) are used to minimize the energy will now be shown. In this process, the energy will be minimized by determining the stationary points of the functional. This is a procedure that is comparable to the standard minimization of functions. The key difference is that energy is given by an energy functional (a mathematical operation that takes in a function and returns a number). Beginning with the energy functional for a trial Slater determinant $\tilde{\Phi}$ gives

$$E[\tilde{\Phi}] = \langle \tilde{\Phi} | H | \tilde{\Phi} \rangle. \tag{1.44}$$

The wave function will be varied by a small amount

$$E[\tilde{\Phi} + \delta\tilde{\Phi}] = \langle \tilde{\Phi} + \delta\tilde{\Phi} | H | \tilde{\Phi} + \delta\tilde{\Phi} \rangle \tag{1.45}$$

$$= E[\tilde{\Phi}] + \{ \langle \delta\tilde{\Phi} | H | \tilde{\Phi} \rangle + \langle \tilde{\Phi} | H | \delta\tilde{\Phi} \rangle \} + \cdots \tag{1.46}$$

$$= E[\tilde{\Phi}] + \delta E[\tilde{\Phi}] + \cdots \tag{1.47}$$

where δE is the collection of all linear terms in the variation of the wave function. Similar to function minimization, the wave function that gives

$$\delta E = 0 \tag{1.48}$$

is stationary and is usually a minimum. [17, 18]

The standard methods for finding the stationary states are found in many references for

several different possibilities.[9, 11, 12, 14, 16, 18, 19] The full derivation of the minimization using the second quantization notation is found in subsubsection 2.2.1.8.

1.2.5 Electron correlation

Correlation is the statistical impact that the presence of a factor has on other factors. An analogy is the sequential drawing of cards as compared to the rolling dice. In the card draw, the identity of the drawn cards effects the probability of subsequent cards. This is an example of correlated behavior.

The behavior of electrons is correlated. The coordinates of one electron affect the coordinates of all other electrons. There are two important factors that lead to the correlated behavior between electrons:

1. the requirement that no two fermions have the same complete set of quantum numbers.[3, 6]

2. the repulsive interaction between two like charged particles.

The electron-electron correlation is fundamental to the correct physics of these systems as evidenced by the Kato cusp condition.[20] The Kato cusp condition requires that the wave function contain the correct behavior when $r_{ee} = 0$ to cancel the Coulomb singularity. Due to the inherent physics that rule the interaction between electrons, the electronic wave functions must show correlation between electrons. The Hartree-Fock method is taken as the uncorrelated basis in quantum chemistry. The correlation energy is defined as[6, 12, 14, 16, 17]

$$E_{\text{corr}} = E_{\text{exact}} - E_{\text{HF}}. \tag{1.49}$$

In most cases, E_{corr} is small, often less than 1% of E_{exact}. However, this difference is often on the order of chemical importance (accuracy of less than 1 kcal/mol).[6, 11, 14, 15, 16, 17] Highly accurate treatments must address electron-electron correlation, whether by post-Hartree-Fock "fixes" to the correlation treatment, by choosing an ansatz (choice of wave function) that addresses the correlation (that is, an explicitly correlated ansatz), or by developing a method that is correlated from first principles (an example of this is density functional theory).

1.3 Excited electronic states

In the preceding section, the ground state of an electron system was discussed. In the applications of interest in semiconductors, the important processes occur in the excitation, lifetime, and relaxation of the excited electronic states. An excited electronic state is one in which all electrons are not in the lowest possible energy levels. This state is reached by the addition of some amount of energy, which must be equal to the difference in energy levels, which may occur either by the absorption of a photon or as the result of a chemical reaction.[15] In Figure 1.1, the ground state is excited by the interaction with a photon of energy $h\nu$ to give an excited state. The change in energy is

$$\Delta E = h\nu = \frac{2\pi\hbar c}{\lambda}, \tag{1.50}$$

where h is Planck's constant, c is the speed of light, and λ is the wavelength of the radiation.[3, 6, 12, 15] While in this state, there are two possibilities[21]

1. the molecule can return to the ground state either directly or by means of combination of

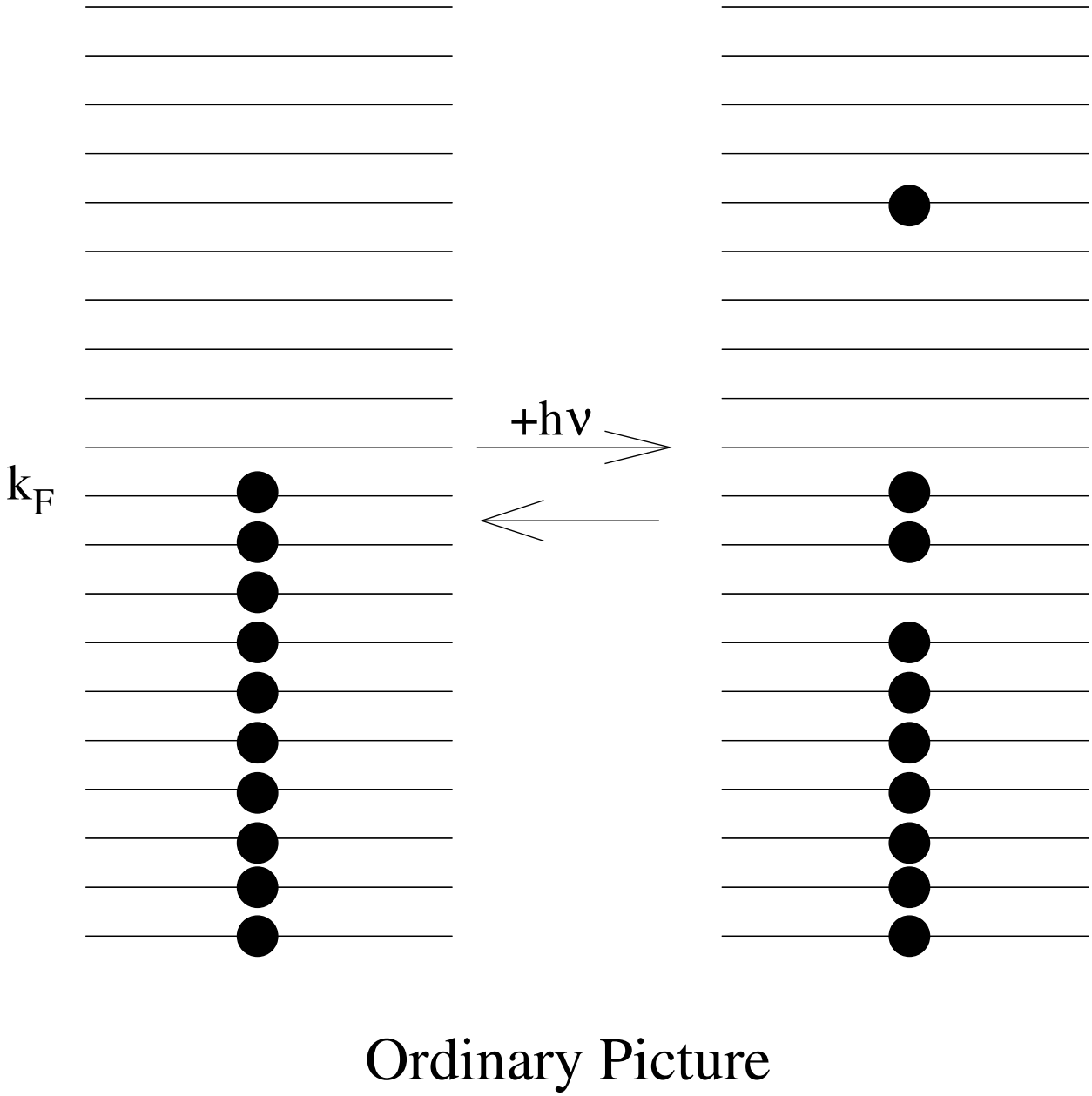

Figure 1.1: Example of an electronic transition due to the addition of energy via a photon.

processes.

2. the excited molecule can interact with another molecule transferring energy into some process that molecule is undergoing.

The photon emitted in the first case can either be of the same energy as absorbed photon or (by non-radiative processes which change the excited state energy level) different energy.[12, 15] The generation and fate of excited electron states is an essential component of understanding the properties of certain applications of a molecule.

1.3.1 Optical properties

The optical properties of an atom or molecule are closely tied to the excited electronic states of the atom or molecule. One of the methods for generating an excited electronic state is the addition of energy, by way of a photon, to the system. Optical spectroscopy in the forms of absorption spectroscopy and photoluminescence spectroscopy are particularly useful for studying excited electronic systems. In absorption spectroscopy, the degree to which photons of particular energies (wavelengths) are absorbed is measured. In photoluminescence, the system is excited by photons and the system's response is measured. These properties allow the system to be characterized and to determine how the material may be used.

1.3.2 Computational methods for excited electronic states

The calculation of excited electronic states is a challenging undertaking. There are several methods for calculating the properties of the excited electronic states.[12, 22]. The single-configuration methods usually use the Hartree-Fock as the reference wave function. The config-

uration interaction singles (CIS) and its various refinements, such as CISD (singles and doubles), CISDT (singles, doubles, and triples), produce excited states from the Hartree-Fock reference wave function by replacing spin orbitals with virtual (unoccupied higher energy) orbitals. The key difference from CI methods used to improve the ground state energy (by including electron-electron correlation) is that one must use at least the singles and doubles in the electron correlation problem because the ground state does not couple to the singly excited states (by the Slater-Condon rules) and in the calculation of the excited states the singles since it is the sets of molecular orbitals themselves that are important.[15] One of the pitfalls of the methods is that the basis sets are usually optimized for the ground state and are of limited quality in the description of the excited states.[15] A further pitfall is that the CI methods lack electron correlation in the excited states which leads to error in the energies of the excited states.[12] Higher accuracy methods include symmetry-adapted cluster configuration interaction (SAC-CI),[23, 24] equation-of-motion coupled-cluster (EOM-CC),[25] and linear response coupled-cluster methods.[26]

The problem of determination of the excited states may also be approached from the point of view of time-dependence using propagator methods, such as time-dependent Hartree-Fock (TDHF) and time-dependent DFT (TDDFT).[15] Both methods are largely the application of the Random Phase Approximation to the time-independent methods.[15] TDDFT has the advantage of containing electron-correlation in the formalization which leads to potentially higher quality than the CIS or time-dependent Hartree-Fock (TDHF) results.[15]

The calculation of the excited electron states remains a challenge which has yet to be solved in a manner which is general and cheap, especially for large systems. Large systems are often computational prohibitive in the all-electron picture.

1.4 Quantum dots

Quantum dots are nanocrystalline materials that have tunable optical and electronic properties.[27, 28] For instance, the interesting relationship between the number of atoms (size and shape combined) and the intermediate electronic properties (between those of molecules and of bulk semiconductors) can be seen in Figure 1.2. As this is one example, each of the tunability factors can

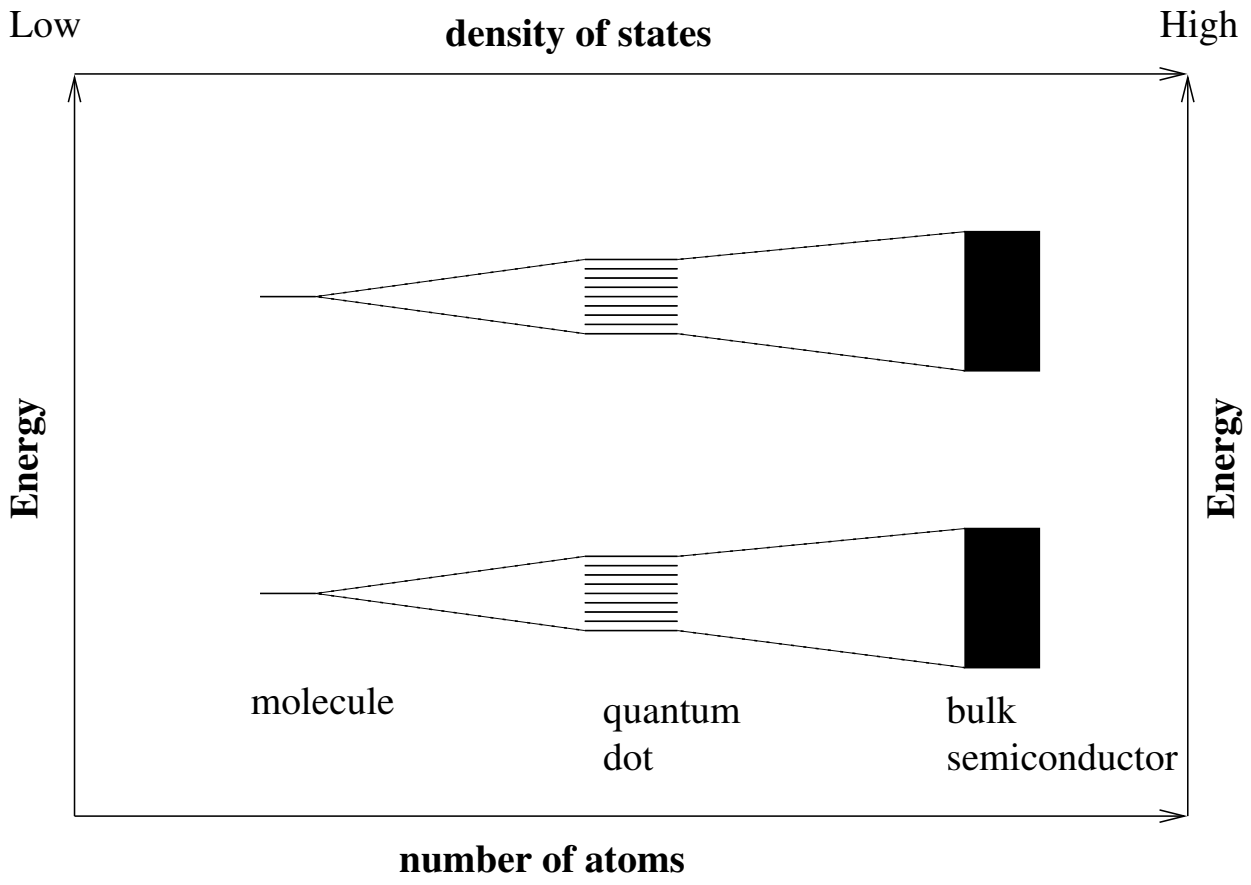

Figure 1.2: Energy levels as the number of atoms increases.

be observed to allow the optical and electronic properties of the system to be customized while holding the other factors as close to constant as possible.

1.4.1 Tunable factors

In this subsection, a more in-depth discussion of each tuning factor will in turn described. The key to wide application of qdots has been the control of optical and electronic properties by several parameters, including size and shape[29, 30, 31, 32, 33, 34, 35, 36], composition[37, 38], applied electromagnetic fields[39, 40, 41, 42, 43, 44], and ligands[45, 46, 47, 48, 49].

1.4.1.1 Size

The electronic and optical properties of quantum dots (QD) depend strongly on the size of the dots. [35, 50, 51, 52] This allows unprecedented opportunity to modify quantum dots for customized applications. The fundamental reason behind the strong structural dependence of optical properties of QDs can be understood in terms of the density of electronic states in quantum dots. As shown in Figure 1.2, the density of states in QDs are higher than isolated molecules but is lower than the bulk material.[35] By changing the size, one can control the density of states in quantum dots and directly modify the optical and electronic properties. Increasing the size of a quantum dot increases the density of states and in the limit of very large number of atoms, the optical properties of quantum dots become identical to that of bulk material.

1.4.1.2 Shape

The changing of the shape of the nanoparticle can greatly influence the optical and electronic properties of the system.[36, 53, 54] Shapes that have been prepared include spheres,[54, 55] rods,[51, 52, 56, 57] wires,[54, 58] pyramid,[59, 60] lens,[61, 62] cubic,[63, 64, 65] tetrapod,[57] hexapod,[66] and others shapes.[55] In each of these studies, the shape of the nanoparticle has had

a significant impact on the optical and electronic properties.

1.4.1.3 Composition

The composition of the quantum dot is an important factor in the optical and electronic properties of the quantum dot. The quantum dot can be made of an single element or combination of different elements. Some of the materials used to prepare quantum dots are Si,[67, 68, 69], Ge,[70, 71, 72] CdSe,[32, 46, 49, 54, 73, 74, 75, 76] CdS,[73, 77, 78, 79] CdTe,[46, 73, 80] PbS,[77, 81, 82] GaAs,[83], InP,[84], ZnS,[77] and others. Core-shell (systems where materials are layered) are structural motifs that have been explored.[30, 31, 38, 85, 86, 87] The notation used here is X/Y where X is the core material and Y is shell material. Core-shell material combinations include CdSe/ZnS,[30, 38, 86, 87, 88], CdTe/CdSe,[89] CdSe/CdS,[31] InGa/GaAs,[60] and CdS/CdSe.[85] The various possibilities for the composition of the quantum dot give an amazing variety of possibilities.

1.4.1.4 Ligands

The capping ligands play an important role in the formation and have sizable impacts in the optical and electronic properties of quantum dots.[45] The choice of the ligands has been made for many reasons, including solubility, functionalization, and specific targeting of chemicals and biomolecules. The most common ligands are phosphine oxides (in particular, tri-*n*-ocytlphosphine oxide (TOPO)), amines, thiols, and carboxylic acids.[45]

The surface chemistry of quantum dots is a very complex and difficult study component of the quantum dot system. In this work, the ligand length has been isolated as one of the many

parameters that exist in the surface chemistry of quantum dots. A central problem in the study of even modest size quantum dots is the large number of electrons that are within the quantum dot core. Even at a relatively modest ligand density, many ligands are present on the surface of the quantum dot. Each ligand is a polyelectronic system that adds more complexity to the already complex quantum dot system. Smaller systems, such as $Cd_{33}Se_{33}$ with trimethylphosphine oxide ligands, have been treated using DFT.[48, 90] The ligand can also influence the shape of the quantum dot, as seen by McPhail and Weiss in their study of the effect of change of shape from cubic to hexapodal by changing ligand parameters.[66]

1.4.1.5 Applied electric fields

The presence of an applied electric field can alter the optical and electronics of quantum dots. The influence of an external electric field on optical properties of semiconductors has been studied extensively using both experimental and theoretical techniques. In bulk semiconductors the shift in the optical absorbtion due to the external field is known as the Franz-Keldysh effect.[91, 92] In quantum wells and quantum dots, application of electric field has shown to modify the optical properties of nanosystems and is known as the quantum-confined Stark effect (QCSE).[93, 94] The application of the external field induces various modifications in the optical properties of the nanomaterial including, absorption coefficient, spectral weight of transitions, and change in λ_{max} of the absorption spectra. In certain cases, the applied field can lead to exciton ionization.[95] The quantum-confined Stark effect has found application in the field of electro-absorption modulators,[96] solar cells,[97] and light-emitting devices.[98] Recent experiments by Weiss et al. on semiconductor quantum dots have shown that the QCSE can also be

enhanced by the presence of heterojunctions.[39] In some cases, the QCSE can be induced chemically because of close proximity to ligands.[97] The QCSE also plays a major role in electric field dependent photoconductivity in CdS nanowires and nanobelts. [99] Application of electric field has emerged as one of the tools to control and customize quantum dots as novel light sources. In a recent study, electric field was used in generation and control of polarization-entangled photons using gallium arsenide (GaAs) quantum dots.[100] It has been shown that the coupling between stacked quantum dots can be modified using electric field. [101] A particularly intriguing method for controlling and producing an electric field is the use of plasmonic active materials such as gold as shell for quantum dots. Jin and Gao demonstrated that a gold shell on a quantum dot could have plasmonic activity and that the fluoresent properties of the quantum dot could be controlled by changing the spacing between the quantum dot and gold shell.[102] Erogbogdo and co-workers have developed gold-encapsulated silicon quantum dots for use in cancel cell imaging which uses the plasmonic enhancement of the gold shell.[103] Liaw and Liu have studied the plasmonic enhancement of silicon quantum dots which showed a relationship between metal layer thickness and the enhancement.[104] Jin and co-workers have used quantum dots to harvest light which led to an plasmonic enhancement due to the presence of silver nanoparticles.[105] West and Sadgeghi has shown how FRET can be influenced in quantum dots in the region of metal nanoparticles.[106] The QCSE has been investigated using various theoretical techniques including perturbation theory,[19, 107, 108, 109, 110, 111] variational techniques,[112, 113, 114, 115, 116, 117, 118] and configuration interaction method.[119, 120, 121, 122, 123, 124, 125, 126, 127, 128, 129]

1.4.2 Applications of quantum dots

The many tuning parameters that have been reviewed in subsection 1.4.1 have led to application in development and fabrication of novel materials including light-harvesting devices, light-emitting devices, and varius sensors. The tunable parameteters allow for both the course and fine tuning of the optical and electronic properties of the material. This tuning can lead to the engineering of materials to very tight specifications.

1.4.2.1 Light-harvesting devices

The harvesting of light to conversion of light energy to electrical energy is one of the most popular applications for quantum dots.[130, 131, 132, 133, 134, 135, 136, 137, 138, 139, 140, 141] Greenham and co-workers prepared early quantum cell solar cells.[130] Kongkanand and co-workers prepared CdSe solar cells and improved the efficiency by use of size and shape controls.[131] López and co-workers have prepared CdSe quantum dots capped with thioglycolic acid with N-doped TiO_2 solar cells that had much higher efficiency than either undoped TiO_2 or N-doped TiO_2 without CdSe quantum dots.[132] Kamat has discussed several methods for improving efficiency in solar cells by using CdSe quantum dots.[133] Sargent and co-workers have prepared solar cells with PbS quantum dot components that have exhibited efficiency of up to 4.2%.[134, 135, 136, 137] Si and co-workers have prepared CdSe on TiO_2 nanotube solar cells which showed a strong dependence on CdSe quantum dot size.[138] Plass and co-workers have made solar cells sensitized with PbS quantum dots that energy conversion efficiencies of up to 0.49%.[139] Zaban and co-workers prepared solar cells that used InP quantum dots that greatly increased the sensitivity of photoconductivity in TiO_2.[140] Yu and co-workers prepared InAs

quantum dot TiO_2 solar cells that had an efficiency of 0.3% but were air stable for at least a week.[141]

1.4.2.2 Light-emitting devices

Quantum dots have been of interest as the material for light-emitting as well as light-harvesting devices.[60, 80, 98, 142, 143, 144, 145, 146, 147, 148] These applications have included lasers,[60, 142, 143, 144, 145] and solid-state lighting.[80, 146, 147, 148] Bimberg and co-workers have produced lasers with InAs/GaAs and InGaAs/GaAs quantum dots.[60] Klimov and co-workers have produced lasers from CdSe quantum dots.[142] Foucher and co-workers have produced a hybrid material laser with a collodial quantum dot film with a polymer on a glass background.[143] Wang and co-workers have produced a laser from CdSe/CdS/ZnS core-muitishell materials.[145] De and co-worker shave produced InGaN/GaN light emitting diodes.[98] Anikeeva and co-workers have produced light-emitting devices with a mixture of red-green-blue quantum dots in a monolayer.[146] Jang and co-workers have used green- and red-light-emitting quantum dots combined with blue InGaN LEDs to create white quantum dot LEDs with high quantum efficiencies.[147] Sohn and co-workers have improved the white light-emitting diodes using a non-conventional packing technique that uses multiple core-shell $CuInS_2$/ZnS quantum dot with silica-coated quantum dots to form color conversion film.[148] Shea-Rohwer and co-workers have produced red-emitting CdTe quantum dots for use with InGaN blue LEDs.[80] Quantum dots have great potential for the production and design of light-emitting devices.

1.4.2.3 Photocatalysis

The ability of the quantum dot to be tuned towards particular energies leads to applications in photocatalysis.[69, 78, 149, 150, 151, 152, 153, 154, 155, 156, 157] Labiadh and co-workers have used ZnS quantum dots to catalysis the degradation of salicylic acid.[149] Sun and co-workers have used CdS quantum dots to catalyze charge transfer processes.[78] Yan and co-workers have PbS/CdS quantum dots to produce H_2 photocatalytically.[150] Li and co-workers have used CdS in TiO_2 to photocatalytically oxidize NO in air and degrade organic compounds in aqueous solution.[151] Kang and co-workers have used Si quantum dots in the photocatalysis of benzene to phenol.[69] Soni and co-workers have performed a size-dependent CdSe quantum dot study of the photocatalyzed degradation of organic dye.[152] Singh and co-workers have developed an artificial photosynthesis using CuInS quantum dots.[153] Mansur and co-workers have studied the "green" degradation of organic dye pollutants using ZnS.[154] Li and co-workers have developed carbon quantum dots as photocatalysts for highly selective oxidation of benzyl alcohol and its derivatives.[155] Pourahmad has integrated PbS quantum dots into molecular sieves for the photocatalyic production of H_2.[156] Holmes and co-workers have used CdSe quantum dots to photocatalyze the splitting of water and found a size-dependent rate.[157] Quantum dots have been used in a wide array of photocatalyic systems.

1.4.2.4 Sensors

Quantum dots have found applications as sensors for many analyates.[28, 39, 41, 86, 87, 89, 158, 159, 160] Chan and co-workers used the functional flexibility of the surface ligands to attach biorecognition molecules that target certain cells.[28] Chen and Wu have used ZnSe quantum

dots capped with mercaptoacetic acid to determine pH by fluorescence spectroscopy.[158, 159] Yu and co-workers have used quantum dot-based pH probes for the study of enzyme reaction kinetics.[161] Yang and co-workers has used CdTe/CdSe core/shell quantum dots as pH-sensitive fluorescence probe with ascorbic acid as the added acid.[89] Deng and co-workers reported green and orange CdTe quantum dots, capped with specially marked ligands, as pH probes and for detection of viruses.[160] Tomasulo and co-workers produced CdSe/ZnS core/shell quantum dots with ligands which allowed the pH could be probed from 3 to 11.[86, 87] Teubert and co-workers investigated the electric-field dependence of the optical properties of INGaN/GaN quantum dots in contact with an electrolyte, finding that pH variation corresponds with photoluminescence.[41] Another application is the use of the quantum dots as nanoscale electric probes. Park and co-workers have used quantum dots to measure electrical fields on the nanoscale by taking advantage of the quantum-confined Stark effect using a variety of nanocrystals, including CdSe nanorods, CdSe quantum dot in CdS nanorods, CdTe/CdSe core/shell quantum dots, and ZnSe in CdS nanorod.[39] In each of these application, the change in the optical and electronic properties in quantum dots was used to determine the presence of some compound or characteristic of the system.

1.4.2.5 Bioimaging

A special application has been the use of quantum dots to determine the location of certain types of cells in living systems. [162, 163, 164, 165, 166, 167, 168, 169, 170, 171, 172, 173, 174, 175, 176, 177, 178, 179] Lovriá and co-workers examined the subcellular localization of CdTe quantum dots and also studied the toxcity of CdTe quantum dots finding that smaller quantum dots were more toxic.[175] Selvan and co-workers have used CdSe quantum dots to target cell

membranes.[176] Yong and co-workers have used InP/ZnS quantum dots conjugated with pancreatic cancer specific antibodies for efficient optical imaging of cancer cells in vitro.[177] Yang and co-workers have produced innovative carbon quantum dots which were demonstrated in use for bioimaging and staining.[178] Luo and co-workers have prepared carbon quantum dots which have high performance but are nontoxic in comparison to the txocity of the heavy metals in traditional quantum dots and comparable bioimaging performance.[179]

1.5 Organization

The remainder of this work is organized as follows. In chapter 2, a newly defined quantity call the electron-hole correlation length will be determined for CdSe quantum dots. It will also be demonstrated that the electron-hole correlation length can be used to improve the determination of the explicit correlation operator. In chapter 3, the development of the variational polaron transformation for use in the study of the optical and electronic properties in GaAs quantum dots under an applied electric field will be discussed. In chapter 4, the influence of electric fields on CdSe quantum dots will be explored, particularly the influence of ligand length and environment pH on the exciton binding energy for these systems. In chapter 5, conclusions from these projects will be given and avenues for future work along these tracks will be discussed.

Chapter 2: Determination of electron-hole correlation length in CdSe quantum dots using explicitly correlated two-particle cumulant

2.1 Introduction

Electron-hole excitations in semiconductor quantum dots are influenced by their size, shape and chemical composition. Controlling the generation and the dissociation of electron-hole (eh) pairs have important technological applications in the field of light-harvesting materials,[133, 180, 181, 182] photovoltaics,[85, 183, 184, 185] solid-state lighting,[80, 146, 147, 148] and lasing[142, 143, 144, 145]. In order to control the generation and dissociation of the eh-pair, it is important to understand the underlying interaction between the quasiparticles. Theoretical treatment of electron-hole interaction in quantum dots is challenging because of the computational bottleneck associated with quantum mechanical treatment of many-electron systems. In principle, a simplified description of the electron-hole pair can be achieved by ignoring the eh interaction and treating them as independent quasiparticles. Although this approach can dramatically reduce the computational cost, such simplifications can lead to qualitatively wrong results. For example, optical spectra calculation using independent quasiparticle approach often shows significant deviation from the experimental results. One of the main limitations of the independent quasiparticle method is its inability in describing bound excitonic states. Multiexcitonic interaction,

exciton and biexciton binding energies, radiative and Auger recombination are some of the properties whose calculations depend on the accurate treatment of electron-hole correlation. Theoretical investigation of electron-hole correlation has been performed using various methods such as time-dependent density functional theory (TDDFT)[186, 187, 188, 189, 190, 191, 192, 193], perturbation theory[194], GW combined with Bethe-Salpeter equation[195, 196, 197, 198, 199, 200, 201, 202, 203], configuration interaction[81, 119, 128, 204, 205, 206, 207, 208, 209], quantum Monte Carlo[206, 210, 211, 212], path-integral Monte Carlo,[213, 214] explicitly correlated Hartree-Fock method,[40, 215, 216, 217, 218] and electron-hole density functional theory.[219]

In this work, we are interested in the calculation of electron-hole correlation length (eh-CL) in CdSe quantum dots. Our goal is to provide a statistical definition of the electron-hole correlation length. The concept of correlation length has been widely used in many fields, including statistical mechanics[220, 221, 222, 223] and polymer science.[221, 222, 223, 224, 225, 226, 227] One of the important features of the eh-CL is that is it provides an intrinsic length scale for describing the electron-hole interaction. Because of this, it can play an important role in describing excitonic effects in quantum dots and other nanomaterials such as carbon nanotubes.[228, 229, 230] The eh-CL can also be used for construction of electron-hole correlation functional for multicomponent density functional theory.[219] For example, Salahub and co-workers have developed a series of exchange-correlation functions that are based on electron-electron correlation length[231, 232, 233, 234] and a similar strategy can be used for construction of electron-hole correlation functionals using eh-CL. The eh-CL can also aid in the development of explicitly correlated wave functions (such as Jastrow and Gaussian-type geminal functions) which depend directly on the electron-hole separation distance.[40, 212, 215, 216, 217, 218]

We have used the 2-particle electron-hole density matrix for the definition and calcula-

tion of the eh-CL. Two-particle reduced density matrix (2-RDM) has been used extensively for investigation of electron-electron correlation[235, 236, 237, 238, 239, 240, 241] and electronic excitation[242] in many-electron systems. For the present system, the 2-RDM is the appropriate mathematical quantity that contains all the necessary information about electron-hole correlation. Specifically, the cumulant associated with the electron-hole 2-RDM is the component of the 2-RDM that cannot be expressed as a product of 1-particle electron and hole densities. In principle, the 2-RDM can be obtained directly without the need for an underlying wave function as long as the N-representability of 2-RDM can be satisfied. However, in the present work, we have obtained the 2-RDM from an explicitly correlated electron-hole wave function. The remainder of the article is organized as follows. The basic theory of second quantization in electronic systems is presented in subsection 2.2.1. Electronic density matrices definitions and properties are shown in subsection 2.2.2. The derivation of eh-CL from the electron-hole cumulant is presented in subsection 2.2.4, transformation to intracular and extracular coordinates is described in subsection 2.2.6, and details of the explicitly correlated electron-hole wave function are presented in subsection 2.2.7 and section 2.3. The method was applied to a series of CdSe quantum dots and the results are presented in section 2.4.

2.2 Theory

2.2.1 Second quantization

Second quantization has been shown to be great use in several textbooks.[6, 17, 243, 244] Second quantization is an another representation of quantum mechanics that reduces all operators and wave functions to a set of elementary operators. The elementary operators create and annihilate

states in a standard reference state. The creation and annihilation operator may be defined for any particle type. In this section, the electronic creation and annihilation operators will be presented. In subsubsection 2.2.3.1, the creation and annihilation operators for a multi-component system will be presented. While the standard representation of quantum mechanics is widely used, it requires the imposition of certain properties of the system and requires the foreknowledge of certain aspects of the system (such as the number of electrons). This representation offers the advantages of built-in antisymmetry (which does not have to be imposed, since the creation and annihilation operators enforce the property) and simplified manipulation of wave functions and operators. On the other hand, second quantization introduces additional relationships and rules.

2.2.1.1 Creation and Annihilation Operators

The electronic creation operator is defined as [6, 17, 243, 244]

$$a_i^\dagger |\text{vac}\rangle = |\chi_i\rangle, \tag{2.1}$$

which means that a electron is placed in the molecular orbital χ_i. It follows logically that

$$a_1^\dagger |\chi_1\rangle = 0, \tag{2.2}$$

since the state cannot hold two particles in the same position.

The electronic annihilation operator is then defined as [6, 17, 243, 244]

$$a_i |\chi_i\rangle = |\text{vac}\rangle. \tag{2.3}$$

Two cases will yield zero for an annihilation operator:

$$a_i|\text{vac}\rangle = 0 \tag{2.4}$$

and

$$a_i|\chi_j\rangle = 0 \quad \text{if} \quad i \neq j. \tag{2.5}$$

Now, we wish to know what occurs when creation and annihilation operators operate to the left (on bras). For annihilation operators, we have[6, 17, 243, 244]

$$\begin{aligned}\langle\text{vac}|a_i &= \langle\text{vac}|(a_i)^\dagger \\ &= \langle\text{vac}|a_i^\dagger \\ &= \langle\chi_i|.\end{aligned}$$

For creation operators, we have[6, 17, 243, 244]

$$\begin{aligned}\langle\chi_i|a_i^\dagger &= \langle\chi_i|(a_i^\dagger)^\dagger \\ &= \langle\chi_i|a_i \\ &= \langle\text{vac}|\end{aligned}$$

2.2.1.2 Important Relations

In order to manipulate the creation and annihilation operators, three relations are used[6, 17, 243, 244]

$$a_i^\dagger a_j^\dagger + a_j^\dagger a_i^\dagger = 0 \tag{2.6}$$

$$a_i a_j + a_j a_i = 0 \tag{2.7}$$

$$a_i^\dagger a_j + a_j a_i^\dagger = \delta_{ij}. \tag{2.8}$$

The use of these relations, in particular the last, is the key to rearranging the operators into useful expressions.

2.2.1.3 Normal Order and Contractions

For the case of the vacuum state, it is useful to define a *normal order*. This ordering is such that all annihilation operators are to the right of all creation operators. This is,

$$A^\dagger B^\dagger C^\dagger \cdots XYZ$$

Now, we define a contraction[245]

$$\overbrace{a_i a_j^\dagger} = a_i a_j^\dagger - \{a_i a_j^\dagger\} \tag{2.9}$$

which also introduces the notation $\{\cdots\}$ which is the enclosed string in normal order (for operation on a vacuum). It is important to realize that $\{\cdots\}$ includes a factor $(-1)^P$ where P is the number

of permutations (or transpositions) required to bring the string of operators into normal order.

We note that

$$\overbrace{a_i a_j} = 0 \tag{2.10}$$

$$\overbrace{a_i^\dagger a_j^\dagger} = 0 \tag{2.11}$$

$$\overbrace{a_i^\dagger a_j} = 0 \tag{2.12}$$

$$\overbrace{a_i a_j^\dagger} = \delta_{ij} \tag{2.13}$$

$$\overbrace{a_i a_j a_k^\dagger} a_l^\dagger = \delta_{ik} a_j a_l^\dagger \tag{2.14}$$

We also define *full contractions* as the case where all operators are pairwise contracted. For example,

$$\overbrace{a_i \overbrace{a_j a_k^\dagger} a_l^\dagger} = -\delta_{ik}\delta_{jl}$$

is fully contracted. A rule of thumb to note here is that the sign of a full contraction is negative if the number of crossings is odd and positive otherwise.

2.2.1.4 Wick's Theorem

For an arbitrary string of annihilation and creation operators $ABC\cdots XYZ$, the string may be written as a linear combination of normal ordered strings.[245, 246]

$$ABC\cdots XYZ = \{ABC\cdots XYZ\} + \sum_{\text{singles}} \{\overbrace{AB}C\cdots XYZ\}$$

$$+ \sum_{\text{doubles}} \{\overbrace{ABC\cdots XYZ}\}$$
$$+ \cdots \tag{2.15}$$

The generalized Wick's theorem simplifies the matter further because it states that if a string can be divided into normal ordered substrings, then only contractions between the strings need be evaluated, not those contractions within the strings.[246]

$$\begin{aligned}\{ABC\cdots\}\{XYZ\cdots\} = \{&ABC\cdots XYZ\cdots\} \\ &+ \sum_{\text{singles}} \{\overbrace{ABC\cdots XYZ}\cdots\} \\ &+ \sum_{\text{doubles}} \{\overbrace{ABC\cdots XYZ}\cdots\} \\ &+ \cdots\end{aligned}$$

2.2.1.5 Operators in Second Quantization

With the tools to express and manipulate creation and annihilation operations to give any wavefunction from a vacuum state, it remains necessary to express the single and two particles operators in terms of creation and annihilation operators. We define the operators O_1, the sum of a one-particle operators, h as[246]

$$O_1 = \sum_{ij} \langle i|h|j\rangle a_i^\dagger a_j. \tag{2.16}$$

and the two particle operator, O_2 as

$$O_2 = \sum_{ijkl} \langle ij|kl\rangle a_i^\dagger a_j^\dagger a_l a_k, \tag{2.17}$$

in which one should carefully note the order of $a_l a_k$. One should also note that O_2 can be expressed to explicitly show the operator g as

$$O_2 = \sum_{ijkl} \langle ij|g|kl\rangle a_i^\dagger a_j^\dagger a_l a_k, \tag{2.18}$$

as will be seen in the example (*vide infra*).

2.2.1.6 Fermi Vacuum

It is useful to consider a state that is filled with N-particles, such as $|\chi_1\chi_2\cdots\chi_N\rangle$. If we consider what operators will cause a these states to vanish, it becomes clear that the normal order should be such that all creation operators are to the left of all annihilation operators. This ordering is denoted as $:\cdot:$ and the only not-zero contraction are[246]

$$\overbrace{a_i^\dagger a_j} = \delta_{ij}. \tag{2.19}$$

2.2.1.7 Energy of a N-particle Slater Determinant

For a system such that

$$H = \underbrace{\sum_{ij} \langle i|h|j\rangle a_i^\dagger a_j}_{H_0} + \underbrace{\sum_{ijkl} \langle ij|V_{ee}|kl\rangle a_i^\dagger a_j^\dagger a_l a_k}_{H_2} \tag{2.20}$$

with $|\Psi_0\rangle = |\chi_1\chi_2\cdots\chi_N\rangle$, show that

$$E = \langle\Psi_0|H|\Psi_0\rangle \tag{2.21}$$

We consider the first term. Given the form of $|\Psi_0\rangle$, the creation and annihilation string should be converted to normal order for an occupied system

$$a_i^\dagger a_j =: a_i^\dagger a_j : +\delta_{ij} = \delta_{ij} - a_j a_i^\dagger. \tag{2.22}$$

Using Eq. (2.22) in the first term with the wavefunctions gives

$$H_0 = \sum_{ij}^{N} \langle i|h|j\rangle \langle\Psi_0|\delta_{ij} - a_j a_i^\dagger|\Psi_0\rangle = \sum_{ij}^{N} \langle i|h|j\rangle (\delta_{ij}\langle\Psi_0|\Psi_0\rangle - \langle\Psi_0|a_j a_i^\dagger|\Psi_0\rangle) \tag{2.23}$$

For this term to be nonzero, $i = j$ and the upper limit must be N since the rearrangement simplification assumes that the strings are operating on an N-particle Slater determinant, so we have

$$H_0 = \sum_{i=1}^{N} \langle i|h|i\rangle. \tag{2.24}$$

The second term, H_2, is now determined. Let us consider the creation and annihilation operators

$$\begin{aligned} a_i^\dagger a_j^\dagger a_l a_k =& : a_i^\dagger a_j^\dagger a_l a_k : \\ &+ : \overbrace{a_i^\dagger a_j^\dagger} a_l a_k : + : \overbrace{a_i^\dagger a_j^\dagger a_l} a_k : \\ &+ : a_i^\dagger \overbrace{a_j^\dagger a_l} a_k : + : a_i^\dagger \overbrace{a_j^\dagger a_l a_k} : \end{aligned}$$

$$
\begin{aligned}
&+ :\overbrace{a_i^\dagger a_j^\dagger a_l a_k}: + :\overbrace{a_i^\dagger a_j^\dagger a_2 a_k}: \\
&= a_l a_k a_i^\dagger a_j^\dagger \\
&\quad - \delta_{il} a_k a_j^\dagger + \delta_{ik} a_l a_j^\dagger \\
&\quad - \delta_{jl} a_k a_i^\dagger + \delta_{jk} a_l a_i^\dagger \\
&\quad + \delta_{ik}\delta_{jl} - \delta_{il}\delta_{jk}
\end{aligned}
$$

Let us consider the implications of this rearrangement. Clearly, the conditions on H_2 do not allow $i = j$ or $k = l$ to give nonzero terms, but place no limitation on $i = k$ or $i = l$ and $j = k$ $j = l$. Consider the case $i = l, j = k$, then we have

$$
\begin{aligned}
a_i^\dagger a_j^\dagger a_j a_i &= a_j a_i a_i^\dagger a_j^\dagger \\
&\quad - \delta_{ii} a_j a_j^\dagger + \delta_{ij} a_i a_j^\dagger \\
&\quad - \delta_{ji} a_j a_i^\dagger + \delta_{jj} a_i a_i^\dagger \\
&\quad + \delta_{ij}\delta_{ji} - \delta_{ii}\delta_{jj}
\end{aligned}
$$

Similarly, the case $i = k, j = l$ gives

$$
\begin{aligned}
a_i^\dagger a_j^\dagger a_i a_j &= a_i a_i a_j^\dagger a_j^\dagger \\
&\quad - \delta_{ij} a_i a_j^\dagger + \delta_{ii} a_j a_j^\dagger \\
&\quad - \delta_{jj} a_i a_i^\dagger + \delta_{ji} a_j a_i^\dagger \\
&\quad + \delta_{ii}\delta_{jj} - \delta_{ij}\delta_{ji}
\end{aligned}
$$

Assuming that these operators are operating on a N-particle Slater determinant gives

$$a_i^\dagger a_j^\dagger a_l a_k = \delta_{ik}\delta_{jl} - \delta_{il}\delta_{jk} \tag{2.25}$$

with the consideration that this is not a general term but is limited to an N-particle Slater determinant.

With this determination in hand and the consideration that $i = k$, $i = l$, $j = k$, or $j = l$, we may now determine the H_2 term

$$\begin{aligned} H_2 &= \sum_{ij}^{N} \langle ij|V_{\text{ee}}|ij\rangle(\delta_{ii}\delta_{jj} - \delta_{ij}\delta_{ji}) + \sum_{ij}^{N} \langle ij|V_{\text{ee}}|ij\rangle(\delta_{ij}\delta_{ji} - \delta_{ii}\delta_{jj}) \\ &= \sum_{ij}^{N} \langle ij|V_{\text{ee}}|ij\rangle - \langle ij|V_{\text{ee}}|ji\rangle. \end{aligned}$$

Therefore, it is shown that

$$E = \langle \Psi_0|H|\Psi_0\rangle = \sum_{i=1}^{N} \langle i|h|i\rangle + \left(\sum_{ij}^{N} \langle ij|V_{\text{ee}}|ij\rangle - \langle ij|V_{\text{ee}}|ji\rangle \right). \tag{2.26}$$

2.2.1.8 Minimization of The Energy

With Eq. (2.26) in hand, we now turn to the minimization of energy. We may do so by Lagrange's method of undetermined multipliers. We note that a boundary condition is determined by

$$\int \mathrm{d}x_1 \chi_a^*(1)\chi_b(1) = [a|b] = \delta_{ab}. \tag{2.27}$$

From this, the constraints are expressed as

$$[i|j] - \delta_{ij} = 0. \tag{2.28}$$

In order to minimize the energy, we consider the functional $\mathscr{L}[\{\chi_i\}]$, given as

$$\mathscr{L}[\{\chi_i\} = E[\{\chi\}] - \sum_{i=1}^{N}\sum_{j=1}^{N} \varepsilon_{ji}([i|j] - \delta_{ij}). \tag{2.29}$$

We may then minimize the energy by minimizing $\mathscr{L}$, that is

$$\delta\mathscr{L} = \delta E[\{\chi\}] - \sum_{i=1}^{N}\sum_{j=1}^{N} \varepsilon_{ji}\delta[i|j] = 0. \tag{2.30}$$

To do so, we must find δE. We do so by

$$\begin{aligned}
\delta E[\chi] &= E[\chi + \delta\chi] - E[\chi] \\
&= \sum_{i=1}^{N} \langle(\chi_i + \delta\chi_i)|h|(\chi_i + \delta\chi_i)\rangle \\
&\quad + \left(\sum_{1=1}^{N}\sum_{j=1}^{N} \langle(\chi_i + \delta\chi_i)(\chi_j + \delta\chi_j)|V_{\text{ee}}(1 - P_{12})|(\chi_i + \delta\chi_i)(\chi_j + \delta\chi_j)\rangle\right) \\
&\quad - \sum_{i=1}^{N} \langle\chi_i|h|\chi_i\rangle + \left(\sum_{i=1}^{N}\sum_{j=1}^{N} \langle\chi_i\chi_j|V_{\text{ee}}(1 - P_{12})|\chi_i\chi_j\rangle\right).
\end{aligned}$$

Rewriting in integral form and dropping the integrals and differentials for clarity gives

$$\begin{aligned}
\delta E &= \sum_{i=1}^{N} (\chi_i^* + \delta\chi_i^*) h (\chi_i + \delta\chi_i) \\
&\quad + \sum_{i=1}^{N}\sum_{j=1}^{N} (\chi_i^* + \delta\chi_i^*)(\chi_j^* + \delta\chi_j^*) V_{\text{ee}}((\chi_i + \delta\chi_i)(\chi_j + \delta\chi_j) - (\chi_j + \delta\chi_j)(\chi_i + \delta\chi_i))
\end{aligned}$$

$$
\begin{aligned}
&- \sum_{i=1}^{N} \chi_i^* h \chi_i + \sum_{i=1}^{N} \sum_{j=1}^{N} (\chi_i^* \chi_j^*) V_{\mathrm{ee}} (\chi_i \chi_j - \chi_j \chi_i) \\
&= \sum_{i=1}^{N} \chi_i^* h \chi_i - \chi_i^* h \delta\chi_i + \delta\chi_i^* h \chi_i + \delta\chi_i^* h \delta\chi_i \\
&\quad + \sum_{i=1}^{N} \sum_{j=1}^{N} (\chi_i^* \chi_j^* + \chi_i \delta\chi_j^* + \delta\chi_i^* \chi_j^* + \delta\chi_i^* \delta\chi_j^*) V_{\mathrm{ee}} ((\chi_i \chi_j + \chi_i \delta\chi_j + \delta\chi_i \chi_j + \delta\chi_i \delta\chi_j)) \\
&\quad - \sum_{i=1}^{N} \sum_{j=1}^{N} (\chi_i^* \chi_j^* + \chi_i \delta\chi_j^* + \delta\chi_i^* \chi_j^* + \delta\chi_i^* \delta\chi_j^*) V_{\mathrm{ee}} ((\chi_j \chi_i + \chi_j \delta\chi_i + \delta\chi_j \chi_i + \delta\chi_j \delta\chi_i)) \\
&\quad - \sum_{i=1}^{N} \chi_i^* h \chi_i + \sum_{i=1}^{N} \sum_{j=1}^{N} (\chi_i^* \chi_j^*) V_{\mathrm{ee}} (\chi_i \chi_j - \chi_j \chi_i) \\
&= \sum_{i=1}^{N} \chi_i^* h \chi_i - \chi_i^* h \delta\chi_i + \delta\chi_i^* h \chi_i + \delta\chi_i^* h \delta\chi_i \\
&\quad + \sum_{i=1}^{N} \sum_{j=1}^{N} \chi_i^* \chi_j^* V_{\mathrm{ee}} \chi_i \chi_j + \chi_i^* \chi_j^* V_{\mathrm{ee}} \chi_i \delta\chi_j + \chi_i^* \chi_j^* V_{\mathrm{ee}} \delta\chi_i \chi_j + \chi_i^* \chi_j^* V_{\mathrm{ee}} \delta\chi_i \delta\chi_j \\
&\quad + \chi_i^* \delta\chi_j^* V_{\mathrm{ee}} \chi_i \chi_j + \chi_i^* \delta\chi_j^* V_{\mathrm{ee}} \chi_i \delta\chi_j + \chi_i^* \delta\chi_j^* V_{\mathrm{ee}} \delta\chi_i \chi_j + \chi_i^* \delta\chi_j^* V_{\mathrm{ee}} \delta\chi_i \delta\chi_j \\
&\quad + \delta\chi_i^* \chi_j^* V_{\mathrm{ee}} \chi_i \chi_j + \delta\chi_i^* \chi_j^* V_{\mathrm{ee}} \chi_i \delta\chi_j + \delta\chi_i^* \chi_j^* V_{\mathrm{ee}} \delta\chi_i \chi_j + \delta\chi_i^* \chi_j^* V_{\mathrm{ee}} \delta\chi_i \delta\chi_j \\
&\quad + \delta\chi_i^* \delta\chi_j^* V_{\mathrm{ee}} \chi_i \chi_j + \delta\chi_i^* \delta\chi_j^* V_{\mathrm{ee}} \chi_i \delta\chi_j + \delta\chi_i^* \delta\chi_j^* V_{\mathrm{ee}} \delta\chi_i \chi_j + \delta\chi_i^* \delta\chi_j^* V_{\mathrm{ee}} \delta\chi_i \delta\chi_j \\
&\quad - \sum_{i=1}^{N} \sum_{j=1}^{N} \chi_i^* \chi_j^* V_{\mathrm{ee}} \chi_j \chi_i + \chi_i^* \chi_j^* V_{\mathrm{ee}} \chi_j \delta\chi_i + \chi_i^* \chi_j^* V_{\mathrm{ee}} \delta\chi_j \chi_i + \chi_i^* \chi_j^* V_{\mathrm{ee}} \delta\chi_j \delta\chi_i \\
&\quad + \chi_i^* \delta\chi_j^* V_{\mathrm{ee}} \chi_j \chi_i + \chi_i^* \delta\chi_j^* V_{\mathrm{ee}} \chi_j \delta\chi_i + \chi_i^* \delta\chi_j^* V_{\mathrm{ee}} \delta\chi_j \chi_i + \chi_i^* \delta\chi_j^* V_{\mathrm{ee}} \delta\chi_j \delta\chi_i \\
&\quad + \delta\chi_i^* \chi_j^* V_{\mathrm{ee}} \chi_j \chi_i + \delta\chi_i^* \chi_j^* V_{\mathrm{ee}} \chi_j \delta\chi_i + \delta\chi_i^* \chi_j^* V_{\mathrm{ee}} \delta\chi_j \chi_i + \delta\chi_i^* \chi_j^* V_{\mathrm{ee}} \delta\chi_j \delta\chi_i \\
&\quad + \delta\chi_i^* \delta\chi_j^* V_{\mathrm{ee}} \chi_j \chi_i + \delta\chi_i^* \delta\chi_j^* V_{\mathrm{ee}} \chi_j \delta\chi_i + \delta\chi_i^* \delta\chi_j^* V_{\mathrm{ee}} \delta\chi_j \chi_i + \delta\chi_i^* \delta\chi_j^* V_{\mathrm{ee}} \delta\chi_j \delta\chi_i \\
&\quad - \sum_{i=1}^{N} \chi_i^* h \chi_i - \sum_{i=1}^{N} \sum_{j=1}^{N} \chi_i^* \chi_j^* V_{\mathrm{ee}} \chi_i \chi_j - \chi_i^* \chi_j^* V_{\mathrm{ee}} \chi_j \chi_i \\
&= \sum_{i=1}^{N} \chi_i^* h \delta\chi_i + \delta\chi_i^* h \chi_i \\
&\quad + \sum_{i=1}^{N} \sum_{j=1}^{N} \chi_i^* \chi_j^* V_{\mathrm{ee}} \chi_i \delta\chi_j + \chi_i^* \chi_j^* V_{\mathrm{ee}} \delta\chi_i \chi_j + \chi_i^* \delta\chi_j^* V_{\mathrm{ee}} \chi_i \chi_j + \delta\chi_i^* \chi_j^* V_{\mathrm{ee}} \chi_i \chi_j \\
&\quad - \sum_{i=1}^{N} \sum_{j=1}^{N} \chi_i^* \chi_j^* V_{\mathrm{ee}} \chi_j \delta\chi_i + \chi_i^* \chi_j^* V_{\mathrm{ee}} \delta\chi_i \chi_j + \chi_i^* \delta\chi_j^* V_{\mathrm{ee}} \chi_j \chi_i + \delta\chi_i^* \chi_j^* V_{\mathrm{ee}} \chi_j \chi_i
\end{aligned}
$$

Returning to standard notation gives us

$$\begin{aligned}\delta E = &\sum_{i=1}^{N}[\chi_i|h|\delta\chi_i] + [\delta\chi_i|h|\chi_i] \\ &+ \sum_{i=1}^{N}\sum_{j=1}^{N}\langle\chi_i\chi_j|V_{\text{ee}}|\chi_i\delta\chi_j\rangle + \langle\chi_i\chi_j|V_{\text{ee}}\delta\chi_i\chi_j\rangle + \langle\chi_i\delta\chi_j|V_{\text{ee}}|\chi_i\chi_j\rangle + \langle\delta\chi_i\chi_j|V_{\text{ee}}|\chi_i\chi_j\rangle \\ &- \sum_{i=1}^{N}\sum_{j=1}^{N}\langle\chi_i\chi_j|V_{\text{ee}}|\chi_j\delta\chi_i\rangle + \langle\chi_i\chi_j|V_{\text{ee}}|\delta\chi_j\chi_i\rangle + \langle\chi_i\delta\chi_j|V_{\text{ee}}|\chi_j\chi_i\rangle + \langle\delta\chi_i\chi_j|V_{\text{ee}}|\chi_j\chi_i\rangle.\end{aligned} \tag{2.31}$$

This may completely rewritten in chemist's notation as

$$\begin{aligned}\delta E = &\sum_{i=1}^{N}[\chi_i|h|\delta\chi_i] + [\delta\chi_i|h|\chi_i] \\ &+ \sum_{i=1}^{N}\sum_{j=1}^{N}[\chi_i\chi_i|V_{\text{ee}}|\chi_j\delta\chi_j] + [\chi_i\chi_i|V_{\text{ee}}|\delta\chi_j\chi_j] + [\chi_i\delta\chi_i|V_{\text{ee}}|\chi_j\chi_j] + [\delta\chi_i\chi_i|V_{\text{ee}}|\chi_j\chi_j] \\ &- \sum_{i=1}^{N}\sum_{j=1}^{N}[\chi_i\chi_j|V_{\text{ee}}|\chi_j\delta\chi_i] + [\chi_i\chi_j|V_{\text{ee}}|\delta\chi_j\chi_i] + [\chi_i\delta\chi_j|V_{\text{ee}}|\chi_j\chi_i] + [\delta\chi_i\chi_j|V_{\text{ee}}|\chi_j\chi_i].\end{aligned} \tag{2.32}$$

This equation is shown to be

$$\begin{aligned}\delta E = &\sum_{i=1}^{N}[\chi_i|h|\delta\chi_i] + [\delta\chi_i|h|\chi_i] \\ &+ \sum_{i=1}^{N}\sum_{j=1}^{N}[\chi_i\chi_i|V_{\text{ee}}|\chi_j\delta\chi_j] + [\chi_i\chi_i|V_{\text{ee}}|\delta\chi_j\chi_j] + [\chi_i\delta\chi_i|V_{\text{ee}}|\chi_j\chi_j] + [\delta\chi_i\chi_i|V_{\text{ee}}|\chi_j\chi_j] \\ &- \sum_{i=1}^{N}\sum_{j=1}^{N}[\chi_i\chi_j|V_{\text{ee}}|\chi_j\delta\chi_i] + [\chi_i\chi_j|V_{\text{ee}}|\delta\chi_j\chi_i] + [\chi_i\delta\chi_j|V_{\text{ee}}|\chi_j\chi_i] + [\delta\chi_i\chi_j|V_{\text{ee}}|\chi_j\chi_i] \\ = &\sum_{i=1}^{N}[\chi_i|h|\delta\chi_i] + [\chi_i|h|\delta\chi_i]^* \\ &+ 2\sum_{i=1}^{N}\sum_{j=1}^{N}[\delta\chi_i\chi_i|V_{\text{ee}}|\chi_j\chi_j] + [\chi_j\chi_j|V_{\text{ee}}|\delta\chi_i\chi_i]^* \\ &- 2\sum_{i=1}^{N}\sum_{j=1}^{N}[\delta\chi_i\chi_j|V_{\text{ee}}|\chi_j\chi_i] + [\chi_j\chi_i|V\text{ee}|\delta\chi_i\chi_j]\end{aligned} \tag{2.33}$$

$$
\begin{aligned}
&= \sum_{i=1}^{N} [\chi_i|h|\delta\chi_i] + \quad \text{complex conjugate} \\
&\quad + 2\sum_{i=1}^{N}\sum_{j=1}^{N} [\delta\chi_i\chi_i|V_{\text{ee}}|\chi_j\chi_j] + \quad \text{complex conjugate} \\
&\quad - 2\sum_{i=1}^{N}\sum_{j=1}^{N} [\delta\chi_i\chi_j|V_{\text{ee}}|\chi_j\chi_i] + \quad \text{complex conjugate.}
\end{aligned}
$$

We now turn to the second term in Eq. (2.30) and find that since

$$
\delta[i|j] = [\delta\chi_i|\chi_j] + [\chi_i|\delta\chi_j]
$$

and $\varepsilon_{ji} = \varepsilon_{ij}^*$, we have

$$
\begin{aligned}
\sum_{i=1}^{N}\sum_{j=1}^{N} \varepsilon_{ji}[\delta\chi_i|\chi_j] + [\chi_i|\delta\chi_j] &= \sum_{i=1}^{N}\sum_{j=1}^{N} \varepsilon_{ji}[\delta\chi_i|\chi_j] + \sum_{i=1}^{N}\sum_{j=1}^{N} \varepsilon_{ij}[\chi_j|\delta\chi_i] \\
&= \sum_{i=1}^{N}\sum_{j=1}^{N} \varepsilon_{ji}[\delta\chi_i|\chi_j] + \sum_{i=1}^{N}\sum_{j=1}^{N} \varepsilon_{ji}^*[\delta\chi_i|\chi_b]^* \\
&= \sum_{i=1}^{N}\sum_{j=1}^{N} \varepsilon_{ji}[\delta\chi_i|\chi_j] + \quad \text{complex conjugate.}
\end{aligned}
$$

We now write $\delta\mathscr{L}$ as

$$
\begin{aligned}
\delta\mathscr{L} &= \sum_{i=1}^{N} [\delta\chi_i|h|\chi_i] \\
&\quad + 2\sum_{i=1}^{N}\sum_{j=1}^{N} [\delta\chi_i\chi_i|V_{\text{ee}}|\chi_j\chi_j] - [\delta\chi_i\chi_j|V_{\text{ee}}|\chi_j\chi_i] \\
&\quad + \quad \text{complex conjugate} \\
&= 0.
\end{aligned}
$$

At this point, it is advantageous to introduce the exchange operator $\mathscr{K}_j(1)$ and coulomb operator

$\mathscr{J}_j(1)$ as

$$\mathscr{K}_j(1)\chi_i(1) = \left[\int \mathrm{d}x_1 \chi_j^*(2) V_{\mathrm{ee}} \chi_i(2)\right] \chi_j(1) \tag{2.34}$$

$$\mathscr{J}_j(1)\chi_i(1) = \left[\int \mathrm{d}x_2 \chi_j^*(2) V_{\mathrm{ee}} \chi_j(2)\right] \chi_i(1) \tag{2.35}$$

We may then also write

$$\langle \chi_i(1)|\, \mathscr{J}_j(1)|\chi_i(1)\rangle = \int \mathrm{d}x_1 \mathrm{d}x_2 \chi_i^*(1)\chi_i(1) V_{\mathrm{ee}} \chi_j^*(2)\chi_j(2) = [ii|V_{\mathrm{ee}}|jj] \tag{2.36}$$

$$\langle \chi_i(1)|\mathscr{K}_j(1)|\chi_i(1)\rangle = \int \mathrm{d}x_1 \mathrm{d}x_2 \chi_i^*(1)\chi_j(1) V_{\mathrm{ee}} \chi_j^*(2)\chi_i(2) = [ij|V_{\mathrm{ee}}|ji] \tag{2.37}$$

In addition, we may use the exchange and coulomb operators to define the Fock operator f as

$$f(1) = h(1) + \sum_{1=1}^{N} \mathscr{J}_b(1) - \mathscr{K}_b(1). \tag{2.38}$$

Returning to Eq. (2.34), we use $\mathscr{K}_j(1)$ and $\mathscr{J}_j(1)$ and return to integral form, and factor out the common $\delta\chi_i$ to get

$$\begin{aligned}\delta\mathscr{L} = \sum_{i=1}^{N} \int \mathrm{d}x_1 \delta\chi_i^*(1) \left[h(1)\chi_i(1) + \sum_{j=1}^{N} (\mathscr{J}_j(1) - \mathscr{K}_j(1))\chi_i(1) - \sum_{j=1}^{N} \varepsilon_{ji}\chi_j(1)\right] \\ + \text{complex conjugate} = 0.\end{aligned} \tag{2.39}$$

Since $\delta\chi_i$ is an arbitrary infinitesimal but non-zero value, the bracket expression must be zero for

all i, giving

$$\left[h(1)+\sum_{j=1}^{N}\mathscr{J}_j(1)-\mathscr{K}_j(1)\right]\chi_i(1)=\sum_{j=1}^{N}\varepsilon_{ji}\chi_j(1)\quad i=1,2,\ldots,N \tag{2.40}$$

The bracketed operators match our definition of the Fock operator f giving us

$$f|\chi_i\rangle=\sum_{j=1}^{N}\varepsilon_{ji}|\chi_j\rangle. \tag{2.41}$$

2.2.2 Density matrices

Density matrices are powerful tools for expressing both pure and ensemble states. For pure states (states that can be expressed as a single state vector), the density matrix is an alternative representation. For mixed states, which can only be expressed as multiple state vectors, the density matrix is a highly useful method for expressing the necessary statistical average of the states. For an ensemble of N systems $n_i(i=1,2,\ldots,k)$ of which some are in state $|i\rangle$. The operator which selects only the desired state is given by

$$\rho=\sum_i p_i|i\rangle\langle i| \tag{2.42}$$

where p_i is the probability that a state picked randomly will be in the state $|i\rangle$.

2.2.2.1 Density Operators

To describe a more general form of the density operator, consider that[247]

$$\Psi_N(x_1x_2\cdots x_N)\Psi_N^*(x_1x_2\cdots x_N) \tag{2.43}$$

is the probability distribution. The quantity in (2.43) will be expressed as

$$\gamma_N(x_1'x_2'\cdots x_N', x_1x_2\cdots x_N) \equiv \Psi_N(x_1'x_2'\cdots x_N')\Psi_N^*(x_1x_2\cdots x_N). \tag{2.44}$$

If $x_i = x_i'$ for all i, we get the elements of (2.43). We may also express (2.44) as[247]

$$|\Psi_n\rangle\langle\Psi_n| = \hat{\gamma}_N \tag{2.45}$$

since

$$(x_1'x_2'\cdots x_N'|\hat{\gamma}_N|x_1x_2\cdots x_N) = (x_1'x_2'\cdots x_N'|\Psi_N\rangle\langle\Psi_N|x_1x_2\cdots x_N) \tag{2.46}$$

$$= \Psi_N(x_1'x_2'\cdots x_N')\Psi_N^*(x_1x_2\cdots x_N), \tag{2.47}$$

noting that $|\cdots)$ signifies a conversion from discrete values (with associated δ) to continuous values (with use of the function $\delta(x)$).

Clearly, $\hat{\gamma}$ is a projection operator. The normalized Ψ_N is

$$\mathrm{tr}(\hat{\gamma}) = \int \Psi_N(x^N)\Psi_N^* \mathrm{d}x^N, \tag{2.48}$$

where tr is the *trace* of the operator in Hilbert space and is the sum of the diagonal elements of the operator matrix. This is useful since it also occur st that for any operator $\hat{A}$, the expectation value is found as

$$\langle \hat{A} \rangle = \mathrm{tr}(\hat{\gamma}\hat{A}) = \mathrm{tr}(\hat{A}\hat{\gamma}). \tag{2.49}$$

This operator description is necessary since in large systems, a particular state may not be represented by a linear superposition of eigenstates of a particular Hamiltonian. However, some states, called *pure*, may be described by a wave function. States which may not be described a wave function are termed *mixed*.

Systems may be described by the probability distribution of the accessible pure states. This is done by the use of the *ensemble density operator*, which is

$$\hat{\Gamma} = \sum_i p_i |\Psi_i\rangle\langle\Psi_i|, \tag{2.50}$$

where p_i is the probability of the system being in state $|\Psi_i\rangle$ For a single pure state $\hat{\Gamma}$ reduces to $\hat{\gamma}$.[247]

The operator $\hat{\Gamma}$ is constructed such that is normalized. For any basis $|f_k\rangle$, it gives[247]

$$\begin{aligned} \mathrm{Tr}(\hat{\Gamma}) &= \sum_i \sum_k p_i \langle f_k|\Psi_i\rangle\langle\Psi_i|f_k\rangle \\ &= \sum_i p_i \langle\Psi_i \sum_k |f_k\rangle\langle f_k|\Psi_i\rangle \\ &= \sum_i p_i \langle\Psi_i|\Psi_i\rangle = \sum_i p_i = 1 \end{aligned} \tag{2.51}$$

The symbol Tr is the trace in *Fock*-space rather than strict Hilbert space. It also shown that $\hat{\Gamma}$ is

Hermitian since[247]

$$\begin{aligned}\langle f_k|\hat{\Gamma}|f_l\rangle &= \sum_i p_i \langle f_k|\Psi_i\rangle\langle\Psi_i|f_l\rangle \\ &= \sum_i p_i \{\langle f_l|\Psi_i\rangle\langle\Psi_i|f_k\rangle\}^* \\ &= \langle f_l|\hat{\Gamma}|f_k\rangle^* \end{aligned} \tag{2.52}$$

It is useful to note that $\hat{\gamma}$ is idempotent[247]

$$\hat{\gamma}\cdot\hat{\gamma} = |\Psi\rangle\langle\Psi|\Psi\rangle\langle\Psi| = |\Psi\rangle\langle\Psi| = \hat{\gamma}, \tag{2.53}$$

but the ensemble density operator $\hat{\Gamma}$ is not:

$$\hat{\Gamma}\cdot\hat{\Gamma} = \sum_i p_i^2 |\Psi_i\rangle\langle\Psi_i| \neq \hat{\Gamma}. \tag{2.54}$$

The expectation value for observable $\hat{A}$ is found, similarly to (2.49), as

$$\langle\hat{A}\rangle = \mathrm{Tr}(\hat{\Gamma}\hat{A}) = \sum_i p_i \langle\Psi_i|\hat{A}|\Psi_i\rangle. \tag{2.55}$$

2.2.2.2 Reduced Density Matrices for Fermion Systems

The most basic Hamiltonian operator is the sum of two symmetric "one-electron" operators and a symmetric "two-electron" operator, of which none depend on spin. With these observations,

the concept of the *reduced density matrix*. The *reduced density matrix of order p* is given by[247]

$$\hat{\gamma}_p(x'_1x'_2\cdots x'_p, x_1x_2\cdots x_p) = \begin{pmatrix} N \\ p \end{pmatrix} \int\cdots\int \hat{\gamma}(x'_1x'_2\cdots x_px_{p+1}\cdots x_N, x_1x_2\cdots x_p\cdots x_N)\mathrm{d}x_{p+1}\cdots\mathrm{d}x_N. \tag{2.56}$$

Consider

$$\hat{\gamma}_2(x'_1x'_2, x_1x_2) = \frac{N(N-1)}{2}\int\cdots\int \Psi(x'_1x'_2x_3\cdots x_N)\Psi^*(x_1x_2x_3\cdots x_N)\mathrm{d}x_3\cdots\mathrm{d}x_N \tag{2.57}$$

and

$$\gamma_1(x'_1, x_1) = N\int\cdots\int \Psi(x'_1x_2\cdots x_N)\Psi^*(x_1x_2\cdots x_N)\mathrm{d}x_2\cdots x\mathrm{d}x_N. \tag{2.58}$$

The reduced density matrices $\hat{\gamma}_1$ and $\hat{\gamma}_2$ are semifinite (zero or positive), Hermitian, and are antisymmetric (exchange of two particles gives a negative value).[247]

The operators $\hat{\gamma}_1$ and $\hat{\gamma}_2$ each give eigenfunctions and eigenvalues such that[247]

$$\int \hat{\gamma}_1(x'_1, x_1)\psi_i(x_1)\mathrm{d}x_1 = n_i\psi_i(x'_1) \tag{2.59}$$

and

$$\int\int \hat{\gamma}_2(x'_1x'_2, x_1x_2)\theta_i(x_1x_2)\mathrm{d}x_1\mathrm{d}x_2 = g_i\theta_i(x'_1x'_2). \tag{2.60}$$

For $\hat{\gamma}_1$, $\psi_i(x)$ are the eigenfunctions called *natural spin orbitals* and the eigenvalues n_i are called

the occupation numbers. These are are also represented by

$$\hat{\gamma}_1 = \sum_i n_i |\psi_i\rangle\langle\psi_i| \tag{2.61}$$

or

$$\hat{\gamma}_1(x_1', x_1) = \sum_i n_i \psi_i(x_1')\psi_i^*(x_1). \tag{2.62}$$

For $\hat{\gamma}_2$, it is

$$\hat{\gamma}_2 = \sum_i |\theta_i\rangle\langle\theta_i|, \tag{2.63}$$

where the g_i are called occupation numbers; the $|\theta_i\rangle$ are two-particle functions called *natural geminals*. These values are defined to be antisymmetric and are also semidefinite.[247]

In the case of mixed states, corresponding definitions of reduced density matrices and operators with the same properties are used. In the case where all participating states have the same particle number, N, the operator $\hat{\Gamma}$ is used as the Nth-order density operator $\hat{\Gamma}_N$. The pth-order mixed state density matrix is[247]

$$\begin{aligned}\hat{\Gamma}_p \quad & (x_1'x_2'\cdots x_p', x_1x_2\cdots x_p) \\ &= \begin{pmatrix} N \\ p \end{pmatrix} \int\cdots\int \hat{\Gamma}_N(x_1'x_2'\cdots x_p'x_{p+1}'\cdots x_n, x_1x_2\cdots x_N)\mathrm{d}x_{p+1}\cdots\mathrm{d}x_N.\end{aligned} \tag{2.64}$$

The operators $\hat{\Gamma}_2$ and $\hat{\Gamma}_1$ also exist, the latter of which is of special importance. It is

$$\hat{\Gamma}_1(x_1', x_1) = N\int\cdots\int \sum_i p_i\Psi_i(x_1'x_2\cdots x_N)\Psi_i^*(x_1x_2\cdots x_N)\mathrm{d}x_2\cdots\mathrm{d}x_N, \tag{2.65}$$

where the Ψ are various N-electron states entering the mixed state under consideration.

The one electron operator is given as[247]

$$\hat{O}_1 = \sum_{i=1}^{N} \hat{O}_1(x_i, x_i'). \tag{2.66}$$

The expectation value of this operator is

$$\langle \hat{O}_1 = \mathrm{tr}(\hat{O}_1 \hat{\gamma}_1) = \int \hat{O}_1(x_1 x_1') \hat{\gamma}_1(x_1', x_1) \mathrm{d}x_1 \mathrm{d}x_1'. \tag{2.67}$$

If the one-electron operator is local ($\hat{A}(r', r) = \hat{A}(r)\delta(r' - r)$), then only the diagonal part is written down giving[247]

$$\hat{O}_1 = \sum_{i=1}^{N} \hat{O}_1(x_i) \tag{2.68}$$

and the expectation-value is given by

$$\langle \hat{O}_1 \rangle = \int \left[\hat{O}_1(x_1) \hat{\gamma}_1(x_1', x_1) \right]_{x_1' = x_1} \mathrm{d}x_1 \tag{2.69}$$

All the two-electron operators under consideration are local, so these operators are written as their diagonal parts, giving[247]

$$\hat{O}_2 = \sum_{i<j}^{N} \hat{O}_2(x_i, x_j) \tag{2.70}$$

with expectation-value of

$$\langle \hat{O}_2 \rangle = \mathrm{tr}(\hat{O}_2 \hat{\gamma}_N)$$

$$= \int\int \left[\hat{O}_2(x_1,x_2)\hat{\gamma}_2(x_1'x_2',x_1x_2)\right]_{x_1'=x_1,x_2'=x_2} \mathrm{d}x_1\mathrm{d}x_2. \tag{2.71}$$

The expectation value of the Hamiltonian, all these parts are combined to give

$$\begin{aligned} E &= tr(\hat{H}\hat{\gamma}_N = E[\hat{\gamma}_1,\hat{\gamma}_2] = E[\hat{\gamma}_2] \\ &= \int [(-\frac{1}{2}\nabla_1^2 + v(r_1))\hat{\gamma}_1(x_1',x_1)]_{x_1'=x_1}\mathrm{d}x_1 + \int\int \frac{1}{r_{12}}\hat{\gamma}_2(x_1x_2,x_1,x_2)\mathrm{d}x_1\mathrm{d}x_2. \end{aligned} \tag{2.72}$$

2.2.3 Electron-hole picture

The importance and difficulty of highly accurate calculations of the excited electronic states was discussed in section 1.3. In this section, the use of the multi-component electron-hole picture will be described. There are many systems in which the renormalization of different components can aid in simplifying aspects of the systems. The renormalized particles are called "dressed-particles" or (preferred in this work) quasi-particles. By analogy, concrete examples would be similar to describe a bottle of water by describing the air bubble (quasi-particle) rather than the water (all-electron) or by describing a crowded auditorium by describing the empty seats ("there are three empty seats") rather than attempted to describe it by the attendance ("we have 347 attendees"). The renormalization constant is quite powerful and is used in the solution of many problems, with some representative (but not exhaustive) examples being[248]

1. The modeling of a gas as N interacting particles in a box.

2. The modeling of a magnetic material as set of individual magnets in a lattice.

3. The random arrangement of polymers in solution.

The greatest strength of renormalization is the reduction in the number of degrees of freedom in the system.[248]

The key renormalization that is used in this work is the quasi-particle transformation. The quasi-particle transformation is an exact mathematical transformation that allows a compact representation of excited electronic states.[249] In the quasi-particle representation, the excitation of a single electron from the ground to the excited electronic state is described by generation of an electron-hole pair. This process is illustrated in Figure 2.1.[249, 250] The electron and the hole generated during the excitation process are known as quasi-particles and the interaction between them is described by the electron-hole Hamiltonian.

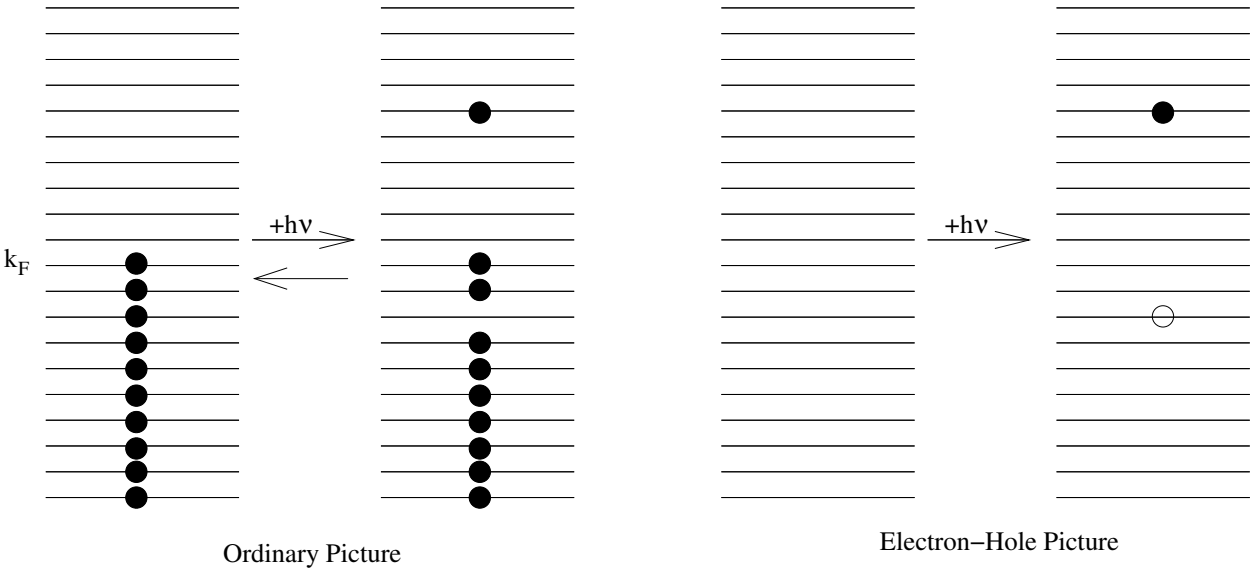

Figure 2.1: Comparison of the all-electron picture (on the left) with the electron-hole picture (on the right) of an arbitrary excitation.

A schematic representation of the transformation is presented in Figure 2.1.[249, 250] On the left, the electrons are represented as particles at various energy levels, up to k_{F}, the Fermi level. Excitation of a electron creates an unoccupied energy level below the Fermi level and occupies an energy level above the Fermi level. On the right in Figure 2.1, the electron-hole representation has

been invoked. The excited electron is now represented by a quasi-electron (the full circle) and the set of the $N-1$ electrons is now represented by the hole (the empty circle).

2.2.3.1 Second quantization for the electron-hole picture

In analogy to the electronic picture, second quantization can be useful in expressing quantum mechanical systems in the electron-hole picture.

2.2.3.1.1 Creation and annihilation operators

In analogy to the electronic system, creation and annihilation operators may be defined. The quasi-particles electron and hole are both fermion-type particles.[249**?**] The rules as related in subsection 2.2.1 apply. In the electron-hole picture, the reference space is a direct product of the Fock space for the electron and the Fock space for the hole,

$$|\Phi_k\rangle = |\Phi^{\mathrm{e}}\rangle \otimes |\Phi^{\mathrm{h}}\rangle. \tag{2.73}$$

The creation and annihilation operators for the electron will be denoted

$$e_i^\dagger|\rangle = |\chi_i^{\mathrm{e}}\rangle \tag{2.74}$$

$$e_i|\chi_i^{\mathrm{e}}\rangle = |\rangle. \tag{2.75}$$

The creation and annihilation operators for the hole will be denoted

$$h_i^\dagger|\rangle = |\chi_i^{\mathrm{h}}\rangle \tag{2.76}$$

$$h_i|\chi_i^{\mathrm{h}}\rangle = |\rangle. \tag{2.77}$$

2.2.3.1.2 Important relations

The relationships between the electron and hole creation and annhilation operators are given as[249]

$$[e_k, e_l^\dagger]_+ = \delta_{kl}, \tag{2.78}$$

$$[e_k, e_l]_+ = [e_k^\dagger, e_l^\dagger]_+ = 0, \tag{2.79}$$

$$[h_k, h_l^\dagger]_+ = \delta_{kl}, \tag{2.80}$$

$$[h_k, h_l]_+ = [h_k^\dagger, h_l^\dagger]_+ = 0, \tag{2.81}$$

$$[e_k, h_m]_+ = [e_k, h_m^\dagger]_+ = [e_k^\dagger, h_m]_+ = [e_k^\dagger, h_m^\dagger]_+ = 0, \tag{2.82}$$

where

$$[A, B]_+ = AB + BA. \tag{2.83}$$

2.2.3.1.3 Electron and hole operators

The key difference from the single component second quantization is the appearance of an additional two-body operator. Observe that the electron-electron (and hole-hole) Coulomb interaction terms has the property that the order of the annihilation operators is reversed in Eq. (2.92). However, since the electron and holes are different particle types, the two-body electron-hole op-

erator is

$$\sum_{ijj'j'} \langle ijj'j'|\varepsilon^{-1} r_{\mathrm{eh}}^{-1}|ijj'j'\rangle e_i^\dagger e_j h_{i'}^\dagger h_{j'}. \tag{2.84}$$

With the tool of second quantization for the electron and hole picture, the electron-hole quasiparticle transformation will be developed in the next section.

2.2.3.2 Electron-hole quasiparticle transformation

The electron-hole quasiparticle transformation may be shown in the following manner. In excited state, the excited electron is higher than the Fermi level, as seen in Figure 2.1. With that in mind, the Hamiltonian for the simple system in the figure is

$$H = \sum_{k<k_{\mathrm{F}}} \varepsilon_k - \sum_{k<k_{\mathrm{F}}} \varepsilon_k h_k^\dagger h_k + \sum_{k>k_{\mathrm{F}}} e_k^\dagger e_k, \tag{2.85}$$

where k_{F} is the Fermi energy level. Beginning with the electronic Hamiltonian

$$H = \sum_{pq}^{\infty} \langle p|h(1)|q\rangle p^\dagger q + \sum_{pqrs}^{\infty} \langle pq|rs\rangle p^\dagger q^\dagger sr. \tag{2.86}$$

The one-body operator will be expressed as

$$\sum_{pq}^{\infty} \langle p|h(1)|q\rangle p^\dagger q = \sum_{ij} \langle i|h(1)|j\rangle i^\dagger j + \sum_{ab} \langle a|h(1)|b\rangle a^\dagger b, \tag{2.87}$$

where indices of i, j are over occupied states and indices of a, b are unoccupied states. By changing the operators for the occupied states (in the electronic picture) to hole operators and the unoccupied

states (corresponding to quasielectron) gives

$$\sum_{pq}^{\infty}\langle p|h(1)|q\rangle p^{\dagger}q=\sum_{ij}\langle i|h(1)|j\rangle h_i^{\dagger}h_j+\sum_{ab}\langle a|h(1)|b\rangle e_a^{\dagger}e_b. \tag{2.88}$$

The two-particle term leads to a much more complicated set of equations. The equations are given as[251]

$$\begin{aligned}\sum_{pqrs}^{\infty}\langle pq|rs\rangle p^{\dagger}q^{\dagger}sr=&\frac{1}{2}\sum_{abcd}\langle ab|cd\rangle\{a_a^{\dagger}a_b^{\dagger}a_da_c\}+\frac{1}{2}\sum_{ijkl}\langle ij|jl\rangle\{a_i^{\dagger}a_j^{\dagger}a_la_k\}+2\sum_{iabj}\langle ia|bj\rangle\{a_i^{\dagger}a_a^{\dagger}a_ja_b\}\\&+\sum_{aibc}\langle ai|bc\rangle\{a_a^{\dagger}a_i^{\dagger}a_ca_b\}+\sum_{ijka}\langle ij|ka\rangle\{a_i^{\dagger}a_j^{\dagger}a_ka_a\}+\sum_{abci}\langle ab|ci\rangle\{a_a^{\dagger}a_b^{\dagger}a_ia_c\}\\&+\sum_{iajk}\langle ia|jk\rangle\{a_i^{\dagger}a_a^{\dagger}a_ka_j\}+\frac{1}{2}\sum_{abij}\langle ab|ij\rangle\{a_a^{\dagger}a_b^{\dagger}a_ja_i\}+\frac{1}{2}\sum_{ijab}\langle ij|ab\rangle\{a_i^{\dagger}a_j^{\dagger}a_ba_a\},\end{aligned} \tag{2.89}$$

where the notation $\{\cdots\}$ indicates that the string of creation and annihilation operators must be placed in normal order. The terms on the left-hand side in Eq. (2.89) can also be expressed in diagrams which can be seen in Figure 2.2 Eq. (2.89) will now be written in terms of electron and hole creation and annihilation operators

$$\begin{aligned}\sum_{pqrs}^{\infty}\langle pq|rs\rangle p^{\dagger}q^{\dagger}sr=&\frac{1}{2}\sum_{abcd}\langle ab|cd\rangle\{e_a^{\dagger}e_b^{\dagger}e_de_c\}+\frac{1}{2}\sum_{ijkl}\langle ij|jl\rangle\{h_ih_jh_l^{\dagger}h_k^{\dagger}\}+2\sum_{iabj}\langle ia|bj\rangle\{h_ie_a^{\dagger}h_j^{\dagger}e_b\}\\&+\sum_{aibc}\langle ai|bc\rangle\{e_a^{\dagger}h_ih_c^{\dagger}h_b^{\dagger}\}+\sum_{ijka}\langle ij|ka\rangle\{e_i^{\dagger}e_j^{\dagger}e_kh_a^{\dagger}\}+\sum_{abci}\langle ab|ci\rangle\{e_a^{\dagger}e_b^{\dagger}e_ih_c^{\dagger}\}\\&+\sum_{iajk}\langle ia|jk\rangle\{h_ih_ah_k^{\dagger}h_j^{\dagger}\}+\frac{1}{2}\sum_{abij}\langle ab|ij\rangle\{e_a^{\dagger}e_b^{\dagger}h_j^{\dagger}h_i^{\dagger}\}+\frac{1}{2}\sum_{ijab}\langle ij|ab\rangle\{h_ih_je_be_a\},\end{aligned} \tag{2.90}$$

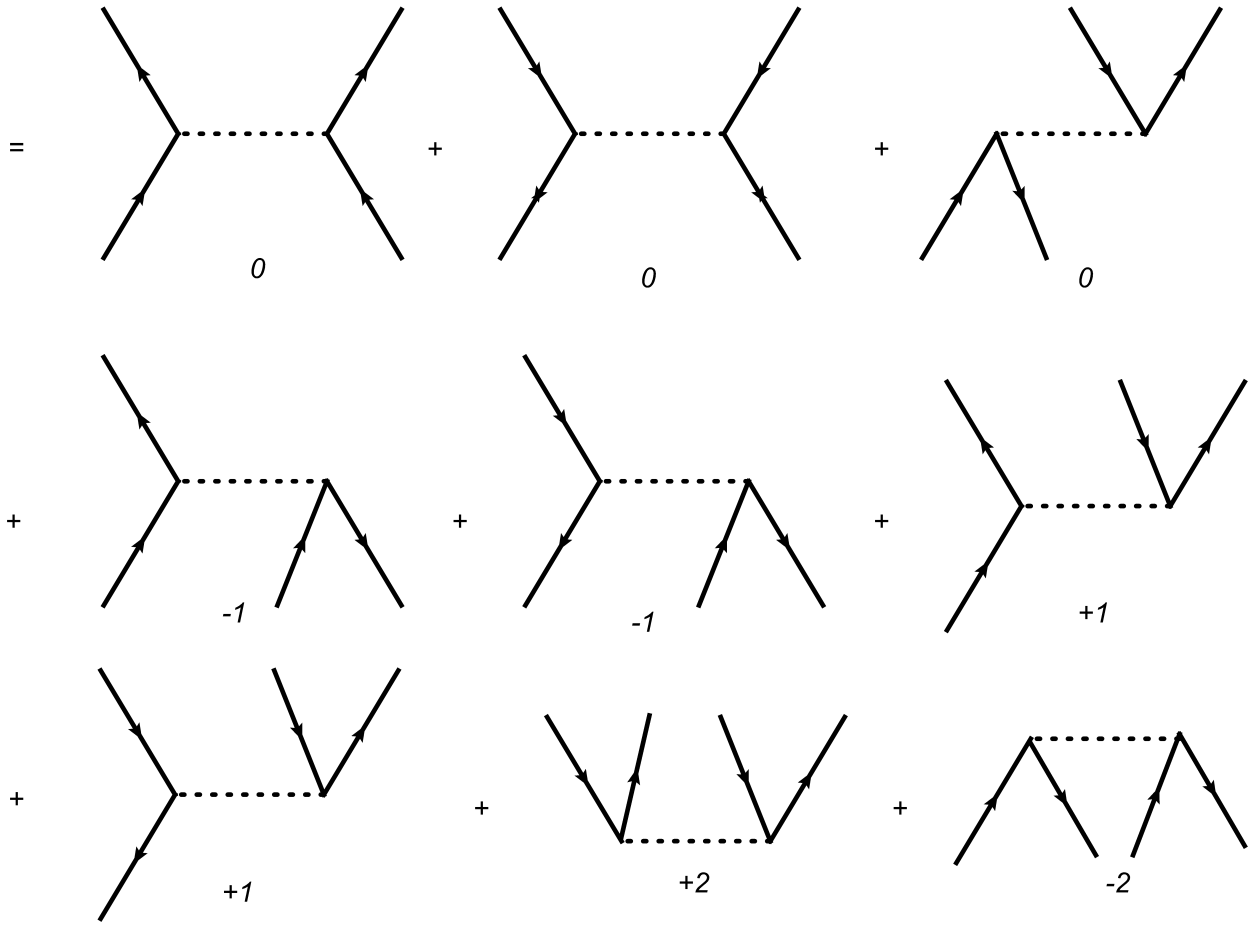

Figure 2.2: The two-body terms expressed in diagrams. The numbers under each diagram correspond to the excitation levels.

The only terms which contribute to the group state are those with excitation index 0 (see Figure 2.2). The full electron-hole Hamiltonian will shown in the next section.

2.2.3.3 Electron-Hole Hamiltonian

The exact transformation of the excited electron state into the electron-hole representation gives, as a consequence, the electron-hole Hamiltonian which describes the electron, the hole, and the interactions between the electron and the hole and is given as[40, 126, 128, 205, 206, 212, 215, 216, 218, 252, 253, 254, 255, 256, 257, 258]

$$
\begin{aligned}
H = & \sum_{ij} \langle i| \frac{-\hbar^2}{2m_{\mathrm{e}}} + v^{\mathrm{e}}_{\mathrm{ext}} |j\rangle e^{\dagger}_i e_j \\
& + \sum_{ij} \langle i| \frac{-\hbar^2}{2m_{\mathrm{h}}} + v^{\mathrm{h}}_{\mathrm{ext}} |j\rangle h^{\dagger}_i h_j \\
& + \sum_{iji'j'} \langle iji'j'| \varepsilon^{-1} r^{-1}_{\mathrm{eh}} |iji'j'\rangle e^{\dagger}_i e_j h^{\dagger}_{i'} h_{j'} \\
& + \sum_{ijkl} w^{\mathrm{ee}}_{ijkl} e^{\dagger}_i e^{\dagger}_j e_l e_k + \sum_{ijkl} w^{\mathrm{hh}}_{ijkl} h^{\dagger}_i h^{\dagger}_j h_l h_k \\
= & \underbrace{\hat{T}_{\mathrm{e}} + \hat{V}_{\mathrm{ee}} + \hat{V}^{\mathrm{ext}}_{\mathrm{e}}}_{\text{electronic}} + \underbrace{\hat{T}_{\mathrm{e}} + \hat{V}_{\mathrm{hh}} + \hat{V}^{\mathrm{ext}}_{\mathrm{h}}}_{\text{hole}} + \underbrace{\hat{V}_{\mathrm{eh}}}_{\text{interaction}}
\end{aligned}
\tag{2.91}
$$

where $\hat{T}_{\mathrm{e}}$ is the electron kinetic energy operator, $\hat{V}_{\mathrm{ee}}$ is the electron-electron interaction potential, $\hat{V}^{\mathrm{ext}}_{\mathrm{e}}$ is the electron external potential (nuclear-electron interaction) term, $\hat{T}_{\mathrm{h}}$ is the hole kinetic energy operator, $\hat{V}_{\mathrm{hh}}$ is the hole-hole interaction potential, $\hat{V}^{\mathrm{ext}}_{\mathrm{h}}$ is the hole external potential (nuclear-hole interaction) term, and $\hat{V}_{\mathrm{eh}}$ is the electron-hole Coulomb interaction term. In this presentation, the second quantization version of the Hamiltonian is used. Second quantization for electron-hole systems will be presented in subsection 2.2.5.

2.2.3.3.1 Methods for electron-hole systems

There are a number of methods for performing calculations within the electron-hole regime. Electron-hole systems have been investigated using various theoretical techniques including perturbation theory,[19, 107, 108, 109, 110, 111] variational techniques,[112, 113, 114, 115, 116, 117, 118] and configuration interaction method.[119, 120, 121, 122, 123, 124, 125, 126, 127, 128, 129]

2.2.3.4 Electron-hole correlation

The $\hat{V}_{\text{eh}}$ term couples the electron and hole coordinates and is responsible for electron-hole correlation. Electron-hole correlation has been treated by a number of traditional methods including Hartree-Fock, configuration interaction,[127, 128, 204, 205] many-body perturbation theory,[259, 260, 261] many-body Green's function theory,[200, 203, 261, 262, 263] and quantum Monte Carlo.[210, 211, 212, 213, 264, 265, 266, 267, 268] The inherent physics of the electron-hole system leads to the systems requiring strong correlation effects. The attractive Coulomb interaction between the electron and hole should lead to enhancement of the probability of finding electron and hole particles at short spatial separations. Highly accurate determination of the properties of electron-hole systems should incorporate this requirement. Theoretical investigation of electron-hole correlation has been performed using various methods such as time-dependent density functional theory (TDDFT)[186, 187, 188, 189, 190, 191, 192, 193], perturbation theory[194], GW combined with Bethe-Salpeter equation[195, 196, 197, 198, 199, 200, 201, 202, 203], configuration interaction[81, 119, 128, 204, 205, 206, 207, 208, 209], quantum Monte Carlo[206, 210, 211, 212], path-integral Monte Carlo[213, 214], and explicitly correlated Hartree-Fock method.[40, 215, 216, 217, 218]

2.2.3.5 Explicitly correlated electron-hole methods

In this work, the methods will be explicilty correlated electron-hole methods. In each of these methods, the electron-hole correlation will be explicitly addressed by incorporation of the electron-hole interaction into the wave function. Of particular use in this work is the electron-hole explicitly correlated Hartree-Fock (XC)[215, 216, 217] and Full Configuration Interaction.[40]

2.2.3.5.1 Ansatz

The ansatz for an XC method is

$$\Psi_{\text{eh}-\text{XCHF}} = G\Phi^{\text{eh}}, \tag{2.92}$$

where G is the explicit correlation operator and Φ^{eh} is a reference wave function. The reference wave function can be a Hartree-Fock (HF) wave function, Full Configuration Interaction (FCI), or nearly any other multi-component wave function. The explicit correlation operator can lead to many possible methods.

2.2.3.5.2 Explicit correlation operator

The explicit correlation operator G (or sometimes called geminal operator) is defined as[40, 215, 216, 217]

$$G = \sum_{i=1}^{N_{\text{e}}} \sum_{j=1}^{N_{\text{h}}} g(i,j), \tag{2.93}$$

where N_e is the number of electrons, N_h is the number of holes, and

$$g(i,j) = \sum_{k=1}^{N_{gem}} b_k \exp(-\gamma_k r_{ij}^2), \tag{2.94}$$

where N_{gem} is the number of geminal parameter sets and $\{b_k, \gamma_k\}$ are sets of geminal parameters. This is called an explicitly correlated method because the electron-hole separation distance r_{eh} is found directly in the operator. Explicit correlation operators of this form have been shown to improve:

1. the quality of the wave function at small electron-hole separation distances.[215, 216, 218]

2. speed the convergence of energy with smaller basis sets.[40, 217]

Each of these qualities helps greatly in the calculation of highly accurate electron-hole properties.

2.2.3.5.3 Electron-hole explicitly correlated Hartree-Fock

The multi-component Hartree-Fock reference wave function is a single Slater determinant for the electron and the hole,[216]

$$\Phi^{eh} = \Phi^e \Phi^h. \tag{2.95}$$

The ansatz for the electron-hole explicitly correlated Hartree-Fock method is[215, 216, 217]

$$\Psi_{eh-XCHF} = G\Phi^{eh}. \tag{2.96}$$

The energy for the method is determined by the minimization

$$E_{\mathrm{eh-XCHF}} = \min_{G,\Phi^{\mathrm{e}},\Phi^{\mathrm{h}}} \frac{\langle G\Phi^{\mathrm{e}}\Phi^{\mathrm{h}}|H|G\Phi^{\mathrm{e}}\Phi^{\mathrm{h}}\rangle}{\langle G\Phi^{\mathrm{e}}\Phi^{\mathrm{h}}|G\Phi^{\mathrm{e}}\Phi^{\mathrm{h}}\rangle}. \tag{2.97}$$

This minimization may be done by several methods. A very useful method is to use the transformations

$$\tilde{H} = G^{\dagger}HG, \tag{2.98}$$

$$\tilde{1} = G^{\dagger}G, \tag{2.99}$$

so that

$$E_{\mathrm{eh-XCHF}} = \min_{G,\Phi^{\mathrm{e}},\Phi^{\mathrm{h}}} \frac{\langle \Phi^{\mathrm{e}}\Phi^{\mathrm{h}}|\tilde{H}|\Phi^{\mathrm{e}}\Phi^{\mathrm{h}}\rangle}{\langle \Phi^{\mathrm{e}}\Phi^{\mathrm{h}}|\tilde{1}|\Phi^{\mathrm{e}}\Phi^{\mathrm{h}}\rangle}. \tag{2.100}$$

This allows the search to be performed with a relatively simple wave function, while taking advantage of the explicit correlation operator.[215, 216, 217]

2.2.3.5.4 Electron-hole explicitly correlated Full Configuration Interaction

The choice of the reference wave function in this method is the Full Configuration Interaction (FCI) wave function. The form of the wave function is the direct product of FCI wave functions for the electron and the hole[40]

$$\Phi_k^{\mathrm{eh}} = \Phi_i^{\mathrm{e}} \otimes \Phi_j^{\mathrm{h}}. \tag{2.101}$$

The FCI method for multicomponent methods shares the conceptually simple approach to the correlation (in this case, electron-hole) problem. However, due to the nature of FCI wave functions, the untenability of the size of the FCI matrix is reached sooner than in the electron systems since the number of matrix elements grows as the product of two factorial increase quantities. The addition of an explicit correlation operator leads to the explicitly correlated FCI method (XCFCI). The full details of the XCFCI method are given in subsection 3.2.2.

2.2.3.5.5 Particular Applications

The XCHF and related methods have been used to study a wide of variety of systems. Elward and co-workers have studied the electron-hole recombination in CdSe quantum dots.[216] Elward and Chakraborty have studied the effect of dot size on both exciton binding energy and electron-hole recombination probability.[215] Blanton and co-workers have use the explicitly correlated Full Configuration Interaction to study the effect of a homogeneous electric field on the exciton binding energy and electron-hole recombination probability.[40]

2.2.3.6 Electron-hole pair in a parabolic confinement

A system that has been studied extensively for the application of electron-hole systems is the electron-hole pair in a parabolic well. The Hamiltonian for such a system is given by

$$\hat{H} = -\frac{\hbar^2}{2m_e}\nabla_e^2 + \frac{1}{2}k_e r_e^2 + -\frac{\hbar^2}{2m_h}\nabla_h^2 - \frac{1}{\varepsilon r_{eh}}\frac{1}{2}k_h r_h^2 \tag{2.102}$$

$$= \hat{H}_e + \hat{H}_h + \hat{V}_{eh}, \tag{2.103}$$

where m_e is the mass of the quasi-electron, m_h is the mass of the hole, k_e is the force constant for the electron, k_h is the force constant for the hole, and ε is the dielectric constant for the material. This is an example of the effective mass approximation. In the effective mass approximation, the properties of the material are simulated by using an effective mass (as scaled mass relative to the mass of the free electron). The inherent damping of the electron-hole interaction in the material is simulated using the dielectric constant ε. This parabolic potential system has been extensively studied and exact solutions are known in certain limits, which allows for accurate benchmarking.[269, 270, 271, 272, 273, 274, 275, 276, 277]

2.2.3.7 Interesting properties of electron-hole systems

There are a number of interesting properties of electron-hole systems which may be studied. In the current work, exciton binding energy, electron-hole recombination probability, electron-hole correlation length, and electron-hole separation have been studied.

2.2.3.7.1 Exciton binding energy

Exciton binding energy is the amount of energy required to completely dissociate a bound electron-hole pair (exciton). Mathematically, it expressed as

$$E_B = E^{ni} - E^{int}, \tag{2.104}$$

where E_B is the exciton binding energy, E^{ni} is the non-interacting energy (energy for a completely dissociated system), and E^{int} is the interacting energy. Exciton binding energy has been studied by a number of groups.[40, 217, 278, 279]

2.2.3.7.2 Electron-hole recombination probability

Electron-hole recombination probability is a measure of the probability of finding the electron and hole within a small (or directly "on-top") volume. While measuring the lifetime of the electron-hole pair is difficult in the electron-hole picture, determination of the electron-hole recombination probability is approachable. The electron-hoe recombination probability has been studied by several groups.[40, 205, 216, 217]

2.2.3.7.3 Electron-hole separation distance

The average separation of the electron and hole is often an interesting and useful property to study. Often, either the expectation value of the distance $\langle |r_e - r_h| \rangle$ or the expectation value of the square of the separation will be studied.

2.2.3.7.4 Electron-hole correlation length

Electron-hole correlation length is this context is quantity that has been determined through a new definition in this work. In general, the electron-hole correlation length has been explored with many definitions as a measure of the influence that the attractive interaction between the electron and hole has on the properties of the system. The electron-hole correlation length is the subject of this chapter.

2.2.4 Electron-hole cumulant

The interaction between the quasi-particles in the quantum dot is described the electron-hole Hamiltonian,[40, 126, 128, 205, 206, 212, 215, 216, 218, 252, 253, 254, 255, 256, 257, 258] which

has the following general expression

$$
\begin{aligned}
H = & \sum_{ij} \langle i| \frac{-\hbar^2}{2m_{\mathrm{e}}} \nabla_{\mathrm{e}}^2 + v_{\mathrm{ext}}^{\mathrm{e}} |j\rangle e_i^\dagger e_j \\
& + \sum_{ij} \langle i| \frac{-\hbar^2}{2m_{\mathrm{h}}} \nabla_{\mathrm{h}}^2 + v_{\mathrm{ext}}^{\mathrm{h}} |j\rangle h_i^\dagger h_j \\
& + \sum_{iji'j'} \langle iji'j'| \varepsilon^{-1} r_{\mathrm{eh}}^{-1} |iji'j'\rangle e_i^\dagger e_j h_{i'}^\dagger h_{j'} \\
& + \sum_{ijkl} w_{ijkl}^{\mathrm{ee}} e_i^\dagger e_j^\dagger e_l e_k + \sum_{ijkl} w_{ijkl}^{\mathrm{hh}} h_i^\dagger h_j^\dagger h_l h_k .
\end{aligned}
\tag{2.105}
$$

We define the electron-hole wave function for a multiexcitonic system consisting of N_{e} and N_{h} number of electrons and holes, respectively by $\Psi_{\mathrm{eh}}(\mathbf{x}_1^{\mathrm{e}}, \ldots, \mathbf{x}_{N_{\mathrm{e}}}^{\mathrm{e}}, \mathbf{x}_1^{\mathrm{h}}, \ldots, \mathbf{x}_{N_{\mathrm{h}}}^{\mathrm{h}})$, where $\mathbf{x}$ is a compact notation for both the spatial and spin coordinate of the particles. The spin-integrated 2-particle reduced density can be obtained from the electron-hole by integration over the $N_{\mathrm{e}} - 1$ and $N_{\mathrm{h}} - 1$ coordinates as shown in the following equation

$$
\rho_{\mathrm{eh}}(\mathbf{r}_{\mathrm{e}}, \mathbf{r}_{\mathrm{h}}) = \frac{N_{\mathrm{e}} N_{\mathrm{h}}}{\langle \Psi_{\mathrm{eh}} | \Psi_{\mathrm{eh}} \rangle} \int ds_1^{\mathrm{e}} ds_1^{\mathrm{h}} d\mathbf{x}_2^{\mathrm{e}}, \ldots, \mathbf{x}_{N_{\mathrm{e}}}^{\mathrm{e}} \mathbf{x}_2^{\mathrm{h}}, \ldots, \mathbf{x}_{N_{\mathrm{h}}}^{\mathrm{h}} \Psi_{\mathrm{eh}}^* \Psi_{\mathrm{eh}} \tag{2.106}
$$

where, integration over the spin coordinate s_1 is performed for both electron and hole. The single-particle density is obtained from the 2-particle density using the sum-rule condition[280]

$$
\rho_{\mathrm{e}}(\mathbf{r}_{\mathrm{e}}) = \frac{1}{N_{\mathrm{h}}} \int d\mathbf{r}_{\mathrm{h}} \rho_{\mathrm{eh}}(\mathbf{r}_{\mathrm{e}}, \mathbf{r}_{\mathrm{h}}), \tag{2.107}
$$

$$
\rho_{\mathrm{h}}(\mathbf{r}_{\mathrm{h}}) = \frac{1}{N_{\mathrm{e}}} \int d\mathbf{r}_{\mathrm{e}} \rho_{\mathrm{eh}}(\mathbf{r}_{\mathrm{e}}, \mathbf{r}_{\mathrm{h}}). \tag{2.108}
$$

We define the electron-hole cumulant as the difference between the 2-particle density and the product of the 1-particle electron and hole densities as shown in the following equation

$$q(\mathbf{r}_\mathrm{e},\mathbf{r}_\mathrm{h}) = \rho_\mathrm{eh}(\mathbf{r}_\mathrm{e},\mathbf{r}_\mathrm{h}) - \rho_\mathrm{e}(\mathbf{r}_\mathrm{e})\rho_\mathrm{h}(\mathbf{r}_\mathrm{h}). \tag{2.109}$$

This definition is analogous to the definition used by Mazziotti et al.[281] in electronic structure theory. By construction, the cumulant contains information about correlation between the two particles. Consequently, the Coulomb contribution of the electron-hole correlation energy can be directly expressed in terms of the electron-hole cumulant and is given by the following expression

$$\begin{aligned}\langle \Psi_\mathrm{eh}|V_\mathrm{eh}|\Psi_\mathrm{eh}\rangle &= \langle \rho_\mathrm{eh}\varepsilon^{-1}r_\mathrm{eh}^{-1}\rangle \\ &= J_\mathrm{eh} + \langle q(\mathbf{r}_\mathrm{e},\mathbf{r}_\mathrm{h})\varepsilon^{-1}r_\mathrm{eh}^{-1}\rangle,\end{aligned} \tag{2.110}$$

where ε is the dielectric constant and J_eh is the classical Coulomb electron-hole energy

$$J_\mathrm{eh} = \langle \rho_\mathrm{e}\rho_\mathrm{h}\varepsilon^{-1}r_\mathrm{eh}^{-1}\rangle. \tag{2.111}$$

The cumulant has an important property that its integration over all space should be zero due to the density sum-rule conditions[280]

$$\int d\mathbf{r}_\mathrm{e}d\mathbf{r}_\mathrm{h}q(\mathbf{r}_\mathrm{e},\mathbf{r}_\mathrm{h}) = 0. \tag{2.112}$$

We use this relationship for the definition of the electron-hole correlation length.

2.2.5 Electron-hole cumulant in density matrices

The electron-hole cumulant may be expressed in terms of density matrices. The electron-hole reduced density matrix is

$$\Gamma^{\mathrm{eh}}_{ijab} = \langle \Psi | e_i^\dagger e_j h_a^\dagger h_b | \Psi \rangle. \tag{2.113}$$

The single-component electron and hole density matrices are

$$\Gamma^{\mathrm{e}}_{ij} = \langle \Psi | e_i^\dagger e_j | \Psi \rangle, \tag{2.114}$$

$$\Gamma^{\mathrm{h}}_{ab} = \langle \Psi | h_a^\dagger h_j | \Psi \rangle \tag{2.115}$$

The cumulant is then

$$q_{ijab} = \Gamma^{\mathrm{eh}}_{ijab} - \Gamma^{\mathrm{e}}_{ij}\Gamma^{\mathrm{h}}_{ab} \tag{2.116}$$

2.2.6 Intracular and extracular coordinates

Beginning with Coleman's initial definition of the the intracule and extracule matrices in terms of the center of mass (extracule) and relative motion (intracule) coordinates,[282] the concept of the intracule and extracule in the regime of electronic systems has been previously explored in earlier studies.[282, 283, 284, 285, 286, 287, 288] The intracular and extracular coordinates for the

eh-system are defined by

$$\mathbf{r}_{\mathrm{eh}} = \mathbf{r}_{\mathrm{e}} - \mathbf{r}_{\mathrm{h}} \tag{2.117}$$

$$\mathbf{R} = \frac{1}{2}\left(\mathbf{r}_{\mathrm{e}} + \mathbf{r}_{\mathrm{h}}\right). \tag{2.118}$$

The integral of the cumulant is expressed in terms of these coordinates

$$\int d\mathbf{r}_{\mathrm{e}} d\mathbf{r}_{\mathrm{h}} q(\mathbf{r}_{\mathrm{e}}, \mathbf{r}^{\mathrm{h}}) = \int d\mathbf{r}_{\mathrm{eh}} \int d\mathbf{R} q(\mathbf{r}_{\mathrm{eh}}, \mathbf{R}) \tag{2.119}$$

$$= \int_0^\infty dr_{\mathrm{eh}} r_{\mathrm{eh}}^2 \int d\Omega \sin\theta \int d\mathbf{R} q(\mathbf{r}_{\mathrm{eh}}, \mathbf{R}) \tag{2.120}$$

$$= \int_0^\infty dr_{\mathrm{eh}} r_{\mathrm{eh}}^2 q_{\mathrm{r}}(r_{\mathrm{eh}}) \tag{2.121}$$

In the above expression, the integral over the intracular coordinate $\mathbf{r}_{\mathrm{eh}}$ is transformed into spherical polar coordinates. The function q_r is the spherically averaged radial cumulant and the integral of the radial cumulant over a finite limit is used to define the following function $I(d)$

$$I(d) = \int_0^d dr_{\mathrm{eh}} r_{\mathrm{eh}}^2 q_r(r_{\mathrm{eh}}). \tag{2.122}$$

The zero-integral property of q (defined in Eq. (2.112)) ensures that this integral goes to zero at large d

$$\lim_{d\to\infty} I(d) = 0. \tag{2.123}$$

Here, we use $I(d)$ to define the electron-hole correlation length. Specifically, the electron-hole correlation length (r_c) is defined as the value of d at which the value of $I(d)$ is zero

$$|I(r_c)| = 0 \qquad r_c << \infty. \tag{2.124}$$

The description of the electron-hole wave function used for the calculation of the radial cumulant is presented in the following section.

2.2.7 Explicitly correlated electron-hole wave function

We have used the electron-hole explicitly correlated Hartree-Fock method (eh-XCHF) for obtaining the electron-hole wave function. This method has been used in earlier work for the computation of exciton binding energies and electron-hole recombination probabilities in quantum dots.[40, 215, 216, 217, 218] A brief summary of the eh-XCHF method is presented here and the implementation details of this method can be found in work by Elward and co-workers.[216, 217, 218] The ansatz of the eh-XCHF wave function consists of multiplying the mean-field electron-hole reference wave functions with an explicitly correlated function G as shown in the following equation

$$\Psi_{\mathrm{eh-XCHF}} = G\Phi_e\Phi_h, \tag{2.125}$$

where G is the geminal operator

$$G = \sum_{i=1}^{N_e}\sum_{j=1}^{N_h} g(r_{ij}), \tag{2.126}$$

$$g(r_{\mathrm{eh}}) = \sum_{k=1}^{N_{\mathrm{g}}} b_k \exp(-\gamma_k r_{\mathrm{eh}}^2). \tag{2.127}$$

The eh-XCHF method is a variational method in which the correlation function G and the reference wave function are obtained by minimizing the total energy

$$E_{\mathrm{eh-XCHF}} = \min_{G,\Phi_{\mathrm{e}},\Phi_{\mathrm{h}}} \frac{\langle G\Phi_0|H|G\Phi_0\rangle}{\langle G\Phi_0|G\Phi_0\rangle}, \tag{2.128}$$

where $\Phi_0 = \Phi_{\mathrm{e}}\Phi_{\mathrm{h}}$. To perform the above minimization, it is more efficient to work with the following congruent-transformed operators

$$\tilde{H} = G^{\dagger}HG, \tag{2.129}$$

$$\tilde{1} = G^{\dagger}G. \tag{2.130}$$

This transformation is particularly important for the calculation of the 2-particle reduced density matrix in the present work. The set of parameters $\{b_k, \gamma_k\}$ in G were obtained by non-linear optimization, and for a given set of these parameters, the minimization over the reference wave function was performed by determining the self-consistent solution of the coupled Fock equations

$$\tilde{\mathbf{F}}_{\mathrm{e}}\mathbf{C}_{\mathrm{e}} = \tilde{\mathbf{S}}_{\mathrm{e}}\mathbf{C}_{\mathrm{e}}\lambda_{\mathrm{e}}, \tag{2.131}$$

$$\tilde{\mathbf{F}}_{\mathrm{h}}\mathbf{C}_{\mathrm{h}} = \tilde{\mathbf{S}}_{\mathrm{h}}\mathbf{C}_{\mathrm{h}}\lambda_{\mathrm{h}}. \tag{2.132}$$

The tilde in the above expressions represent that the Fock and the overlap matrices incorporate the transformed operators defined in Eq. (2.129).

The transformed operator $\tilde{1}$ can be written as a sum of operators as shown below

$$\tilde{1} = G^{\dagger}G \tag{2.133}$$

$$= \sum_{ii'} g(i,i') \sum_{jj'} g(j,j') \quad (i,j = 1,\ldots,N_{\mathrm{e}}; i',j' = 1,\ldots,N_{\mathrm{h}}) \tag{2.134}$$

$$= \sum_{ii'} g(i,i')g(i,i') + \sum_{i\neq j,i'} g(i,i')g(j,i') \tag{2.135}$$

$$+ \sum_{i'\neq j',i} g(i,i')g(i,j') + \sum_{i\neq j,i'\neq j'} g(i,i')g(j,j').$$

The above expression can be written in a compact notation as a sum of 2, 3, and 4-particle operators

$$G^{\dagger}G = \Omega_{11} + \Omega_{21} + \Omega_{12} + \Omega_{22}. \tag{2.136}$$

The 2-particle density for the eh-XCHF wave function can be expressed in terms of these operators as shown below

$$\rho_{\mathrm{eh}}(\mathbf{r}_{\mathrm{e}},\mathbf{r}_{\mathrm{h}}) = \frac{N_{\mathrm{e}}N_{\mathrm{h}}}{\langle \Psi_{\mathrm{eh-XCHF}} | \Psi_{\mathrm{eh-XCHF}} \rangle} \times \langle \Psi^{*}_{\mathrm{eh-XCHF}} \Psi_{\mathrm{eh-XCHF}} \rangle_{s_1,s'_1,2,2',\ldots,N_{\mathrm{e}},N_{\mathrm{h}}}, \tag{2.137}$$

where the subscript in the above expression is a compact notation for integration over the remaining coordinates described in Eq. (2.106). Substituting the expression from Eq. (2.136), we get the following expression

$$\rho_{\mathrm{eh}}(\mathbf{r}_{\mathrm{e}},\mathbf{r}_{\mathrm{h}}) = \frac{N_{\mathrm{e}}N_{\mathrm{h}}}{\langle \Phi_0 | \tilde{1} | \Phi_0 \rangle} \tag{2.138}$$

$$\times \langle \Phi_0^*(\Omega_{11}+\Omega_{12}+\Omega_{21}+\Omega_{22})\Phi_0\rangle_{s_1,s_1',2,2',\ldots,N_\mathrm{e},N_\mathrm{h}}.$$

For a multiexcitonic system all 2, 3, and 4-particle operators should be used for the computation of the 2-particle density. In a related work on many-electron system, we have shown that it is possible to avoid integration over higher-order operators by using the diagrammatic summation technique and a similar strategy can be used for multiexcitonic systems as well.[289]

2.2.8 Relation to uncorrelated transition density matrices

One of the important features of the correlation function is that it allows for a compact representation of the 2-particle density matrix in the position representation. The relationship can be readily seen by expanding the eh-XCHF wave function in the Slater determinant basis

$$G\Phi_0 = \sum_{ii'}^{\infty} \underbrace{\langle \Phi_i^\mathrm{e}\Phi_{i'}^\mathrm{h}|G|\Phi_0^\mathrm{e}\Phi_0^\mathrm{h}\rangle}_{c_{ii'}} \Phi_i^\mathrm{e}\Phi_{i'}^\mathrm{h} = \sum_{ii'}^{\infty} c_{ii'}\Phi_i^\mathrm{e}\Phi_{i'}^\mathrm{h}. \tag{2.139}$$

Substituting Eq. (2.139) in the expression of ρ_eh gives

$$\begin{aligned}\rho_\mathrm{eh}(\mathbf{r}_\mathrm{e},\mathbf{r}_\mathrm{h}) &= \frac{N_\mathrm{e}N_\mathrm{h}}{\langle\Phi_0|\tilde{1}|\Phi_0\rangle} \qquad (2.140)\\ &\quad\times \langle \sum_{ij}^{\infty}\sum_{i'j'}^{\infty} c_{ii'}^* c_{jj'}\Phi_i^{\mathrm{e}*}\Phi_{i'}^{\mathrm{h}*}\Phi_j^\mathrm{e}\Phi_{j'}^\mathrm{h}\rangle_{s_1,s_1',2,2',\ldots,N_\mathrm{e},N_\mathrm{h}}\\ &= \frac{N_\mathrm{e}N_\mathrm{h}}{\langle\Phi_0|\tilde{1}|\Phi_0\rangle}\sum_{ij}^{\infty}\sum_{i'j'}^{\infty} c_{ii'}^* c_{jj'} d_{ij}^\mathrm{e} d_{i'j'}^\mathrm{h}, \qquad (2.141)\end{aligned}$$

where the transition density matrix d_{ij} is defined as

$$d^{\mathrm{e}}_{ij}(\mathbf{r}_{\mathrm{e}}) = \langle \Phi^{\mathrm{e}*}_i \Phi^{\mathrm{e}}_j \rangle_{s_1,2,\ldots,N_{\mathrm{e}}}. \tag{2.142}$$

It is seen from Eq. (2.140) that the 2-particle density obtained from the eh-XCHF wave function is equivalent to the infinite-order expansion in terms of the transition density matrices.

2.2.9 Determination of geminal coefficient using Gaussian trial wave function

In general, the determination of the correlation length is a computationally intensive process, however, the expression for the radial cumulant can be derived for a model trial Gaussian wave function. This derivation is important because it give useful insight into the inter-relationship between the correlation length r_{c} and the geminal parameters. In subsection 2.4.2, the result from this derivation is used for construction of eh-XCHF wave function.

The model trial wave function consist of only one set of optimizable geminal parameters and is defined as

$$\Psi_{\mathrm{T}}(\mathbf{r}_{\mathrm{e}}, \mathbf{r}_{\mathrm{h}}) = (1 + be^{-\gamma r^2_{\mathrm{eh}}}) e^{-\alpha_{\mathrm{e}} r^2_{\mathrm{e}}} e^{-\alpha_{\mathrm{h}} r^2_{\mathrm{h}}}, \tag{2.143}$$

where, the electron and hole are represented by a single Gaussian basis function. The normalization can be expressed as polynomial in b and is given by the following expression Setting

$$\langle \Psi_{\mathrm{T}} | \Psi_{\mathrm{T}} \rangle = d_0 + d_1 b + d_2 b^2, \tag{2.144}$$

where the terms

$$d_0 = \left(\frac{\pi}{2\alpha_e}\right)^{\frac{3}{2}} \left(\frac{\pi}{2\alpha_h}\right)^{\frac{3}{2}} \tag{2.145}$$

$$d_1 = \left(\frac{\pi}{\sqrt{2}\sqrt{2\alpha_e+\gamma}\sqrt{\frac{\alpha_e\gamma}{2\alpha_e+\gamma}+\alpha_h}}\right)^3 \tag{2.146}$$

$$d_2 = \left(\frac{\pi}{2\sqrt{\alpha_e+\gamma}\sqrt{\frac{\alpha_e\gamma}{\alpha_e+\gamma}+\alpha_h}}\right)^3 \tag{2.147}$$

The two-particle density is given as

$$\rho_2(\mathbf{r}_e,\mathbf{r}_h) = \frac{\Psi_T^2}{\langle\Psi_T|\Psi_T\rangle} \tag{2.148}$$

$$= \frac{1}{\langle\Psi_T|\Psi_T\rangle}(1+2be^{-\gamma r_{eh}^2}+b^2e^{-2\gamma r_{eh}^2})e^{-2\alpha_e r_e^2}e^{-2\alpha_h r_h^2}. \tag{2.149}$$

The 1-particle for the electron density ρ_e is obtained by integrating over the hole coordinates. For the above equation, the expression ρ_e can be expressed as a sum of three Gaussian functions

$$\rho_e(\mathbf{r}) = \frac{1}{\langle\Psi_T|\Psi_T\rangle}e^{-2\alpha_e r^2}(c_0+2c_1be^{-p_1r^2}+c_2b^2e^{-p_2r^2}) \tag{2.150}$$

$$= \frac{1}{\langle\Psi_T|\Psi_T\rangle}e^{-2\alpha_e r^2}\sum_{n=0}^{2} b^n f_n(r) \tag{2.151}$$

where the coefficients are given as

$$c_0 = \left(\frac{\pi}{2\alpha_h}\right)^{3/2} \tag{2.152}$$

$$c_1 = 2\left(\frac{\pi}{2\alpha_h+\gamma}\right)^{3/2} \tag{2.153}$$

$$c_2 = \left(\frac{\pi}{2\alpha_h + 2\gamma}\right)^{3/2} \tag{2.154}$$

$$p_0 = 0 \tag{2.155}$$

$$p_1 = \frac{2\alpha_h\gamma}{2\alpha_h + \gamma} \tag{2.156}$$

$$p_2 = \frac{4\alpha_h\gamma}{2\alpha_h + 2\gamma} \tag{2.157}$$

Combining Eq. (2.149) and (2.151), the cumulant is given by the following equation

$$q(\mathbf{r}_e, \mathbf{r}_h) = \frac{1}{\langle\Psi_T|\Psi_T\rangle} e^{-2\alpha_e r_e^2} e^{-2\alpha_h r_h^2} \left[(1 + 2be^{-\gamma r_{eh}^2} + b^2 e^{-2\gamma r_{eh}^2}) - \frac{1}{\langle\Psi_T|\Psi_T\rangle} \sum_{i,j=0}^{2} b^i b^j f_i(r_e) f_j(r_h)\right] \tag{2.158}$$

$$= \frac{1}{\langle\Psi_T|\Psi_T\rangle^2} e^{-2\alpha_e r_e^2} e^{-2\alpha_h r_h^2} \left[\langle\Psi_T|\Psi_T\rangle(1 + 2be^{-\gamma r_{eh}^2} + b^2 e^{-2\gamma r_{eh}^2}) - \sum_{i,j=0}^{2} b^i b^j f_i(r_e) f_j(r_h)\right] \tag{2.159}$$

To simplify the subsequent step, we evaluate the cumulant at $\mathbf{r}_e = 0$ and perform integration over the hole coordinates as shown in the following expression

$$\int_0^{r_c} dr r^2 \int d\Omega q(0, \mathbf{r}) = 0 \tag{2.160}$$

Preforming the radial integration using the integration rule

$$I(\alpha, r_c) = \int_0^{r_c} r^2 e^{-\alpha r^2} dr \tag{2.161}$$

$$= \frac{\sqrt{\pi}}{4\sqrt{\alpha^3}} \mathrm{Erf}[r_c\sqrt{\alpha}] - \frac{r_c}{2\alpha} e^{-\alpha r_c^2}, \tag{2.162}$$

and substituting the Eq. (2.144) in Eq. (2.160), we get the following equations that relates the geminal parameters with the correlation length.

$$(I(2\alpha_{\mathrm{h}}, r_{\mathrm{c}}) + 2bI(\gamma + 2\alpha_{\mathrm{h}}), r_{\mathrm{c}}) + b^2 I(2(\gamma + \alpha_{\mathrm{h}}), r_{\mathrm{c}}))(d_0 + d_1 b + d_2 b^2) \tag{2.163}$$

$$-(c_0^{\mathrm{e}} + bc_1^{\mathrm{e}} + b^2 c_2^{\mathrm{e}})(c_0^{\mathrm{h}} I(2\alpha_{\mathrm{h}}, r_{\mathrm{c}}) + c_1^{\mathrm{h}} bI(p_1 + 2\alpha_{\mathrm{h}}, r_{\mathrm{c}}) + c_2^{\mathrm{h}} b^2 I(p_2 + 2\alpha_{\mathrm{h}}, r_{\mathrm{c}})) = 0$$

We have used this relationship to obtain geminal parameters using correlation length and the details are provided in subsection 2.4.2.

2.3 Computational method

The method described in subsection 2.2.6 was used for calculating electron-hole correlation length in CdSe quantum dots in the range of 1-20 nm in diameter. We are interested in the effect of dot size on the electron-hole correlation length for a single electron-hole pair in CdSe quantum dots. For a single electron-hole pair, the higher-order operators in Eq. (2.138) rigorously vanish from the expression. This provides considerable simplification in the calculation of the 2-particle density. Because of the dot size, application of either DFT or atom-centered pseudopotential approach is computationally prohibitive. To make the computation tractable, we have used a parabolic confining potential in the electron-hole Hamiltonian described in Eq. (2.105). Parabolic confinement potential in quantum dots has been used extensively for various properties such as total exciton energy[270, 290], exciton dissociation[291], exciton binding energy[215, 216, 218, 292] eh-recombination probability[215, 216, 217], effect of magnetic[107, 293, 294, 295, 296, 297] and electric fields[2, 19, 40, 107, 298], exciton-polariton condensate[299], linear optical properties[300, 301], optical rectification[302], non-linear rectification[2], dynamics[303],

eh-correlation energy[304, 305], resonant tunneling[306], collective modes[307], and thermodynamic properties[308]. The external potential for the electron and hole quasiparticle was defined as

$$v_{\alpha}^{\text{ext}} = \frac{1}{2} k_{\alpha} |\mathbf{r}_{\alpha}|^2 \quad \alpha = \text{e}, \text{h} \tag{2.164}$$

where k_{α} is the force constant which determines the strength of the confinement potential. We have used a particle-number based search procedure for determination of the force constant k_{α}. The central idea of this approach is to find the value of k_{α} such that the computed 1-particle electron and hole densities are confined within the volume of the quantum dot. This is obtained by performing the following minimization

$$\min_{k_{\alpha}^{\min}} \left(N_{\alpha} - \int_{0}^{\frac{D_{\text{dot}}}{2}} dr r^2 \int d\Omega \rho_{\alpha}(\mathbf{r}) \right)^2, \tag{2.165}$$

where D_{dot} is the diameter of the quantum dot and Ω is the angular coordinate. The values of the force constants used for each dot are listed in Table 2.1. The kinetic energy operator was computed using the electron and hole effective masses of 0.13 and 0.38 atomic units, respectively.[253] The interaction between the electrons and hole was described by screened Coulomb potential. We have used the size and distance dependent dielectric function $\varepsilon(\mathbf{r}, R_{\text{dot}})$, which was developed by Wang and Zunger for CdSe.[309] The electron and hole molecular orbitals in Φ_0 were represented using a linear combination of Gaussian type orbitals (GTOs) and the expansion coefficients were obtained by the solving the coupled Fock equations shown in Eq. (2.131). The basis used was a single S Cartesian GTO was used and the exponents of the basis functions are listed in Table 2.2. The

Table 2.1: Force constants for CdSe quantum dots.

Dot diameter (nm)	k_e (atomic units)	k_h (atomic units)
1.24	2.66×10^{-2}	9.10×10^{-3}
1.79	6.22×10^{-3}	2.13×10^{-3}
2.76	1.10×10^{-3}	3.76×10^{-4}
2.98	8.10×10^{-4}	2.77×10^{-4}
3.28	5.52×10^{-4}	1.89×10^{-4}
3.79	3.09×10^{-4}	1.06×10^{-4}
4.80	1.20×10^{-4}	4.12×10^{-5}
5.00	1.02×10^{-4}	3.51×10^{-5}
6.60	3.40×10^{-5}	1.16×10^{-5}
10.00	6.41×10^{-6}	2.19×10^{-6}
15.00	1.26×10^{-6}	4.33×10^{-7}
20.00	4.01×10^{-7}	1.37×10^{-7}

use of GTOs is especially convenient because the integrals involving the GTOs and the Gaussian correlation function, G, are known analytically.[310, 311, 312, 313] For a given value of $\mathbf{r}^e$, the 1-particle density ρ was calculated analytically. The integration over the intracular coordinate in Eq. (2.122) was performed numerically. The correlation function, G, was expanded as a linear combination of six Guassian-type geminal functions[215, 216, 218] and the set of $\{b_k, \gamma_k\}$ parameters were optimized for each dot size. The first set of geminal parameters was set to $b_1 = 1$ and $\gamma_1 = 0$ for all CdSe dot diameters. For each dot diameter, five sets of geminal parameters were determined sequentially by minimizing the energy. The values of the geminal parameters are found in Table 3.3.

Table 2.2: Exponent used in GTO basis $e^{-\alpha r^2}$.

Dot diameter (nm)	α (atomic units)
1.24	2.94×10^{-2}
1.78	1.42×10^{-2}
2.76	5.98×10^{-2}
2.98	5.13×10^{-2}
3.28	4.24×10^{-3}
3.79	3.17×10^{-3}
4.80	1.98×10^{-3}
5.00	1.83×10^{-3}
6.60	1.05×10^{-3}
10.00	4.57×10^{-4}
15.00	2.03×10^{-4}
20.00	1.14×10^{-4}

2.4 Results

2.4.1 Calculation of electron-hole correlation length

The electron-hole correlation length was obtained by integration of the radial cumulant as described in Eq. (2.122). In Figure 2.3, the integral of the cumulant, $I(d)$, for three different dot sizes is presented. As expected, the integral goes to zero at large distances (high d values) and the distance at which the integral converges to zero is defined as the electron-hole correlation length r_c. The determination of an analytic form for the cumulant in Eq. (2.158) has allowed the plotting of the cumulant for as function of the magnitudes of the length of $\mathbf{r}_e$ and $\mathbf{r}_h$ and may be seen in Figure 2.4, Figure 2.5, and Figure 2.6. In each case, there is a relatively small region with maximum enhancement (positive value of the cumulant) with a correponding region of maximum reduction.

The calculated electron-hole correlation lengths are presented in Table 2.4. We find that, in all cases, the correlation length increases with increasing dot diameter. Another quantity that

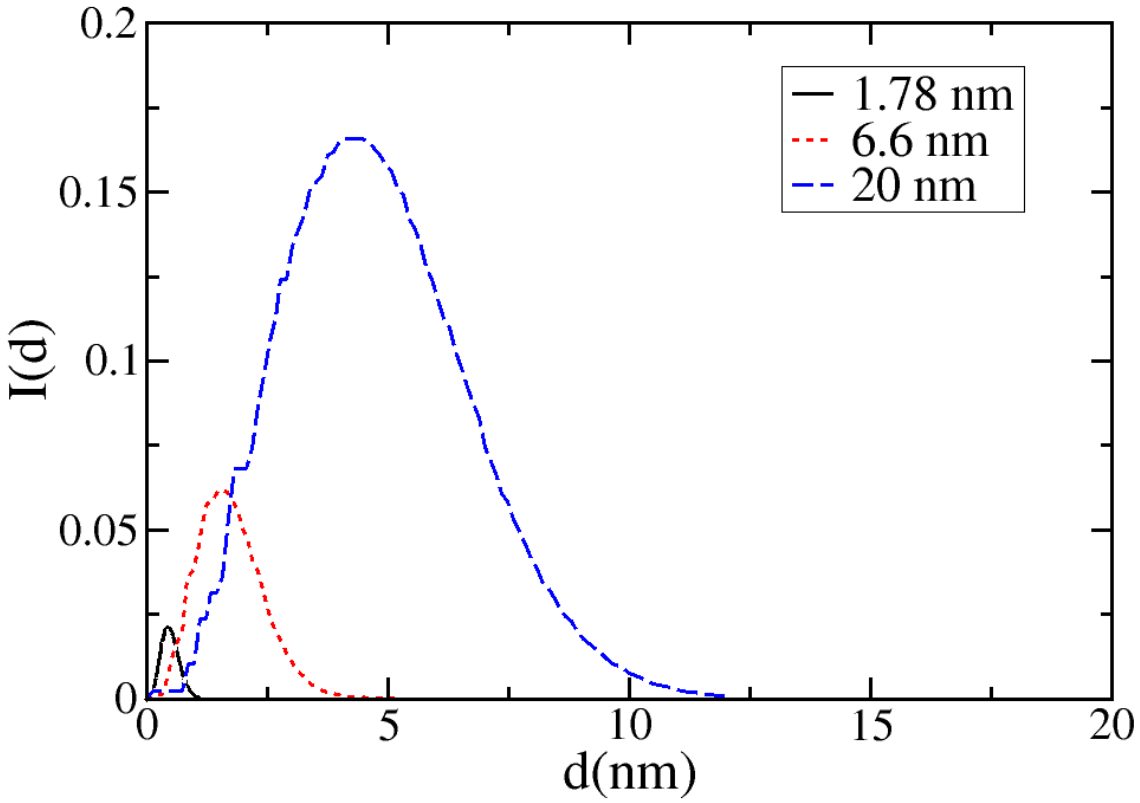

Figure 2.3: The value of $I(d)$ as d, the upper limit in Eq. (2.122), is varied for the 1.78 nm, 6.6 nm, and 20 nm diameter CdSe quantum dots.

is important for investigating electron-hole correlation is the the length scale associated with the first node of the radial cumulant. We define this quantity as r_{node} and the calculated values are presented in Table 2.4. The maximum of the $I(d)$ in Figure 2.3 corresponds to r_{node}. Because the interaction between the electron and hole is attractive, we expect an enhancement in the pair density as compared to mean-field density at small r_{eh} distances. This phenomenon is opposite to the correlation hole observed in electron-electron interaction, in which small r_{ee} shows a decrease in correlated electron-pair density as compared to uncorrelated electron density. The r_{node} can be

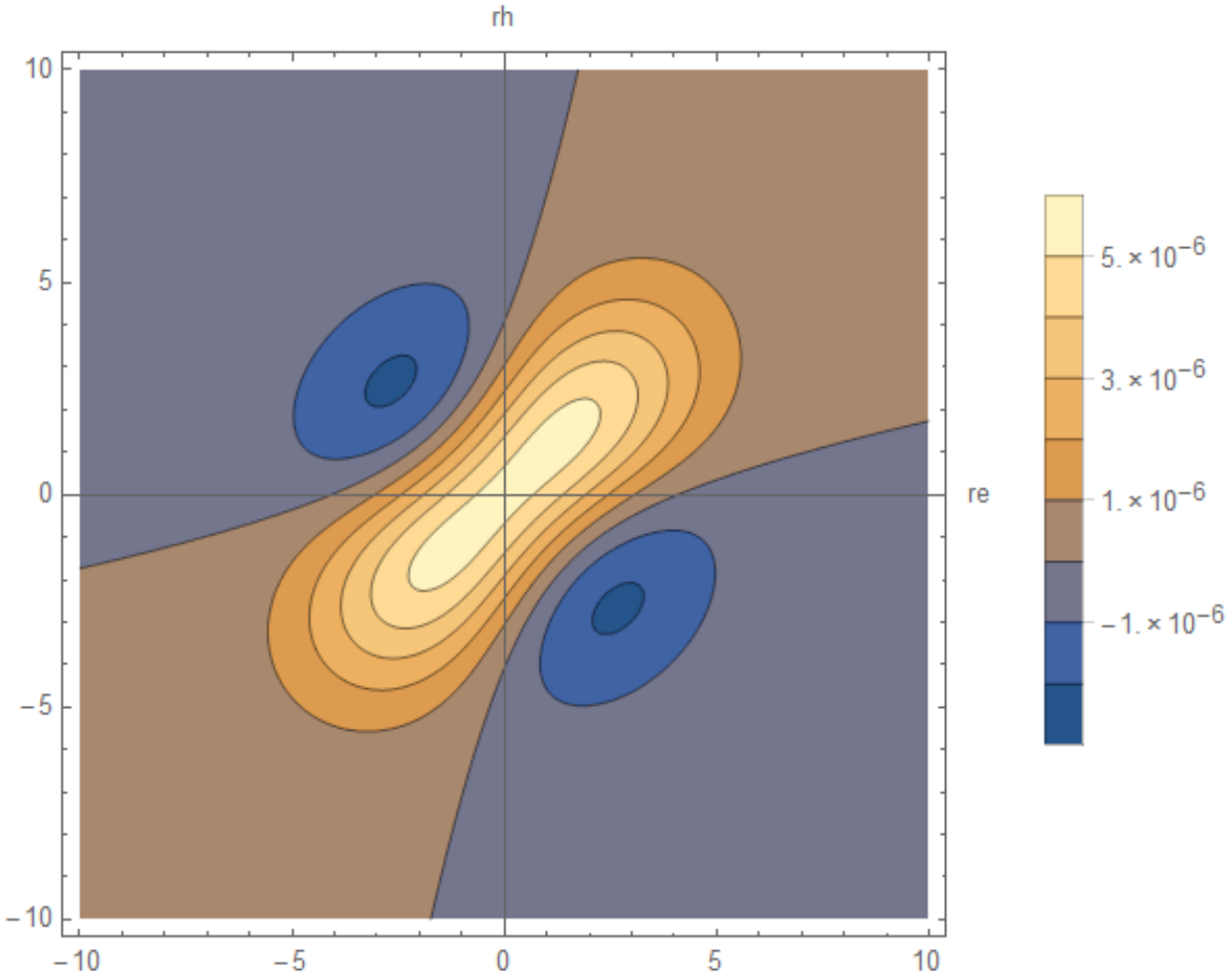

Figure 2.4: The cumulant for the 1.24 nm CdSe quantum dot plotted using the analytic expression in Eq. (2.158). The axes are in atomic units.

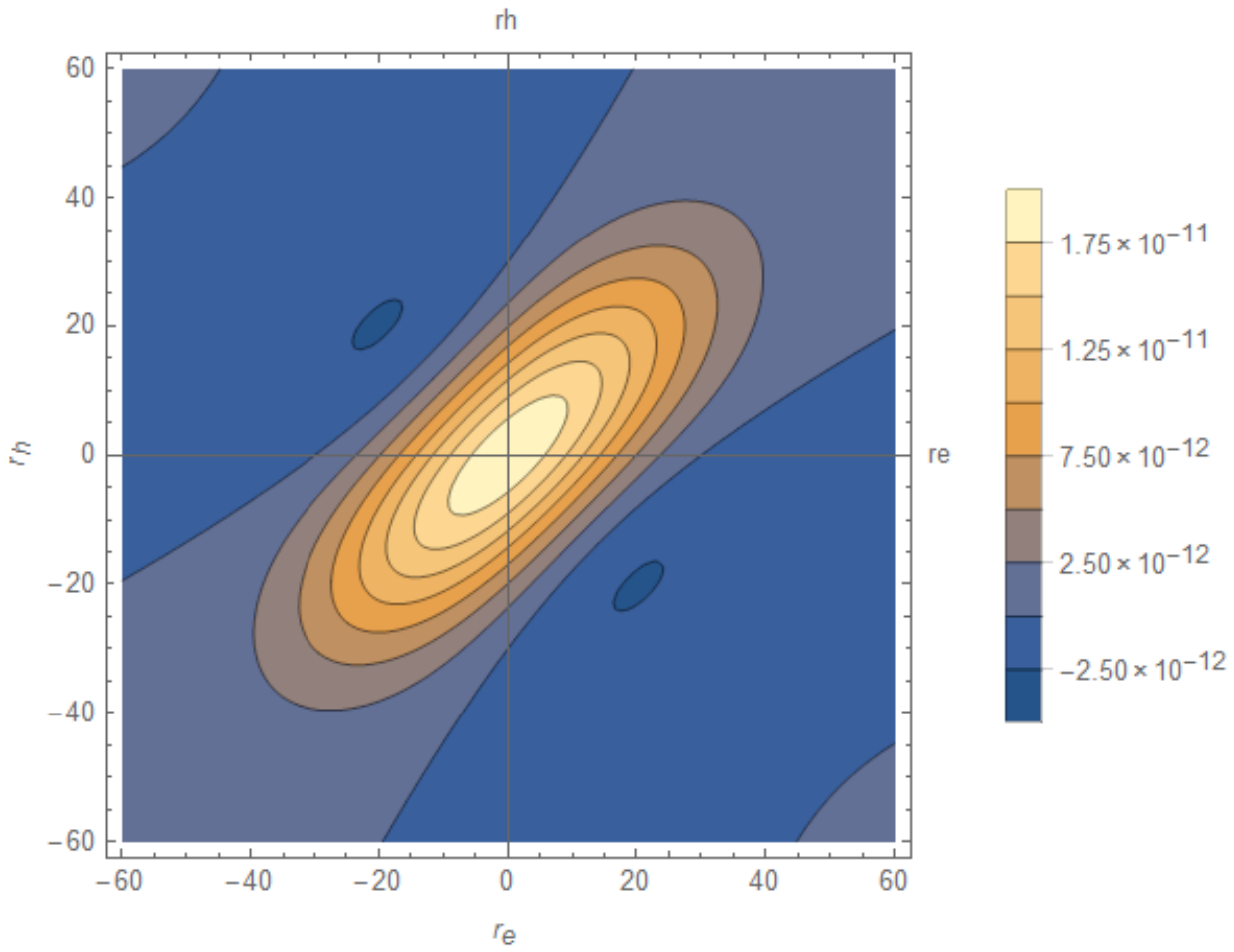

Figure 2.5: The cumulant for the 10 nm CdSe quantum dot plotted using the analytic expression in Eq. (2.158). The axes are in atomic units.

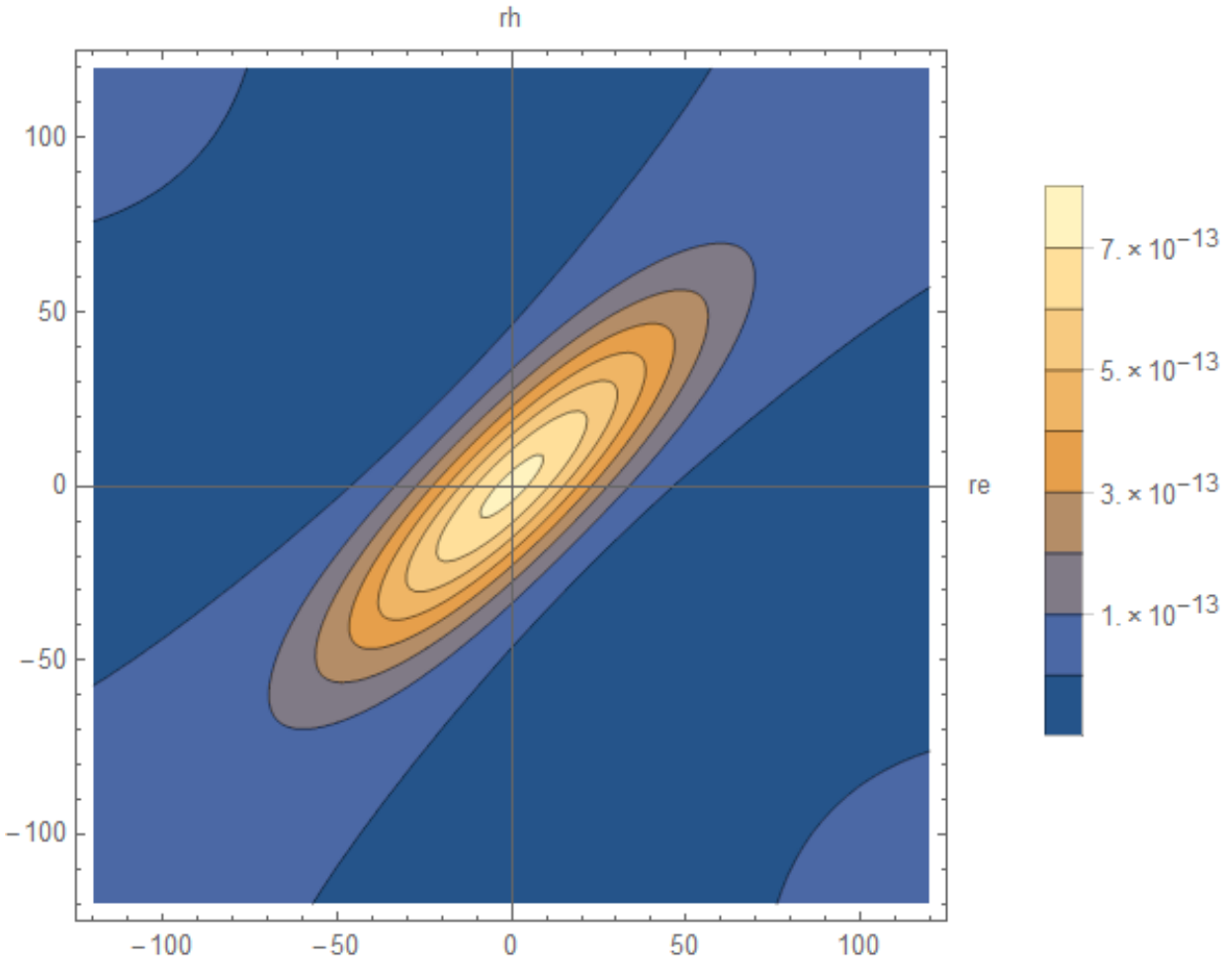

Figure 2.6: The cumulant for the 20 nm CdSe quantum dot plotted using the analytic expression in Eq. (2.158). The axes are in atomic units.

interpreted as the effective radius of the sphere that encloses the region of enhanced probability density. As seen from Table 2.4, r_c and r_{node} are similar in magnitude for small dot sizes, but these quantities differ significantly for larger dots.

2.4.2 Construction of eh-XCHF wave function without geminal optimization

The optimization of the geminal parameters in the eh-XCHF method is computationally intensive process. Therefore, determination of geminal parameters that do not require energy minimization step can significantly reduce the overall computational cost. In this work, we have used a correlation-length based approach to obtain the geminal coefficient. The central idea of this approach is to use obtain approximate correlation lengths for different dot sizes by interpolation and then use the relationship between correlation length and geminal parameters given in Eq. (2.163), to obtain the corresponding $\{b, \gamma\}$ values. From the range of dot size 1-20 nm, we have selected three dots with diameters 1.24 nm, 10 nm, and 20 nm for interpolation. The geminal parameters for these three dots were obtained by minimizing the eh-XCHF energy and the correlation lengths were obtained from the eh-XCHF wave functions. For the remaining dots in the set, the correlation lengths were determined by linear interpolation between the computed correlation lengths. In the next step, the interpolated correlation lengths in Eq. (2.163) and was used to obtain the geminal parameters for the remaining dots by solving the equation numerically. The quality of the geminal parameters obtained using the correlation length based and energy minimized based methods were analyzed by comparing the exciton binding energies obtained using the two methods and the results are presented in Table 2.5. The exciton binding energies calculated using the correlation length method were found to be in good agreement with the energy-minimized results. These

results show that correlation length based eh-XCHF wave function can deliver accurate exciton binding energies at reduced computational cost.

2.5 Conclusion

In conclusion, we have presented a method for calculating electron-hole correlation length in semiconductor quantum dots. We have used the cumulant derived from the electron-hole 2-particle density as the central quantity for defining the correlation length. There are two key features of this method. First, the 2-particle reduced density was obtained from an explicitly correlated electron-hole wave function. Consequently, the reduced density matrix and the corresponding cumulant were explicit functions of the electron-hole separation distance. Second, the calculation of the correlation length was not based on the nodes of the cumulant but was derived from the exact sum rule relationship satisfied by all N-representable cumulants. The developed method was used for calculation of electron-hole correlation length for a series of CdSe quantum dots. The analytical relationship between the correlation length and the geminal parameters were derived and the equation was numerically inverted to obtain geminal parameters for a given correlation length. The results from this study show that correlation-length based explicitly correlated wave functions can give results that are comparable to the energy-minimized wave functions at a reduced computational cost.

The electron-hole correlation length provides a natural length scale for investigating electron-hole correlation in nanoparticles. We envision that in future work, the electron-hole correlation length will be used in the construction of compact explicitly correlated wave functions and also for developing multi-component electron-hole density functionals. [219]

Table 2.3: Value of the geminal parameters for CdSe quantum dots.

Diameter (nm)	b_2	γ_2	b_3	γ_3	b_4	γ_4	b_5	γ_5	b_6	γ_6
1.25	1.338×10^{-1}	2.134×10^{-2}	1.559×10^{-1}	1.150×10^{-3}	3.630×10^{-2}	1.112×10^{0}	2.290×10^{-2}	2.111×10^{-1}	1.099×10^{-1}	1.020×10^{-3}
1.78	1.497×10^{-1}	1.569×10^{-2}	2.099×10^{-1}	1.120×10^{-3}	2.009×10^{-1}	4.400×10^{-4}	4.260×10^{-2}	1.112×10^{0}	3.820×10^{-2}	1.444×10^{-1}
2.76	2.279×10^{-1}	4.700×10^{-3}	5.990×10^{-2}	1.111×10^{-1}	2.119×10^{-1}	4.400×10^{-4}	-1.910×10^{-2}	3.140×10^{-3}	1.540×10^{-2}	1.222×10^{0}
2.98	2.449×10^{-1}	3.960×10^{-3}	6.400×10^{-2}	1.114×10^{-1}	2.099×10^{-1}	3.700×10^{-4}	1.490×10^{-2}	1.434×10^{0}	1.580×10^{-2}	1.012×10^{-1}
3.28	2.589×10^{-1}	3.580×10^{-3}	6.680×10^{-2}	1.112×10^{-1}	2.109×10^{-1}	4.300×10^{-4}	9.990×10^{-2}	1.100×10^{-4}	1.590×10^{-2}	1.253×10^{0}
3.79	2.799×10^{-1}	3.000×10^{-3}	6.990×10^{-2}	1.111×10^{-1}	2.209×10^{-1}	3.700×10^{-4}	1.099×10^{-1}	1.200×10^{-4}	1.540×10^{-2}	1.432×10^{0}
4.80	3.610×10^{-1}	1.660×10^{-3}	8.790×10^{-2}	1.010×10^{-1}	6.180×10^{-2}	2.229×10^{-2}	2.099×10^{-1}	2.200×10^{-4}	9.990×10^{-2}	1.100×10^{-4}
5.00	3.699×10^{-1}	1.570×10^{-3}	8.990×10^{-2}	1.010×10^{-1}	6.680×10^{-2}	2.135×10^{-2}	2.099×10^{-1}	2.200×10^{-4}	9.990×10^{-2}	1.100×10^{-4}
6.60	4.499×10^{-1}	1.380×10^{-3}	6.099×10^{-1}	1.800×10^{-4}	5.280×10^{-2}	1.112×10^{0}	1.299×10^{-1}	1.011×10^{-1}	1.331×10^{-1}	1.335×10^{-2}
10.00	5.899×10^{-1}	1.240×10^{-3}	9.999×10^{-1}	1.300×10^{-4}	6.400×10^{-2}	1.012×10^{0}	1.569×10^{-1}	1.023×10^{-1}	1.799×10^{-1}	1.211×10^{-2}
15.00	6.999×10^{-1}	1.040×10^{-3}	1.110×10^{0}	1.300×10^{-4}	6.580×10^{-2}	1.102×10^{0}	1.589×10^{-1}	1.022×10^{-1}	1.999×10^{-1}	1.999×10^{-1}
20.00	7.999×10^{-1}	1.030×10^{-3}	2.000×10^{0}	1.200×10^{-4}	9.999×10^{-1}	4.000×10^{-5}	5.489×10^{-1}	1.227×10^{-2}	2.899×10^{-1}	1.240×10^{-3}

Table 2.4: Electron-hole correlation lengths and r_{node} for CdSe quantum dots.

Dot Diameter (nm)	Correlation length (nm)	r_{node} (nm)
1.24	0.381	0.283
1.78	0.683	0.431
2.76	1.905	0.595
2.98	2.117	0.653
3.28	2.572	0.732
3.79	2.778	0.833
4.80	3.293	1.082
5.00	3.307	1.124
6.60	4.047	1.653
10.00	6.156	2.749
15.00	10.164	3.257
20.00	11.930	4.733

Table 2.5: Exciton binding energies calculated using energy-minimized and correlation-length based Gaussian-type geminal G function.

Dot Diameter (nm)	Energy-minimized based G (eV)	Correlation-length based G (eV)
1.24	1.260	1.259
1.78	0.759	0.752
2.76	0.430	0.426
2.98	0.391	0.387
3.28	0.347	0.342
3.79	0.290	0.285
4.80	0.219	0.212
5.00	0.209	0.202
6.60	0.151	0.144
10.00	0.095	0.092
15.00	0.061	0.052
20.00	0.046	0.042

Chapter 3: Development of polaron-transformed explicitly correlated full configuration interaction method for investigation of quantum-confined Stark effect in GaAs quantum dots

3.1 Introduction

3.1.1 Background

The influence of an external electric field on optical properties of semiconductors has been studied extensively using both experimental and theoretical techniques. In bulk semiconductors the shift in the optical absorbing due to the external field is known as the Franz-Keldysh effect.[91, 92] In quantum wells and quantum dots, application of electric field has shown to modify the optical properties of nanosystems and is known as the quantum-confined Stark effect (QCSE).[93, 94] The application of the external field induces various modifications in the optical properties of the nanomaterial including, absorption coefficient, spectral weight of transitions, and change in λ_{max} of the absorption spectra. In certain cases, the applied field can lead to exciton ionization.[95] The quantum-confined Stark effect has found application in the field of electro-absorption modulators,[96] solar cells,[97] and light-emitting devices.[98] Recent experiments by Weiss et al. on semiconductor quantum dots have shown that the QCSE can also be enhanced by the presence of heterojunctions.[39] In some cases, the QCSE can be induced chem-

ically by proximity to ligands.[97] The QCSE also plays a major role in electric field dependent photoconductivity in CdS nanowires and nanobelts. [99] Application of electric field has emerged as one of the tools to control and customize quantum dots as novel light sources. In a recent study, electric field was used in generation and control of polarization-entangled photons using gallium arsenide (GaAs) quantum dots.[100] It has been shown that the coupling between stacked quantum dots can be modified using electric field. [101] The QCSE has been investigated using various theoretical techniques including perturbation theory,[19, 107, 108, 109, 110, 111] variational techniques,[112, 113, 114, 115, 116, 117, 118] and configuration interaction method.[119, 120, 121, 122, 123, 124, 125, 126, 127, 128, 129] In the present work, development of explicitly correlated full configuration interaction (XCFCI) method is presented for investigating the effect of an external electric field on quantum dots and wells. The XCFCI method is a variational method in which the conventional CI wave function is augmented by explicitly correlated Gaussian-type geminal functions.[312] The inclusion of explicitly correlated function in the form of the wave function is important for the following two reasons. First, the addition of the geminal function increases the convergence of the FCI energy with respect to the size of the underlying 1-particle basis set.[314] Second, inclusion of explicitly correlated function improves the form of the electron-hole (eh) wave function at small inter-particle distances which is important for accurate calculation of electron-hole recombination probability. [210, 218, 253] The effect of explicitly correlated function on the convergence of CI energy has been investigated by Prendergast et al. and is directly related to accurate treatment of the Coulomb singularity in the Hamiltonian. [314, 315, 316] Varganov et al. have also demonstrated the applicability of geminal augmented multiconfiguration self-consistent field wave function for many-electron systems.[317] For electron-hole systems, Elward et al. have performed variational calculation using explicitly correlated wave function for treating electron-

hole correlated in quantum dots.[216, 218] One of the important features of the XCFCI method presented here is the inclusion of the external field in the ansatz of the wave function. This is achieved by defining a new set of field-dependent coordinates which are generated by performing variational polaron transformation[318] and recasting the original Hamiltonian in terms of the field-dependent coordinates. The variational polaron transformation was introduced by Harris and Silbey for studying quantum dissipation phenomenon in the spin-boson system[318] and is used in the present work because of the mathematical similarity between the spin-boson and the field-dependent electron-hole Hamiltonian. The spin-boson system will be discussed in more detail in subsection 3.1.2

3.1.2 Spin-Boson system

As stated above, the spin-boson system is a model that appears in quantum dissipative systems (or open quantum systems); that is, systems in which the system interacts with the surrounding environment.[319] The spin-boson system is a particle of spin 1/2 that is coupled to environment of bosons that behave as harmonic oscillators. The Hamiltonian for this system is[319]

$$H = T_{\mathrm{TSS}} + H_{\mathrm{B}} + H_{\mathrm{int}}, \tag{3.1}$$

where T_{TSS} is the Hamiltonian for a two state system (TSS), H_{B} is the Hamiltonian for the boson environment, and H_{int} is the Hamiltonian for the interaction between the TSS and the boson environment. The components of the total Hamiltonian will be discussed in turn.

A TSS is a system in which the system exists as a linear combination of states, such as

$$|\Psi\rangle = c_1|1\rangle + c_2|2\rangle. \tag{3.2}$$

A double well can be considered a TSS, with a local state that can be solved in the region about each local minimum. The general wave function for double well may be expressed as

$$|\Psi_{\mathrm{DW}}\rangle = c_R|R\rangle + c_L|L\rangle, \tag{3.3}$$

where R is the right-hand state and L is the left-hand state.[319] The TSS Hamiltonian is[319]

$$H_{\mathrm{TSS}} = -\frac{1}{2}\hbar\Delta\sigma_x - \frac{1}{2}\hbar\sigma_z \tag{3.4}$$

$$= \frac{\hbar}{2}\begin{pmatrix} -\varepsilon & -\Delta \\ -\Delta & +\varepsilon \end{pmatrix} \tag{3.5}$$

where Δ is the tunneling matrix element and ε is the energy splitting between the wells (this Hamiltonian is written so that only the right hand minimum can be biased). The $\sigma_i, i = x, y, z$ are the Pauling spin matrices and are given as

$$\sigma_x = \begin{pmatrix} 0 & 1 \\ 1 & 0 \end{pmatrix} \tag{3.6}$$

$$\sigma_y = \begin{pmatrix} 0 & -i \\ i & 0 \end{pmatrix} \tag{3.7}$$

$$\sigma_z = \begin{pmatrix} 1 & 0 \\ 0 & -1 \end{pmatrix} \tag{3.8}$$

The boson environment behaves as a set of harmonic oscillators and the Hamiltonian is[319]

$$H_{\mathrm{B}} = \sum_{i=1}^{N} \frac{p_i^2}{2m_i} + \frac{1}{2} m_i \omega_i x_i^2 \tag{3.9}$$

$$= \sum_{i=1}^{N} \hbar \omega_i b_i^{\dagger} b_i, \tag{3.10}$$

where p is the momentum operator for particle i, m is the mass of particle i, ω is the frequency of the oscillator i, and N is the number of bosons.

The Hamiltonian for the interaction between the TSS and the boson environment is

$$H_{\mathrm{int}} = -\frac{1}{2} \sigma_z \sum_{i=1}^{N} q_0 c_i x_i \tag{3.11}$$

$$= -\frac{1}{2} \sigma_z \sum_{i=1}^{N} \hbar \lambda_i (b_i + b_i^{\dagger}) \tag{3.12}$$

$$\tag{3.13}$$

where q_0 is the separation between the two minimum of the double well, c_0 is a coupling strength term in first quantized notation, and λ_i is the coupling strength term in second quantized notation. By rewritten the Pauling spin matrices in terms of the two state system basis as

$$\sigma_x = |R\rangle\langle L| + |L\rangle\langle R|, \tag{3.14}$$

$$\sigma_y = i|L\rangle\langle R| - i|R\rangle\langle L|, \tag{3.15}$$

$$\sigma_z = |R\rangle\langle R| - |L\rangle\langle L|, \tag{3.16}$$

the spin-boson Hamiltonian can be written as

$$\begin{aligned} H = & -\frac{\hbar}{2}\Delta(|R\rangle\langle L| + |L\rangle\langle R|) - \frac{\hbar}{2}\varepsilon(|R\rangle\langle R| - |L\rangle\langle L|) \\ & - \sum_{i=1}^{N}(g_i^R|R\rangle\langle R| - g_i^L|L\rangle\langle L|)x_i \\ & + H_{\mathrm{B}}, \end{aligned} \tag{3.17}$$

where g_i^L and g_i^R are coupling terms for the left-hand and right-hand wells.

3.1.2.1 Variational polaron transformation for the spin-boson system

Harris and Silbey presented a solution to the spin-boson system using the variational polaron transformation.[318, 320, 321] The Hamiltonian is transformed so that origins of the oscillator are shifted. This is done by performing the following unitary transformation

$$\tilde{H} = U^{\dagger} H U \tag{3.18}$$

with the unitary operator

$$U = \exp(i\sum_j \frac{f_j}{\omega_j^2} p_j [|L\rangle\langle L| - |R\rangle\langle R|]). \tag{3.19}$$

The parameters $\{f_j\}$ are determined variationaly.[318] The Hamiltonian after transformation appears as

$$\begin{aligned}\tilde{H} = &-\frac{\hbar}{2}\Delta^{\text{new}}(|R\rangle\langle L| + |L\rangle\langle R|) - \frac{\hbar}{2}\varepsilon(|R\rangle\langle R| - |L\rangle\langle L|) \\ &- \sum_{i=1}^{N} g_i^{\text{new}}(|R\rangle\langle R| - |L\rangle\langle L|)x_i \\ &+ H_{\text{B}}\end{aligned} \tag{3.20}$$

where the new operators have been transformed. In more compact notation,

$$H^{\text{new}} = H_{\text{TSS}}^{\text{new}} + H_{\text{int}}^{\text{new}} + H_{\text{B}}. \tag{3.21}$$

3.1.3 Organization

The remainder of this chapter is organized as follows. The important equations and futures of full configuration interaction for electrons and for multicomponent systems will be given in subsection 3.2.1. The important features of the XCFCI method are summarized in subsection 3.2.2, construction of the field dependent basis functions is presented in subsection 3.2.3, the application of the XCFCI method using field-dependent basis is presented in section 3.3, and the conclusions are provided in section 3.4.

3.2 Theory

3.2.1 Full configuration interaction

The wave function for a configuration interaction (FCI) may be written as[17]

$$|\mathbf{C}\rangle = \sum_i c_i |i\rangle, \tag{3.22}$$

where $|i\rangle$ are different configurations of Slater determinants. The coefficients c_i are determined by variational minimization

$$E = \min_{\{c_i\}} \frac{\langle \mathbf{C}|H|\mathbf{C}\rangle}{\langle \mathbf{C}|\mathbf{C}\rangle}. \tag{3.23}$$

The coefficients may be determined by finding the stationary states

$$\frac{\partial}{\partial c_i} \frac{\langle \mathbf{C}|H|\mathbf{C}\rangle}{\langle \mathbf{C}|\mathbf{C}\rangle} = 0, \tag{3.24}$$

which may equivalently be posed as an eigenvalue problem

$$\mathbf{HC} = E\mathbf{C}, \tag{3.25}$$

where the elements of the matrix $\mathbf{H}$ are $H_{ij} = \langle i|H|j\rangle$.

The pertinent details of the full configuration interaction method will be described. Further

details may be found in many references.[6, 11, 14, 16, 17] The wave function for FCI is

$$|\Psi_{\mathrm{FCI}}\rangle = c_0|\Phi_0\rangle + \sum_{a,r} c_a^r|\Phi_a^r\rangle + \sum_{\substack{a<b \\ r<s}} c_{ab}^{rs}|\Phi_{ab}^{rs}\rangle + \sum_{\substack{a<b<c \\ r<s<t}} c_{abc}^{rst}|\Phi_{abs}^{rst}\rangle + \cdots, \tag{3.26}$$

where the subscripts indicate the orbitals that were removed and superscripts indicate the orbitals which were added in the excitation. Note that full in FCI refers to the excitation of all possible electrons for each type of excitation. This equation shows both the simplicity and the expense of the method. The simplicity is that there is a readily available form for expansion which has known rules for the evaluation of the terms (the Slater-Condon rules). The difficulty is that the expansion is both infinite and unordered with regards to the importance of terms.[6, 11] The need to use many of the determinants to obtain sizable improvements on the energies obtained using Hartree-Fock makes FCI infeasible for all but the small systems.[6, 12, 14, 16, 17] The computational expense of FCI methods grows at a factorial rate. Consider for a set of M spin orbitals with N electrons, one can construct[6]

$$\binom{M}{N} = \frac{M!}{N!(M-N)!} \tag{3.27}$$

different Slater determinants. If there are n orbitals, k electrons of spin α, and k electrons of spin β, the total number of possible determinants is

$$N_{\mathrm{det}} = \binom{n}{k}\binom{n}{k} = \binom{n}{k}^2. \tag{3.28}$$

In cases where the FCI wave function is intractable, the FCI wave function may be truncated by

selecting only determinants with certain excitations.[17] For example, in the CIS (configuration interaction singles), only the the ground state and singly excited determinants are used.[17] There are several many possibilites for truncated CI wave functions.

The systems under consideration in treatment have spin. The single excitation operator for an electronic system is

$$E_pq = a^\dagger_{p\alpha} a_{q\alpha} + q^\dagger_{p\beta} q_{q\beta}, \tag{3.29}$$

where the α, β indicates the spin of the electron that is being created. The one-body operator in second quantization becomes[17]

$$\hat{f} = \sum_{pq} f_{pq} E_{pq}. \tag{3.30}$$

The two-body operator, after modification with the single excitation operator, becomes

$$\hat{g} = \frac{1}{2} \sum_{pqrt} g_{pqrt} \sum_{\sigma\tau} q^\dagger_{p\sigma} a^\dagger_{r\tau} a_{s\tau} q_{q\sigma} \tag{3.31}$$

$$= \frac{1}{2} \sum_{pqrs} g_{pqrt} (E_{pq} E_{rs} - \delta_{qr} E_{ps}) \tag{3.32}$$

$$= \frac{1}{2} \sum_{pqrs} g_{pqrs} e_{pqrs}, \tag{3.33}$$

where the two-electron excitation operator has been introduced[17]

$$e_{pqrs} = E_{pq} E_{rs} - \delta_{qr} E_{ps} = \sum_{pqrs} a^\dagger_{p\sigma} a^\dagger_{r\tau} a_{s\tau} a_{q\sigma}. \tag{3.34}$$

The Hamiltonian is written in terms of the electron excitation operators as[17]

$$H = \sum_{pq} h_{pq} E_{pq} + \frac{1}{2} \sum_{pqrs} g_{pqrs} e_{pqrs} + h_{\text{nuc}}, \tag{3.35}$$

where the one-body term is [17]

$$h_p q = \int_{-\infty}^{+\infty} \mathrm{d}\mathbf{r} \phi^*(\mathbf{r}) \left(-\frac{\hbar^2}{2m} \nabla^2 + \sum_A \frac{Z_A q_\mathrm{e}}{r_{1A}} \right) \phi(\mathbf{r}), \tag{3.36}$$

and the two-body term is[17]

$$g_{pqrs} = \int_{-\infty}^{+\infty} \mathrm{d}\mathbf{r}_1 \mathrm{d}\mathbf{r}_2 \phi_p^*(\mathbf{r}_1) \phi^*(\mathbf{r}_2) r_{12}^{-1} \phi_r(\mathbf{r}_1) \phi_s(\mathbf{r}_2). \tag{3.37}$$

The Hamiltonian being used is a spin-free operator. Determinants which have different spin projections lead to Hamiltonian matrix elements which vanish.[17] To avoid possible additional work, the determinants are restricted to those determinants with the same spin projection. For N total electrons restricted to spin projection M, the number of α and β are given as[17]

$$N_\alpha = \frac{1}{2} N + M \tag{3.38}$$

$$N_\beta = \frac{1}{2} N - M. \tag{3.39}$$

The restricted Slater determinants are written as

$$|I_\alpha I_\beta\rangle = \alpha_{I\alpha} \beta_{I\beta} |\text{vac}\rangle, \tag{3.40}$$

where $\alpha_{I\alpha}$ and $\beta_{I\beta}$ are the alpha and beta strings; that is, strings of creation operators which give the proper arrangement of orbitals. The number of alpha strings is given by[17]

$$N_{\text{str}}^{\alpha} = \binom{n}{N_\alpha} = \frac{n!}{N_\alpha!(n-N_\alpha)}. \tag{3.41}$$

The Hamiltonian operator will now be placed in a determinantal representation. Eq.(3.36) can be written for a CI expansion as[17]

$$h^{\text{SD}}_{I_\alpha I_\beta, J_\alpha J_\beta} = \langle I_\alpha I_\beta | h | J_\alpha J_\beta \rangle, \tag{3.42}$$

and Eq.(3.37) can be written as[17]

$$g^{\text{SD}}_{I_\alpha I_\beta, J_\alpha J_\beta} = \langle I_\alpha I_\beta | g | J_\alpha J_\beta \rangle \tag{3.43}$$

For $|J_\alpha J_\beta\rangle$, the non-zero elements for $h^{\text{SD}}_{I_\alpha I_\beta, J_\alpha J_\beta}$ are for the choices of $|I_\alpha I_\beta\rangle$[17]

$$|I_\alpha I_\beta\rangle = |J_\alpha J_\beta\rangle \tag{3.44}$$

$$|I_\alpha I_\beta\rangle = E^{\alpha}_{pq} |J_\alpha J_\beta\rangle \tag{3.45}$$

$$|I_\alpha I_\beta\rangle = E^{\beta}_{pq} |J_\alpha J_\beta\rangle, \tag{3.46}$$

where the excitation operators are[17]

$$E^{\gamma}_{pq} = a^{\dagger}_{p\gamma} a_{q\gamma}, \gamma = \alpha, \beta. \tag{3.47}$$

For the two-electron operator, the matrix elements $g^{\mathrm{SD}}_{I_\alpha I_\beta, J_\alpha J_\beta}$ are nonzero in the same cases as the one-body operator (Eq.(3.44)-(3.46)) with the additional choices

$$|I_\alpha I_\beta\rangle = E^\alpha_{pq} E^\beta_{rs} |J_\alpha J_\beta\rangle \tag{3.48}$$

$$|I_\alpha I_\beta\rangle = E^\alpha_{pq} E^\alpha_{rs} |J_\alpha J_\beta\rangle \tag{3.49}$$

$$|I_\alpha I_\beta\rangle = E^\beta_{pq} E^\beta_{rs} |J_\alpha J_\beta\rangle \tag{3.50}$$

With the previous tools in hand, it is now possible to develop a method for calculating

$$\sigma_{I_\alpha I_\beta} = \sum_{J_\alpha J_\beta} \langle I_\alpha I_\beta | H | J_\alpha J_\beta \rangle C_{J_\alpha J_\beta} \tag{3.51}$$

in an efficient manner. Falling back to the Slater-Condon rules leads to an inefficient algorithm because it requires inspecting each matrix element which means the number of operations scales as the square of the number of Slater determinants.[17] The modern method is to determine for each Slater determinant which determinants are connected by single and double excitations, since these are the contributing terms.[17] Rewriting the spin-free Hamiltonian (Eq.(3.35)) as

$$H = \sum_{pq} h_{pq} E_{pq} + \frac{1}{2} \sum_{pqrs} g_{pqrs} (E_{pq} E_{rs} - \delta_{rq} E_{ps}) \tag{3.52}$$

$$= \sum_{pq} k_{pq} E_{pq} + \frac{1}{2} \sum_{pqrs} g_{pqrs} E_{pq} E_{rs}, \tag{3.53}$$

where the effective one-body integral

$$k_{pq} = h_{pq} - \frac{1}{2} g_{prrq} \tag{3.54}$$

has been introduced and the nuclear-nuclear term has been ignored. Eq.(3.51) can now be written as[17]

$$\sigma_{I_\alpha I_\beta} = \sigma^{(1)}_{I_\alpha I_\beta} + \sigma^{(2)}_{I_\alpha I_\beta}, \tag{3.55}$$

where the terms are

$$\sigma^{(1)}_{I_\alpha I_\beta} = \sum_{pq} \sum_{J_\alpha J_\beta} k_{pq} \langle I_\alpha I_\beta | E_{pq} | J_\alpha J_\beta \rangle C_{J_\alpha J_\beta} \tag{3.56}$$

$$\sigma^{(2)}_{I_\alpha I_\beta} = \frac{1}{2} \sum_{pqrs} \sum_{J_\alpha J_\beta} g_{pqrs} \langle I_\alpha I_\beta | E_{pq} E_{rs} | J_\alpha J_\beta \rangle C_{J_\alpha J_\beta}. \tag{3.57}$$

The focus will be on Eq.(3.57) since the one-electron term will be obtained in the course of the calculation.[17] A completeness relationship is inserted between the excitation operators to give

$$\sigma^{(2)}_{I_\alpha I_\beta} = \frac{1}{2} \sum_{\substack{K_\alpha K_\beta J_\alpha J_\beta \\ pqrs}} \langle I_\alpha I_\beta | E_{pq} | K_\alpha K_\beta \rangle g_{pqrs} \langle K_\alpha K_\beta | E_{rs} | J_\alpha J_\beta \rangle C_{J_\alpha J_\beta} \tag{3.58}$$

where the K_α and K_β contain all alpha and beta strings.[17] Eq. (3.58) is now rewritten to give a sequence of partial summations

$$D_{rs,K_\alpha K_\beta} = \sum_{J_\alpha J_\beta} \langle K_\alpha K_\beta | E_{rs} | J_\alpha J_\beta \rangle C_{J_\alpha J_\beta} \tag{3.59}$$

$$G_{pq,K_\alpha K_\beta} = \frac{1}{2} \sum_{rs} g_{pqrs} D_{rs,K_\alpha K_\beta} \tag{3.60}$$

$$\sigma^{(2)}_{I_\alpha I_\beta} = \sum_{pq,K_\alpha K_\beta} \langle I_\alpha I_\beta | E_{pq} | K_\alpha K_\beta \rangle G_{pq,K_\alpha K_\beta} \rangle. \tag{3.61}$$

In step 1, the matrix **D** is generated. The matrix can be separated into

$$D_{rs,K_\alpha K_\beta} = \sum_{J_\beta} \langle K_\beta | E^\beta_{rs} | J_\beta \rangle C_{K_\alpha J_\beta} + \sum_{J_\alpha} \langle K_\alpha | E^\alpha_{rs} | J_\alpha \rangle C_{J_\alpha K_\beta} \tag{3.62}$$

In step 2, matrix **D** is multiplied by the two-electron matrix. Due to the permutational symmetry of the two-electron integrals, Eq. (3.60) is rewritten as

$$G_{pq,K_\alpha K_\beta} = \frac{1}{2} \sum_{r \geq s} q_{pqrs} (D_{rs,K_\alpha K_\beta} + D_{sr,K_\alpha K_\beta})(1 + \delta_{sr})^{-1}, \tag{3.63}$$

which improves computational efficiency.[17] In step 3, the matrix **G** is contracted with the matrix elements of E_{pq}. As a consequence of this formulation, Eq. (3.56) may be written as[17]

$$\sigma^{(1)}_{I_\alpha I_\beta} = \sum_{pq} k_{pq} D_{pq,I_\alpha I_\beta}. \tag{3.64}$$

This is one of the modern efficient methods for calculating the CI matrix elements. This method is known as the N-resolution method. The application of an explicit correlation operator to the FCI method will be described in subsection 3.2.2.

3.2.2 Explictly correlated full configuration interaction

The many-particle field dependent electron-hole Hamiltonian is defined as [1, 2]

$$\begin{aligned} H = {} & T_\mathrm{e} + V^\mathrm{ext}_\mathrm{e} + V_\mathrm{ee} + \sum_i^{N_\mathrm{e}} \mathbf{F} \cdot \mathbf{r}^\mathrm{e}_i \\ & + T_\mathrm{h} + V^\mathrm{ext}_\mathrm{h} + V_\mathrm{hh} - \sum_i^{N_\mathrm{h}} \mathbf{F} \cdot \mathbf{r}^\mathrm{h}_i \end{aligned} \tag{3.65}$$

$$-\sum_{i=1}^{N_e}\sum_{j=1}^{N_h} r_{ij}^{-1},$$

where T is the kinetic energy operator, ε is the dielectric constant, and $\mathbf{F}$ is the external electric field. The external potential V_e^{ext} and V_h^{ext} represent the confining potential experienced by the quasi-particles. The form of the XCFCI wave function is defined as

$$\Psi_{\mathrm{XCFCI}} = \hat{G}\sum_k c_k \Phi_k, \tag{3.66}$$

where c_k is the CI coefficient and Φ_k are basis functions. Analogous to the conventional CI method, the basis functions Φ_k are obtained by applying excitation operator $\hat{X}_k$ to the reference function Φ_0

$$\Phi_k = \hat{X}_k \Phi_0 \quad \text{and} \quad \langle \Phi_k | \Phi_{k'} \rangle = \delta_{kk'}. \tag{3.67}$$

The reference function is a product of electron and hole Slater determinants

$$\Phi_0 = \Phi_0^e \Phi_0^h, \tag{3.68}$$

and its construction is described in subsection 3.2.3. For a multicomponent electron-hole system with K_e electronic orbitals, N_e electrons, K_h, and N_h, the total number of determinants is

$$N_{\mathrm{det}} = \binom{K_e}{N_e}^2 \binom{K_h}{N_h}^2. \tag{3.69}$$

The operator $\hat{G}$ is known as the geminal operator and is an explicit function of r_{eh} and is

Table 3.1: Total number of determinants in a multicomponent electron-hole FCI.

N_e	K_e	N_{det}^{e}	N_h	K_h	N_{det}^{h}	N_{det}^{total}
1	4	1.60×10^{1}	1	4	1.60×10^{1}	2.56×10^{2}
1	6	3.60×10^{1}	1	6	3.60×10^{1}	1.30×10^{3}
1	8	6.40×10^{1}	1	8	6.40×10^{1}	4.10×10^{3}
1	10	1.00×10^{2}	1	10	1.00×10^{2}	1.00×10^{4}
2	10	2.03×10^{3}	2	10	2.03×10^{3}	4.10×10^{6}
10	30	9.03×10^{14}	10	30	9.03×10^{14}	8.14×10^{29}

defined as a linear combination of Gaussian functions

$$\hat{G} = \sum_{i=1}^{N_e} \sum_{j=1}^{N_h} \sum_{k=1}^{N_g} b_k \exp(-\gamma r_{ij}^2), \tag{3.70}$$

where N_g is the number of Gaussian functions included in the expansion, N_e and N_h are the number of electrons and holes, respectively. The parameters b_k and γ_k used in the definition of the geminal operator are obtained variationally. The presence of the electron-hole distance dependent term in the Gaussian-type geminal (GTG) function plays an important role in improving the form of the electron-hole wave function at small interparticle distances. It is important to note that the GTG function uses Gaussian as opposed to exponential functions and consequently is incapable of describing the electron-hole Kato cusp condition exactly. The derivative of GTG function with respect to the electron-hole distance vanishes at $r_{eh} = 0$

$$\left(\frac{\partial G}{\partial r_{eh}} \right)_{r_{eh}} = 0, \tag{3.71}$$

and therefore it is only capable of improving the structure of the wave function in the neighborhood of the coalescence point. However since the coalescence point is of measure zero, we do not expect this approximation to limit the accuracy of the GTG function. [216, 218, 316] This has also been

found to be true for the electron-electron coalescence point[316] in electronic structure theory and the work of Prendergast et al. demonstrated the importance of medium-range correlation for many-electron systems.[314] The XCFCI calculation is performed in two steps. In the first step, the parameters of geminal operator are obtained variationally by performing the following minimization:

$$E[G_{\min}] = \min_{b_k,\gamma_k} \frac{\langle G\Phi_0|H|G\Phi_0\rangle}{\langle G\Phi_0|G\Phi_0\rangle}. \tag{3.72}$$

In the second step, the expansion coefficients $\{c_k\}$ are obtained variationally and are defined by the following minimization procedure:

$$E_{\text{XCFCI}} = \min_{c} \frac{\langle \Psi_{\text{XCFCI}}|H|\Psi_{\text{XCFCI}}\rangle}{\langle \Psi_{\text{XCFCI}}|\Psi_{\text{XCFCI}}\rangle} \tag{3.73}$$

The above equation can be rewritten as a FCI calculation of transformed operators

$$E_{\text{XCFCI}} = \min_{c} \frac{\langle \Psi_{\text{FCI}}|\tilde{H}|\Psi_{\text{FCI}}\rangle}{\langle \Psi_{\text{FCI}}|\tilde{1}|\Psi_{\text{FCI}}\rangle} \tag{3.74}$$

where the transformed operators are defined as

$$\tilde{H} = G^{\dagger}_{\min} H G_{\min}, \tag{3.75}$$

$$\tilde{1} = G^{\dagger}_{\min} G_{\min}. \tag{3.76}$$

The exact expression of the transformed operators in Eqs. (3.75) and (3.76) and discussion relevant to their derivation has been presented earlier in Refs. [216, 218] and is not repeated here. The

E_{XCFCI} reduces to the conventional FCI energy in the limit of geminal function approaches unity

$$E_{\mathrm{FCI}} = \lim_{G \to 1} E_{\mathrm{XCFCI}}. \tag{3.77}$$

We expect the E XCFCI energy to be lower than the FCI energy for identical set of basis functions and earlier studies have shown this to be true.[216] Since G_{min} is obtained in the first step, the limit in the above equation should be evaluated first before the optimization of the CI coefficients is performed. One of the key features of the optimization of the XCFCI wave function described here is that the G min is obtained in the presence of Φ_0 which results in substantial reduction in the cost of the calculation. In an ideal situation, the parameters of GTG function and the CI coefficient should be minimized simultaneously as shown in the following equation:

$$\min_{c,g} \frac{\langle \Psi_{\mathrm{FCI}} | G^{\dagger} H G | \Psi_{\mathrm{FCI}} \rangle}{\langle \Psi_{\mathrm{FCI}} | G^{\dagger} G | \Psi_{\mathrm{FCI}} \rangle} \leq \min_{c} \frac{\langle \Psi_{\mathrm{FCI}} | G^{\dagger} H G | \Psi_{\mathrm{FCI}} \rangle}{\langle \Psi_{\mathrm{FCI}} | G^{\dagger} G | \Psi_{\mathrm{FCI}} \rangle} \tag{3.78}$$

However, such a procedure will be computationally very expensive and the strategy of two successive subspace minimizations is used in the presented work. The underlying assumption in the minimization procedure is that the G min obtained using Φ_0 is of sufficiently high-quality that the XCFCI energy is lower than the FCI energy. During the course of the calculations, this assumption can be verified easily by numerical comparison of the two energies. In a situation where $E[G_{\mathrm{min}}] < E[G = 1]$ and $E_{\mathrm{FCI}} < E_{\mathrm{XCFCI}}$ indicates that the sequential subspace minimization cannot be used for accurate determination of the geminal parameters, and a search in the full parameters spaces of CI coefficient and geminal parameters must be performed. After the successful completion of the XCFCI calculations, the field dependent exciton binding was calculated from the

difference between the non-interacting and interacting ground state energies. Defining the non-interacting Hamiltonian as

$$H_0 = \lim_{r_{\mathrm{eh}} \to \infty} H, \tag{3.79}$$

the exciton binding energy is computed as

$$E_{\mathrm{B}}[\mathbf{F}] = E_0^{(0)} - E_{\mathrm{XCFCI}}, \tag{3.80}$$

where $E_0^{(0)}$ is defined as

$$E_0^{(0)} = \min_{\Psi} \frac{\langle \Psi | H_0 | \Psi \rangle}{\langle \Psi | \Psi \rangle}. \tag{3.81}$$

The field dependent electron-hole recombination probability is obtained from the XCFCI wave function using the following expression[216, 218] and is related on-top electron-hole pair density[322, 323, 324, 325, 326]

$$P_{\mathrm{eh}}[\mathbf{F}] = \frac{\langle \Psi_{\mathrm{XCFCI}} | \delta(\mathrm{r_e} - \mathbf{r_h}) | \Psi_{\mathrm{XCFCI}} \rangle}{\langle \Psi_{\mathrm{XCFCI}} | \Psi_{\mathrm{XCFCI}} \rangle}. \tag{3.82}$$

The exciton binding energy and the recombination probability are functionals of the applied external field and are indicated explicitly in Eqs. (3.80) and (3.82) , respectively.

3.2.3 Construction of field dependent basis set

One of the key features of the electron-hole Hamiltonian used in the present work is the presence of the field-dependent term in Eq. (3.65) . Since the convergence of the CI expansion depends on the quality of the underlying 1-particle basis, it is desirable to construct and use efficient single particle basis sets. In the present work, we have developed field-dependent basis functions and the details of the derivation are presented as following. Starting with the expression of H_0 in Eq. (3.79), the zeroth-order Hamiltonian is expressed as a sum of non-interacting electronic and hole Hamiltonians

$$H_0 = H_0^{\mathrm{e}} + H_0^{\mathrm{h}}, \tag{3.83}$$

where the expression for the single-component Hamiltonian is given as

$$H_0^{\mathrm{e}} = T_{\mathrm{e}} + V_{\mathrm{e}}^{\mathrm{ext}} + |e|\mathbf{F}\cdot\mathbf{r}_{\mathrm{e}}, \tag{3.84}$$

$$H_0^{\mathrm{h}} = T_{\mathrm{h}} + V_{\mathrm{h}}^{\mathrm{ext}} - |e|\mathbf{F}\cdot\mathbf{r}_{\mathrm{h}}. \tag{3.85}$$

As seen from the above equations, the coupling between the external field and the quasi-particle coordinates is linear. The above Hamiltonian shares mathematical similarity with the spin-boson Hamiltonian that has been used extensively in quantum dissipative systems.[327] In the present method, we perform analogous transformation which is defined by the following equations:

$$\mathrm{q}_{\mathrm{e}} = \mathbf{r}_{\mathrm{e}} + \lambda^{\mathrm{e}}\mathbf{F}, \tag{3.86}$$

$$q_h = \mathbf{r}_h - \lambda^h \mathbf{F}. \tag{3.87}$$

Similar to the polaron transformation in the spin-boson system, the coordinates of the quasi-particle experience a shift due to the presence of the external field.[327] Using the method of variational polaron transformation by Harris and Silbey,[318] the shift parameters λ^e and λ^h are determined variationally. Gaussian-type orbitals (GTOs) are defined using the transformed coordinates and are used in construction of the electronic and hole Slater determinant. The Hartree-Fock energy is obtained by performing double minimization over single Slater determinant and the shift parameters λ^e and λ^h

$$E^e_{HF}[\lambda^e_{min}, \Phi^e_0] = \min_{\lambda^e} \min_{\Phi_{SD}} \langle \Phi_{SD}(\mathbf{q}_e) | H^e_0(\mathbf{q}_e) | \Phi_{SD}(\mathbf{q}_e) \rangle, \tag{3.88}$$

$$E^h_{HF}[\lambda^h_{min}, \Phi^h_0] = \min_{\lambda^h} \min_{\Phi_{SD}} \langle \Phi_{SD}(\mathbf{q}_h) | H^h_0(\mathbf{q}_h) | \Phi_{SD}(\mathbf{q}_h) \rangle, \tag{3.89}$$

For identical set of GTO basis functions, the above minimization will yield energy lower than the conventional HF energy

$$E^e_{HF}[\lambda^e_{min}] \leq E^e_{HF}[\lambda^e = 0]. \tag{3.90}$$

The minimization in Eqs. (3.88) and (3.89) is also related to the earlier work on the floating Gaussian method by Frost.[328, 329, 330] Equations (3.88) and (3.89) also define the electron and hole reference functions that are used for construction of the CI expansion. The electron-hole basis functions for the FCI calculations are constructed by taking a direct product between the set

of electronic and hole single-component basis sets

$$\{\Phi_k\} = \{\Phi_i^{\mathrm{e}}\} \otimes \{\Phi_j^{\mathrm{h}}\}. \tag{3.91}$$

The procedure described above is a general method that is independent of the exact form of the external potential. However, if the external potential is of quadratic form, the field dependent zeroth-order single-component Hamiltonian has an uncomplicated mathematical form and additional simplification can be achieved.

3.3 Results and Discussion

The electron-hole Hamiltonian in Eq. (3.65) has been used extensively for studying optical rectification[1, 2, 111, 115, 119] effect in GaAs quantum dots. In the present work, a single electron-hole pair was used and all the system specific parameters were obtained from previous calculations on the GaAs system.[1, 2] The parabolic confinement potential has found widespread applications[19, 107, 114, 117, 270, 293, 295, 297, 302, 331, 332, 333, 334, 335, 336, 337] in the study of quantum dots and was used in the present work to approximate the external potential term in the Hamiltonian shown below

$$H = -\frac{\hbar^2}{2m_{\mathrm{e}}}\nabla_{\mathrm{e}}^2 - \frac{\hbar^2}{2m_{\mathrm{h}}} + \frac{1}{2}k_{\mathrm{e}}r_{\mathrm{e}}^2 + \frac{1}{2}k_{\mathrm{h}}r_{\mathrm{h}}^2 \tag{3.92}$$

$$-\frac{1}{\varepsilon|\mathbf{r}_{\mathrm{eh}}|} + |e|\mathbf{F}\cdot(\mathrm{r_e} - \mathrm{h}). \tag{3.93}$$

All the parameters that are needed for the complete description of the electron-hole Hamiltonian used in the calculations are presented in Table 3.2 . Following earlier work on the effect of electric

field on nonlinear optical properties of GaAs quantum dots,[1, 2] the external electric field was aligned along the z-axis and the field strength was varied from zero to 500 kV/cm. Similar to the spin-boson Hamiltonian, the polaron transform resulted in shifted harmonic oscillators.[327] The 1-particle GTO basis was constructed from the lowest ten eigenfunction of the harmonic oscillator Hamiltonian in Eq. (3.79) and was used to perform the minimization described in Eqs. (3.88) and (3.89). The reference functions for electron and hole were obtained and a direct product between the electronic and the hole basis sets was performed to generate the electron-hole basis for the FCI calculations. The geminal minimization was performed using a set of three $\{b_k, \gamma_k\}$ parameters at each field strength, and the optimized values are presented in Table 3.3. The total exciton energy for the field-free case was found to be 269.45 meV. The total exciton energy of the system as a function of the field strength is presented in Figure 3.1.

Table 3.2: System dependent parameters used in the electron-hole Hamiltonian for the GaAs quantum dot [1, 2]

Parameter	Value
m_e	$0.067m_0$
m_h	$0.090m_0$
k_e	9.048×10^{-7} a.u.
k_h	1.122×10^{-6} a.u.
ε	$13.1\varepsilon_0$

It is seen that the total energy decreases with increasing field strength. Earlier studies on this system indicate that the exciton energy is a quadratic function of the applied field.[338, 339] To investigate the scaling of the total exciton energy with respect to the field strength, we have performed least-square fit of the calculated values with a second order polynomial and the results are presented in Figure 3.1. The results from these calculations confirm that the quadratic scaling of the exciton energy as a function of the field strength. The exciton binding energy was calculated

Table 3.3: Optimized geminal parameters used in the calculations of energy and recombination probability.

F_z (kV/cm)	0	100	200	300	400	500
b_1	1.00	1.00	1.00	1.00	1.00	1.00
γ_1	0.00	0.00	0.00	0.00	0.00	0.00
b_2	1.40×10^{-1}	9.99×10^{-1}	4.99×10^{-2}	5.78×10^{-3}	1.00×10^{-2}	5.59×10^{-3}
γ_2	2.29×10^{-4}	4.60×10^{-6}	1.11×10^{-2}	1.11	1.00	1.11
b_3	4.35×10^{-2}	1.08×10^{-1}	8.90×10^{-2}	1.67×10^{-2}	2.00×10^{-2}	1.58×10^{-2}
γ_3	1.13×10^{-2}	1.00×10^{-2}	1.01×10^{-3}	1.11×10^{-1}	1.01×10^{-1}	1.02×10^{-1}

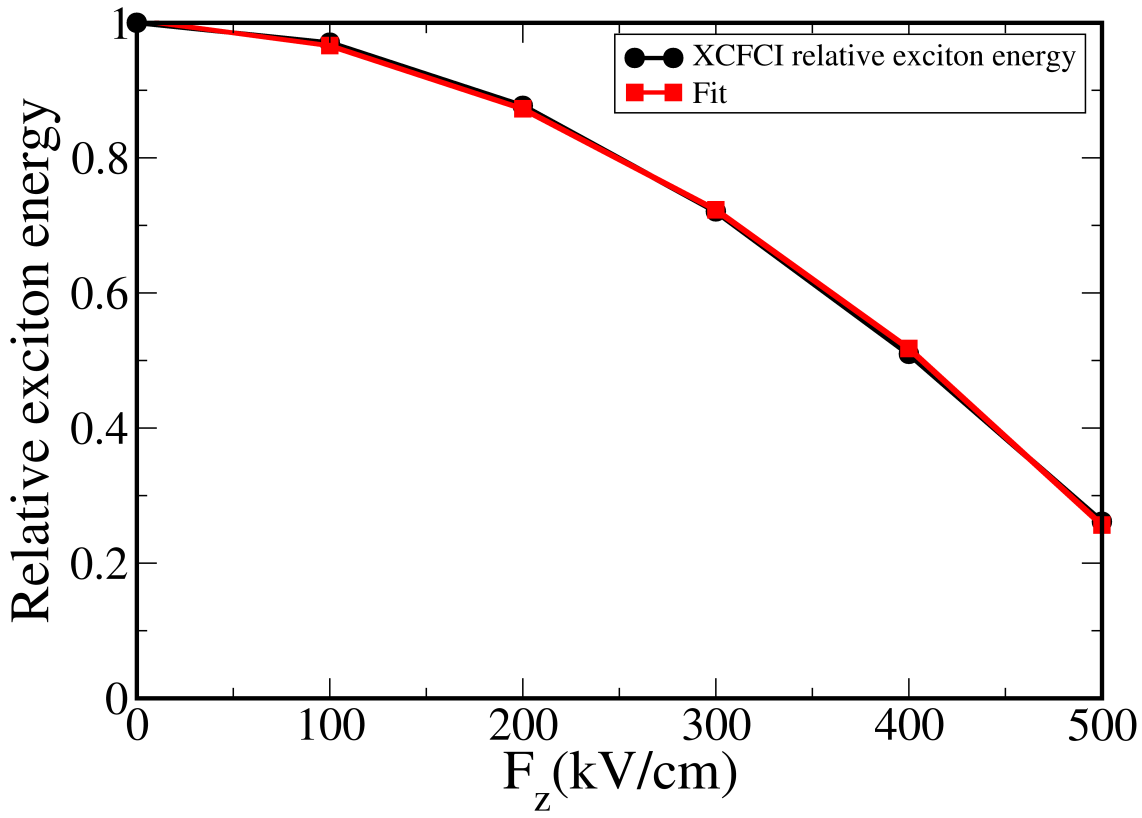

Figure 3.1: Relative exciton energy compared to the fit $E = (-2.7925 \times 10^{-6})F_z^2 + (-7.0938 \times 10^{-5})F_z + 1$.

using Eq. (3.80) and was found to be 28.52 meV for the field-free case. The effect of the external field on the exciton binding energy was investigated by calculating the relative binding energy which is defined by the following equation:

$$\tilde{E}_{\mathrm{B}} = \frac{E_{\mathrm{B}}[\mathbf{F}]}{E_{\mathrm{B}}[\mathbf{F}=0]}. \tag{3.94}$$

It is seen from Figure 3.2 that the exciton binding energy decreases with increasing field strength. As the field strength is increased from 0 to 500 kV/cm, the exciton binding energy

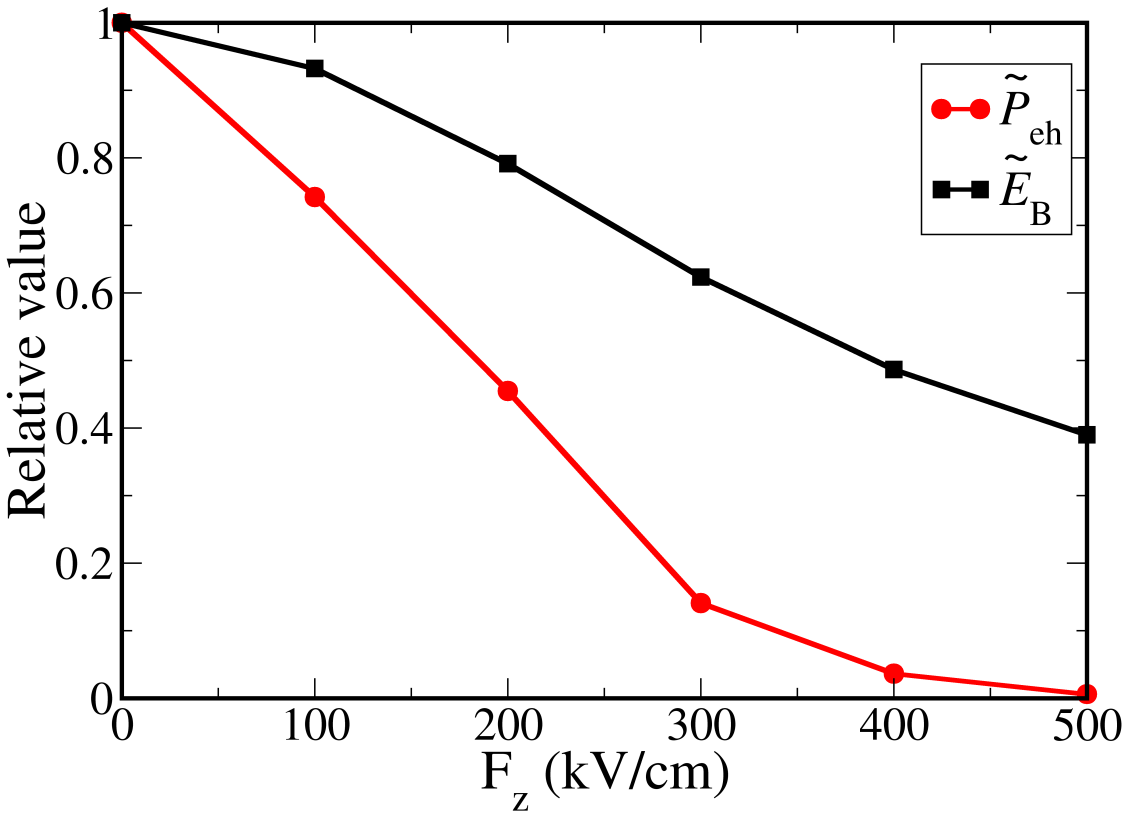

Figure 3.2: Comparison of $\tilde{E}_B$ and $\tilde{P}_{eh}$ as a function of electric field strength.

decreases by a factor of 2.6. In addition to the calculation of binding energy, the effect of the field on electron-hole recombination probability was also investigated. Analogous to the relative binding energy, the relative recombination probability is defined as

$$\tilde{P}_{eh} = \frac{P_{eh}[\mathbf{F}]}{P_{eh}[\mathbf{F}=0]}, \tag{3.95}$$

and is presented in Figure 3.2

It is seen that the there is a sharp decrease in the recombination probability with increasing

field strength and the recombination probability at 500 kV/cm is lower than the field-free case by a factor of 166. One of the key results from this study is that exciton binding energy and eh-recombination probability are affected differently by the external electric field. It is seen that the exciton binding energy and eh-recombination probability follow different scaling with respect to field strength. The effectiveness of the polaron transformation was investigated by computing the exciton binding energy with and without the transformation for identical basis functions. The calculations for the untransformed basis were performed by setting $\lambda^{e} = \lambda^{h} = 0$ and the results are presented in Figure 3.3.

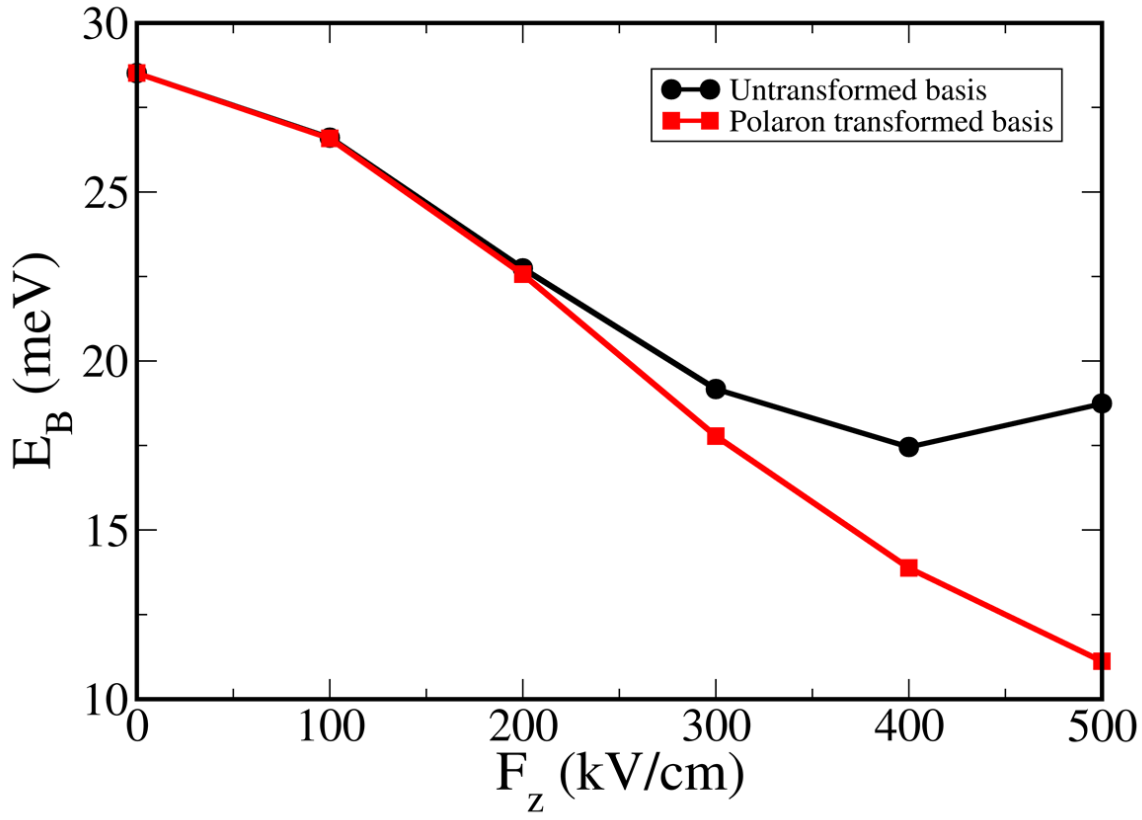

Figure 3.3: Comparison of exciton binding energy obtained using polaron transformed and untransformed method for identical set of electron and hole basis functions.

As expected for low field strengths, we do not see significant difference between the binding energies. However, with increasing field strength the error in the untransformed calculation becomes significant and shows a qualitatively wrong trend in the high field strength limit.

The polaron transformation also provides insight into the effect of the electric field on the exciton binding energy in the limit of high field strengths. Starting with the transformation defined in Eq. (3.86), the electron-hole Coulomb interaction in the transformed coordinate can be expressed as

$$\frac{1}{|\mathbf{r}_\mathrm{e}-\mathbf{r}_\mathrm{h}|} = \frac{1}{|(\mathbf{q}_\mathrm{e}-\mathbf{q}_\mathrm{h})-(\lambda_e+\lambda_h)\mathbf{F}|} = v_\mathrm{eh}(\mathbf{q}). \tag{3.96}$$

It is seen in the above equation that the above expression will be dominated by the field-dependent term in the limit of high field strength. A direct consequence of the above condition is that in the limit of high field strengths, we expect the exciton binding energy to be small

$$H(\mathbf{q}) \approx H_0(\mathbf{q}) \implies E_\mathrm{B} \approx 0 \qquad \text{for } 1 \ll |\mathbf{F}| < \infty. \tag{3.97}$$

It is important to note that the above conclusion is independent of the choice of the external potential.

3.4 Conclusion

The effect of an external electric field on exciton binding energy and electron-hole recombination probability was computed using explicitly correlated full configuration interaction method. Field-dependent basis functions were used in the calculations and a variational polaron transforma-

tion scheme was developed for the construction of field-dependent basis functions. It was found that both exciton binding energy and electron-hole recombination probability decrease with increasing field strength. One interesting conclusion from this study is that the binding energy and recombination probability follow different scaling with respect to the external electric field. For the range of field strengths studied, the recombination probability and exciton binding energy decrease by a factor of 166 and 2.6, respectively. These results give important insights into the application of electric fields for controlling the dissociation of excitons in quantum dots.

Chapter 4: Effect of environmental acidity and ligand length on exciton binding energy of CdSe quantum dots

4.1 Introduction

Quantum dots have interesting optical and electronic properties which have found many applications, including light harvesting materials[340], light-emitting materials[79], photocatalysis[78, 149, 341, 342],bioimaging [88, 162, 163, 164, 165, 166, 167, 168, 169, 170, 171, 172, 173, 174, 303, 343], molecular sensing[165, 166, 172, 344], nanoscale probes[39, 158, 159, 161]. The key to wide application of quantum dots has been the control of optical and electronic properties by several parameters, including size and shape[29, 30, 31, 32, 33, 34], composition[37], applied electromagnetic fields[39, 40, 41, 42, 43, 44],and ligands[45, 46, 47, 48, 49]. The capping ligands play an important role in the formation and have sizable impacts in the optical and electronic properties of quantum dots.[45] The choice of the ligands has been made for many reasons, including solubility, functionalization, and specific targeting of chemicals and biomolecules. The most common ligands are phosphine oxides (in particular, tri-*n*-ocytlphophine oxide (TOPO)), amines, thiols, and carboxylic acids.[45] A key step towards the full understanding and ultimately necessary for the complete ability to engineer quantum dots for specific applications is to understand how the choice of a specific ligand will impact the optical and electronic properties of the

quantum dot systems Many properties of the quantum dots have been studied, including exciton binding energy,[40, 217, 278, 279] recombination probability,[40, 205, 216, 217], and quantum yields.[345]

Of the many parameters that have been used to control the optical and electronic properties of quantum dots, the choice of ligands can be very multifaceted. In an example by Munro and Ginger, the addition of a single octadecanethiol molecule to a CdSe quantum dot caused a 50% decrease in photoluminescence quantum yield.[49] Clearly, the choice of the ligand can have a great impact on the optical and electronic properties. However, it is difficult to isolate one component of the many parameters, but systematic variation of one aspect of ligands has been attempted by the consideration of families of ligands. Aldeek and co-workers have studied the influence on the growth and optical properties by capping CdSe and CdTe quantum dots with mercaptopropionic acid, mercaptohexanoic acid, and mercaptoundeanoic acid.[46] Kwon and co-workers have shown experimentally that the field-effect mobility decreases exponentially as the quantum dot-amine ligand length increases in carbon quantum dots.[346] Ouyang and co-workers studied the effect of changing the ligand length in CdS quantum dots using capric acid and oleic acid, with the longer ligand oleic acid shifting the absorption maximum to the shorter wavelengths.[79] Ma and co-workers have studied the effect of branching isomers of mercaptovaleric acid as ligands for CdTe on the optical properties, finding that branched isomers improved optical properties.[347] Gao and co-workers have studied the impact on photoconductivity in PbSe quantum dots, finding that amines gave higher carrier mobilities than carboxylic acids and gave a lower carrier mobility increases.[47] Newton and co-workers have used TOPO to synthesis ultrasmall and "magic" ($(CdSe)_n \quad n = 13, 19, 33, 34$) CdSe clusters.[76] Dolai and co-workers have produced $(CdSe)_{34}$ in multi-gram quantities without the use of phosphine-ligands, which showed high photoluminescence efficiency.[75] Dolai and

co-workers have studied the "magic" cluster CdSe for the electrochemical properties of the clusters, especially for use in photocatalysts and photovoltaic devices.[74] In each of the preceding cases, the presence and nature of the ligands has shown great impact on the optical and electronic properties of the quantum dot systems.

The relationship between ligand properties and the core quantum dot optical and electronic properties has suggested many applications. An interesting application that suggests itself is the use of the changes in the optical properties as the surface ligands react to the changes in the environment acidity. It has been experimentally shown that this can be accomplished by many groups. Chen and Wu have used ZnSe quantum dots capped with mercaptoacetic acid to determine pH by fluorescence spectroscopy.[158, 159] Yu and co-workers have used quantum dot-based pH probes for the study of enzyme reaction kinetics.[161] Yang and co-workers has used CdTe/CdSe core/shell quantum dots as pH-sensitive fluorescence probe with ascorbic acid as the added acid.[89] Deng and co-workers reported green and orange CdTe quantum dots, capped with specially marked ligands, as pH probes and for detection of viruses.[160] Tomasulo and co-workers produced CdSe/ZnS core/shell quantum dots with ligands such the pH could be probed from 3 to 11.[86, 87] Teubert and co-workers investigated the electric-field dependence of the optical properties of INGaN/GaN quantum dots in contact with an electrolyte, finding that pH variation corresponds with photoluminescence.[41] Another application is the use of the quantum dots as nanoscale electric probes. Park and co-workers have use quantum dots to measure electrical fields on the nanoscale by taking advantage of the quantum-confined Stark effect using a variety of nanocrystals, including CdSe nanorods, CdSe quantum dot in CdS nanorods, CdTe/CdSe core/shell quantum dots, and ZnSe in CdS nanorods.[39] These applications, especially the nanoscale pH probes, are especially interesting since they require a change in the partial electrical field due to

the ligand as the environment acidity changes.

The previous applications suggest the importance of understanding how ligands impact the properties such as exciton binding energy, eh-recombination probability, and others. Towards that goal, it is necessary to consider the quantum dot system with ligands from a theoretical basis. The surface chemistry of quantum dots is a very complex and difficult study component of the quantum dot system. In this work, the ligand length has been isolated as one of the many parameters that impact in the surface chemistry of quantum dots. A central problem in the study of even modest size quantum dots is the large number of electrons that are within the quantum dot core. Even at a relatively modest ligand density, many ligands are present on the surface of the quantum dot. Each ligand is a polyelectronic system that adds more complexity to the already complex quantum dot system. Smaller systems, such as $Cd_{33}Se_{33}$ with trimethylphosphine oxide ligands, have been treated using DFT.[48, 90] Treatment of a large system with a realistic number of ligands is a computational expensive task.

The purpose of this work is to study the effect of ligand length and environmental acidity on the exciton binding energy. The CdSe quantum dot size will be varied while maintaining the constant ligand density but changing the length of the charged ligands and environmental acidity of the system to determine the effect of charged ligands with respect to ligand length and environmental acidity on the exciton binding energy.

The electron-hole in a parabolic potential treatment of spherical quantum dots has been successfully used.[269, 270, 271, 272, 273, 274, 275, 276, 277] Elward and co-workers have used the explicitly correlated Hartree-Fock (XCHF) method to treat parabolic quantum dots.[215, 216, 217] The XCHF method uses a Gaussian-type function that depends directly on the electron-hole separation to improve the form of the wave function at small eh-separations. The attractive nature

of the electron-hole Coulomb interaction increases the importance of the correct behavior in the vicinity of the eh-cusp, which occurs when $r_{\mathrm{eh}} = 0$.[217] Similarly, this method has been shown to improve calculation of the eh-recombination probability due to improved treatment of small eh-separations.[217] Blanton and co-workers have used this method for parabolic quantum dots in a homogeneous field.[40] The XCHF and related methods has been successfully used to treat several electron-hole systems.[40, 215, 216, 217, 218]

The remainder of the chapter is organized as follows. The theory used in these calculations will be detailed briefly in section 4.2. The computational method used in the study will be detailed first in section 4.3. The exciton binding energy will be determined using several combinations of dot size, ligand length, and environmental acidity will be shown and discussed next in section 4.4. Finally, conclusions and future work will appear in section 4.5.

4.2 Theory

The general electron-hole Hamiltonian is[40, 126, 128, 205, 206, 212, 215, 216, 218, 252, 253, 254, 255, 256, 257, 258]

$$
\begin{aligned}
H = & \sum_{ij} \langle i | \frac{-\hbar^2}{2m_{\mathrm{e}}} + v^{\mathrm{e}}_{\mathrm{ext}} | j \rangle e^{\dagger}_i e_j \\
& + \sum_{ij} \langle i | \frac{-\hbar^2}{2m_{\mathrm{h}}} + v^{\mathrm{h}}_{\mathrm{ext}} | j \rangle h^{\dagger}_i h_j \\
& + \sum_{iji'j'} \langle iji'j' | \varepsilon^{-1} r^{-1}_{\mathrm{eh}} | iji'j' \rangle e^{\dagger}_i e_j h^{\dagger}_{i'} h_{j'} \\
& + \sum_{ijkl} w^{\mathrm{ee}}_{ijkl} e^{\dagger}_i e^{\dagger}_j e_l e_k + \sum_{ijkl} w^{\mathrm{hh}}_{ijkl} h^{\dagger}_i h^{\dagger}_j h_l h_k .
\end{aligned}
\tag{4.1}
$$

The wave function used in this work is a N_e and N_h wave function $\Psi_e h(\mathbf{x}_1^\mathrm{e},\ldots,\mathbf{x}_{N_\mathrm{e}}^\mathrm{e},\mathbf{x}_1^\mathrm{h},\ldots,\mathbf{x}_{N_\mathrm{h}}^\mathrm{h})$, where $\mathbf{x}$ is the spatial and spin coordinates for a given coordinate.

The choice of the ansatz is the explicitly correlated Hartree-Fock wave function (XCHF).[40, 215, 216, 217, 218] The method has been full described by Elward and co-workers[216]; therefore, it is briefly described here. The XCHF wave function is

$$\Psi^\mathrm{XCHF} = G\Phi_\mathrm{e}\Phi_\mathrm{h}, \tag{4.2}$$

where Φ_e is the reference wave function for the electron, Φ_h is the reference wave function for the hole, and G is the geminal operator of form

$$G = \sum_{i=1}^{N_\mathrm{e}}\sum_{j=1}^{N_\mathrm{h}} g(r_{ij}), \tag{4.3}$$

$$g(r_\mathrm{eh}) = \sum_{k=1}^{N_g} b_k \exp(\gamma_k r_\mathrm{eh}^2), \tag{4.4}$$

where N_e is the number of electrons, N_h is the number of holes, N_g is the number of sets of geminal parameters. The XCHF method is variational and energy is determined by performing the minimization

$$E_\mathrm{XCHF} = \min_{G,\Phi_\mathrm{e},\Phi_\mathrm{h}} \frac{\langle G\Phi_0|H|G\Phi_0\rangle}{\langle G\Phi_0|G\Phi_0\rangle}, \tag{4.5}$$

where $\Phi_0 = \Phi_\mathrm{e}\Phi_\mathrm{h}$. The minimization is performed more efficiently using the transformed opera-

tors

$$\tilde{H} = G^{\dagger} H G \tag{4.6}$$

$$\tilde{1} = G^{\dagger} G. \tag{4.7}$$

The set of geminal parameters $\{b_k, \gamma_k\}$ were determined by non-linear optimization and the minimization over the reference wave function was performed by self-consistent solution of the coupled Fock equations

$$\tilde{F}_{\mathrm{e}} C_{\mathrm{e}} = \tilde{S}_{\mathrm{e}} C_{\mathrm{e}} \lambda_{\mathrm{e}} \tag{4.8}$$

$$\tilde{F}_{\mathrm{h}} C_{\mathrm{h}} = \tilde{S}_{\mathrm{h}} C_{\mathrm{h}} \lambda_{\mathrm{h}} \tag{4.9}$$

where the tilde indicates that the operators incorporate the transformed operators from Eq. (4.6) and Eq. (4.7).

4.3 Computational method

The system under study is an electron-hole system which is generally described in Eq. (4.1). The values of the effective mass for the electron is $0.13 m_0$, the effective mass of the hole is $0.38 m_0$, where m_0 is the mass of the free electron. The dielectric constant is $6.2 \varepsilon_0$, where ε_0 is the dielectric constant of vacuum. In this system, only generation of a single electron-hole pair is considered. The external potential for system is

$$v_{\mathrm{ext}}^{\alpha} = \frac{1}{2} k_{\alpha} |\mathbf{r}_{\alpha}|^2 + \sum_{A=1}^{N} \frac{Z_A q_{\alpha}}{|\mathbf{r}_{\alpha} - \mathbf{R}_A|} \qquad \alpha = \mathrm{e}, \mathrm{h} \tag{4.10}$$

where $\{Z_A\}$ is the set of point charges, and $\{\mathbf{R}_A\}$ is the set of the point locations, and q_α is the charge on the quasi-particle. A schematic of the charges can be seen in Figure 4.1. The set of point charges for each diameter were determined by placing points on a sphere of the given diameter equidistant. The number of points was determined such that the density of points on the surface of the quantum dot was 3.4 ligands per nm^2. The total number of ligands is given in Table 4.2. The charge vectors were then extended from these points by the length of the ligand. The length of the vectors was determined by using the length of the mercaptocarboxylic acid ligands seen in Figure 4.1.

The number of negative charges corresponding to a quantum dot in an environment pH was calculated by solving the Henderson-Hasselbalch equation to give the ratio of deprotonated to protonated carboxylate groups on the ligands as

$$\%A^- = \frac{10^{\mathrm{p}K_a - \mathrm{pH}}}{1 + 10^{\mathrm{p}K_a - \mathrm{pH}}} \times 100\%. \tag{4.11}$$

Using the $\mathrm{p}K_a = 4.78$ for each carboxylic acid. The percentage of charges at each pH is given in Table 4.1.

The force constants were determined such that the electron and hole would both be found within the diameter of the CdSe qdot by performing the minimization

$$\min_{k_\alpha^{\min}} \left(N_\alpha - \int_0^{\frac{D_{\mathrm{dot}}}{2}} dr r^2 \int d\Omega \rho_\alpha(\mathbf{r}) \right)^2, \tag{4.12}$$

where D_{dot} is the diameter of the quantum dot. The force constants determined by the minimization in Eq. (4.12) are found in Table 4.2. In unoptimized basis calculations, a set of S,P,D Cartesian

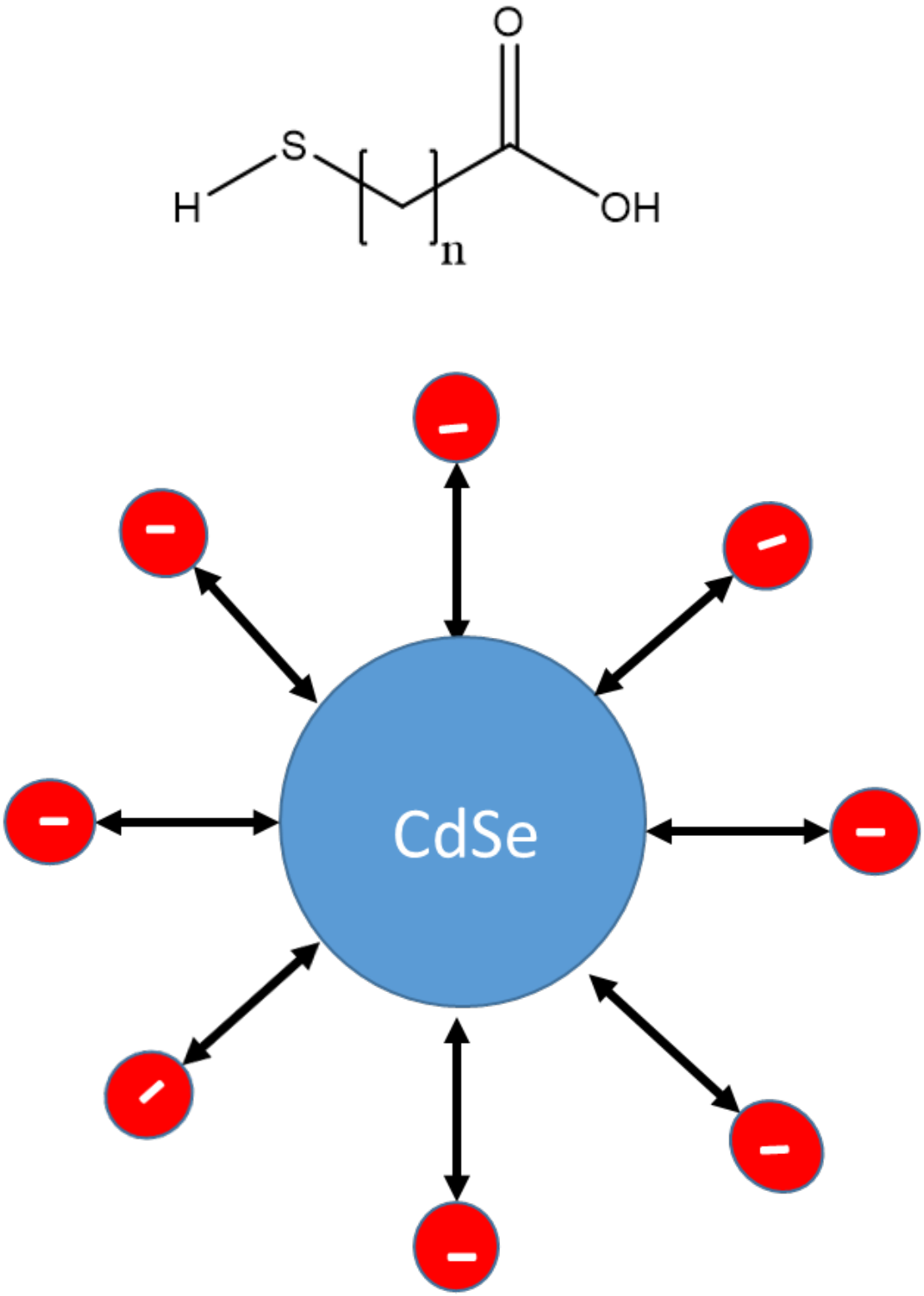

Figure 4.1: Schematic representation of the ligand length system with representative ligand.

Table 4.1: Percentage of negatively charged ligands on a CdSe quantum in a pH environment.

pH	% of negatively charged ligands
1.00	0.02
2.00	0.17
3.00	1.63
4.00	14.23
4.78	50.00
5.00	62.40
6.00	94.40
7.00	99.94
8.00	100.00
9.00	100.00
10.00	100.00
11.00	100.00
12.00	100.00
13.00	100.00
14.00	100.00

Table 4.2: Table of system parameters

Diameter (nm)	Number of Ligands	k_e (atomic units)	k_h (atomic units)
6.0	384	4.016×10^{-5}	1.374×10^{-5}
9.0	864	4.923×10^{-6}	1.684×10^{-6}

Gaussian functions was used, with exponents derived from the force constants in Table 4.2. These exponents are found in Table 4.3.

The geminal parameters in this study were the geminal parameters determined and are found in Table 4.4. The first set of geminal parameters are $b_1 = 1.00$ and $\gamma_1 = 0.00$. The choice of the first set of geminal parameters ensures that the method will contain the Hartree-Fock wave function as a reference, which maintains the correct behavior of wave function at large r_{eh}.

The exciton binding energy is defined as

$$E_B = E^0 - E^{int}, \tag{4.13}$$

Table 4.3: Exponents of basis functions $e^{-\alpha r^2}$.

Dot diameter (nm)	α (atomic units)
6.0	1.14×10^{-3}
9.0	4.00×10^{-4}

Table 4.4: Geminal parameters for 6 nm and 9 nm diameter CdSe qdots.

Dot diameter (nm)	b_2	γ_2	b_3	γ_3
6.0	2.55×10^{-2}	1.86×10^{-2}	1.06×10^{-2}	1.37×10^{-2}
9.0	2.55×10^{-2}	1.86×10^{-2}	1.06×10^{-2}	1.49×10^{-2}

where E^0 is the non-interacting energy, found using the Hamiltonian H^0, and E^{int} is the interacting energy using the fully interacting Hamiltonian H. From the exciton binding energies, a relative difference percentage in exciton binding energy

$$\%D_R = \frac{(E_{\text{B}}^l - E_{\text{B}}^\infty)}{E_{\text{B}}^\infty} \times 100\%, \tag{4.14}$$

where E_B^l is the exciton binding energy at the ligand length l and E_B^∞ is the exciton binding energy for a ligand-free quantum dot.

The non-interacting exciton energies were determined using a full minimization of the non-interacting Hamiltonian

$$H^0 = \lim_{r_{\text{eh}} \to \infty} H, \tag{4.15}$$

to give

$$E^0 = \min_{\Psi} \frac{\langle \Psi | H^0 | \Psi \rangle}{\langle \Psi | \Psi \rangle}. \tag{4.16}$$

The interacting energies were determined using field-free wave functions

$$E = \frac{\langle \Psi | H | \Psi \rangle}{\langle \Psi | \Psi \rangle}. \tag{4.17}$$

4.4 Results

The exciton binding binding energy was determined for 6 nm and 9 nm CdSe quantum dots with a range of ligands containing 1-30 CH_2 units between the thiol and the carboxylic acid and in pH environments from 1 to 14. This range of lengths and environmental acidities gives a full range of possibilities for each parameter. The effect of all ligands protonated to all ligands depronated was observed in these sets of data.

In Figure 4.2, the full set of relative difference percentage of exciton binding energy is seen. In Figure 4.3, a subset of the ligand lengths (1,2,5, 10, 15, 20, 25, 30 CH_2 units) is plotted. Most noticeable in this plot is the regularity with which the relative difference percentage increases as the ligand length becomes longer. With shorter ligands, the decreases in the exciton binding energy was greatest. As the ligands become longer, the effect of the charges decreases as the interaction term is an inverse separation relationship. At pH near the pK_a, the maximum decrease in the exciton binding energy is observed for all ligand lengths.

In Figure 4.4, the full set of relative difference percentage of exciton binding energy for the complete set of pH and ligand lengths for the 9 nm CdSe quantum is shown. The results are similar

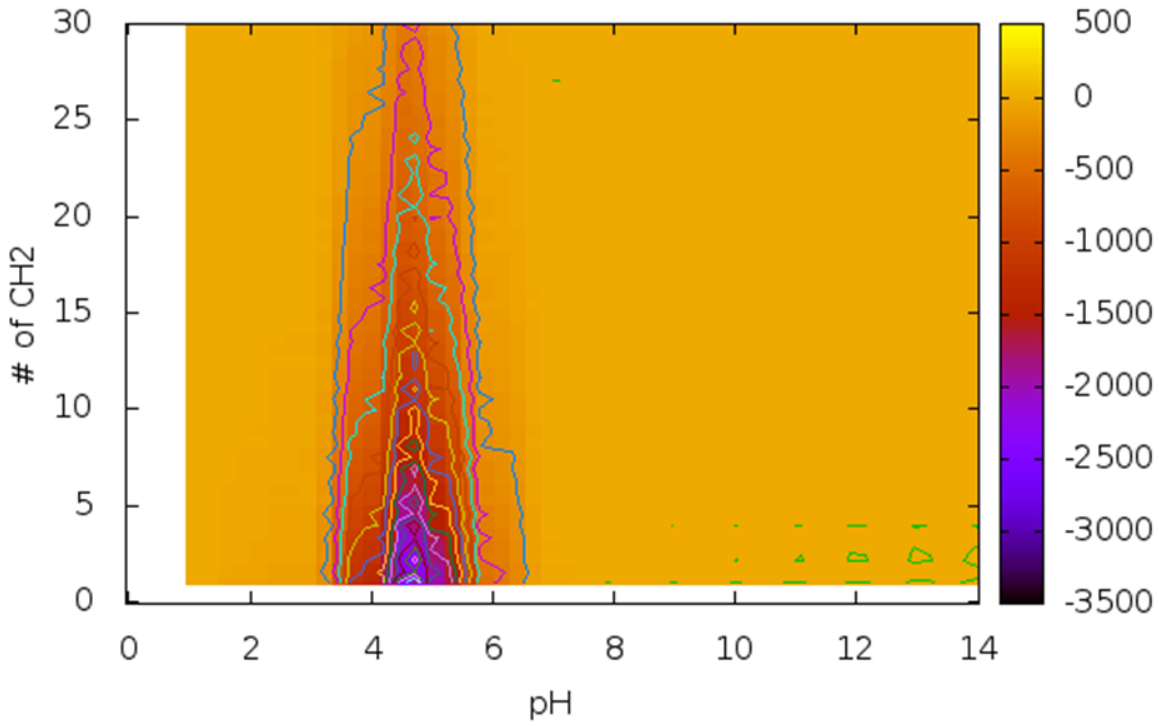

Figure 4.2: Relative difference percentage of exciton binding energy for the 6 nm CdSe quantum dot with ligands from 1-30 CH_2 units and pH 1-14 viewed as a contour plot.

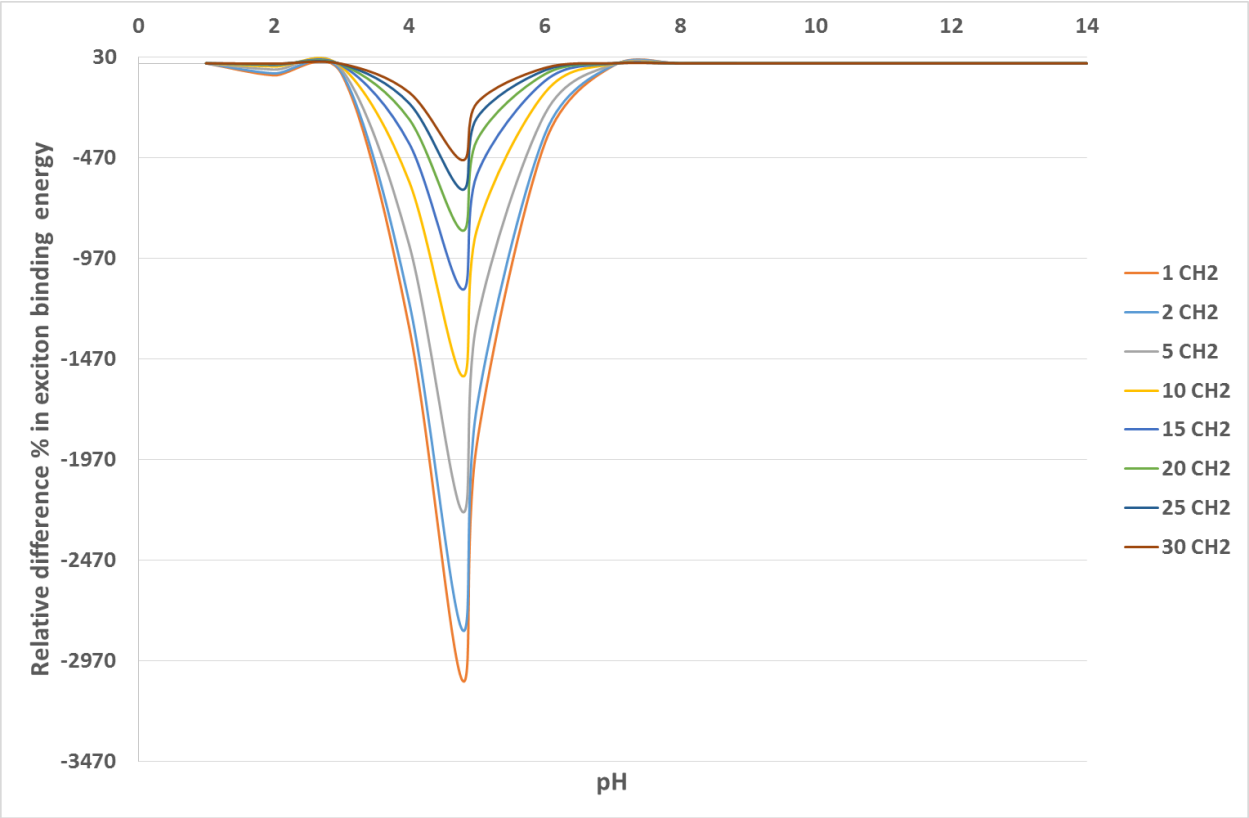

Figure 4.3: Relative difference percentage of exciton binding energy for the 6 nm CdSe quantum dot with ligands from 1-30 CH_2 units and pH 1-14.

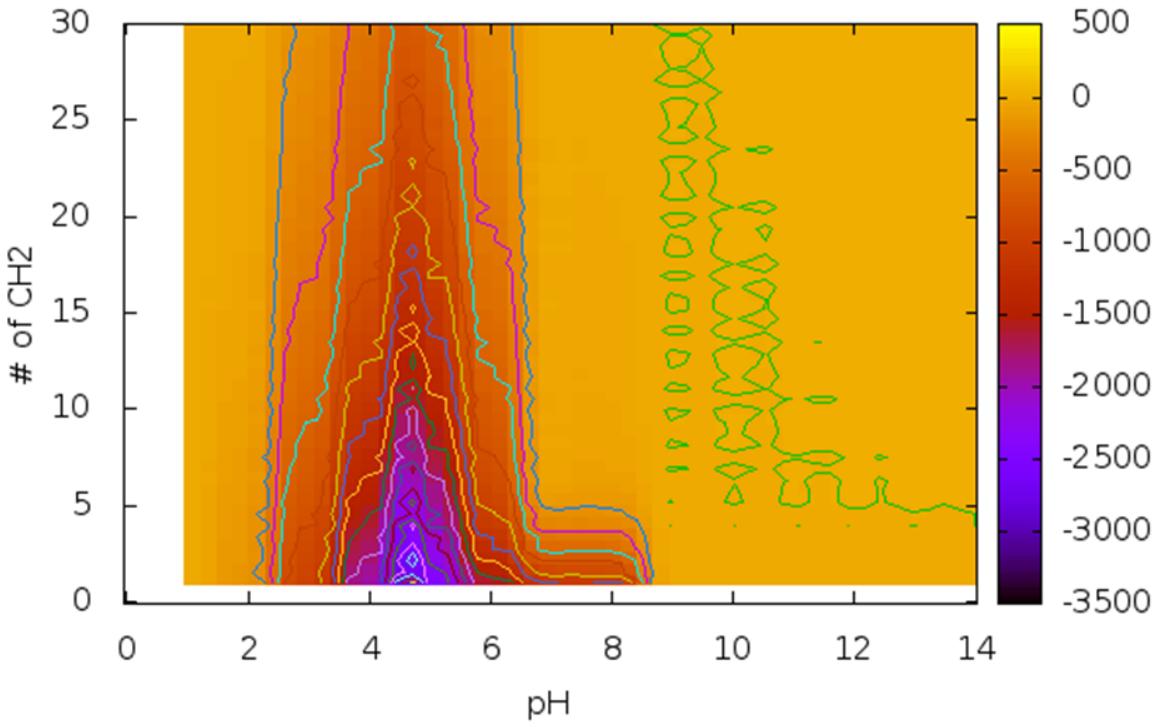

Figure 4.4: Relative difference percentage of exciton binding energy for the 9 nm CdSe quantum dot with ligands from 1-30 CH_2 units and pH 1-14 view as a contour plot.

to Figure 4.2; however, the larger dot shows additional features. The key finding in the 6 nm CdSe quantum dot study was the consistent minimum of the relative difference percentage in the region of pK_a. In Figure 4.2 shows similar results. The greatest decrease in exciton binding energy is in the region about pH = pK_a; however, there is broadening of the region in which the decreases are greatest. In Figure 4.5, a subset of the full data seen in Figure 4.4 is seen in cross-section. In this view, the new feature of the shoulder between pH 6 and 8 is more easily seen.

In both cases 6 nm (Figure 4.2) and 9 nm (Figure 4.4), it is most notable that both low and high pH values gave similar changes in the exciton binding energy. At low pH, the majority (if

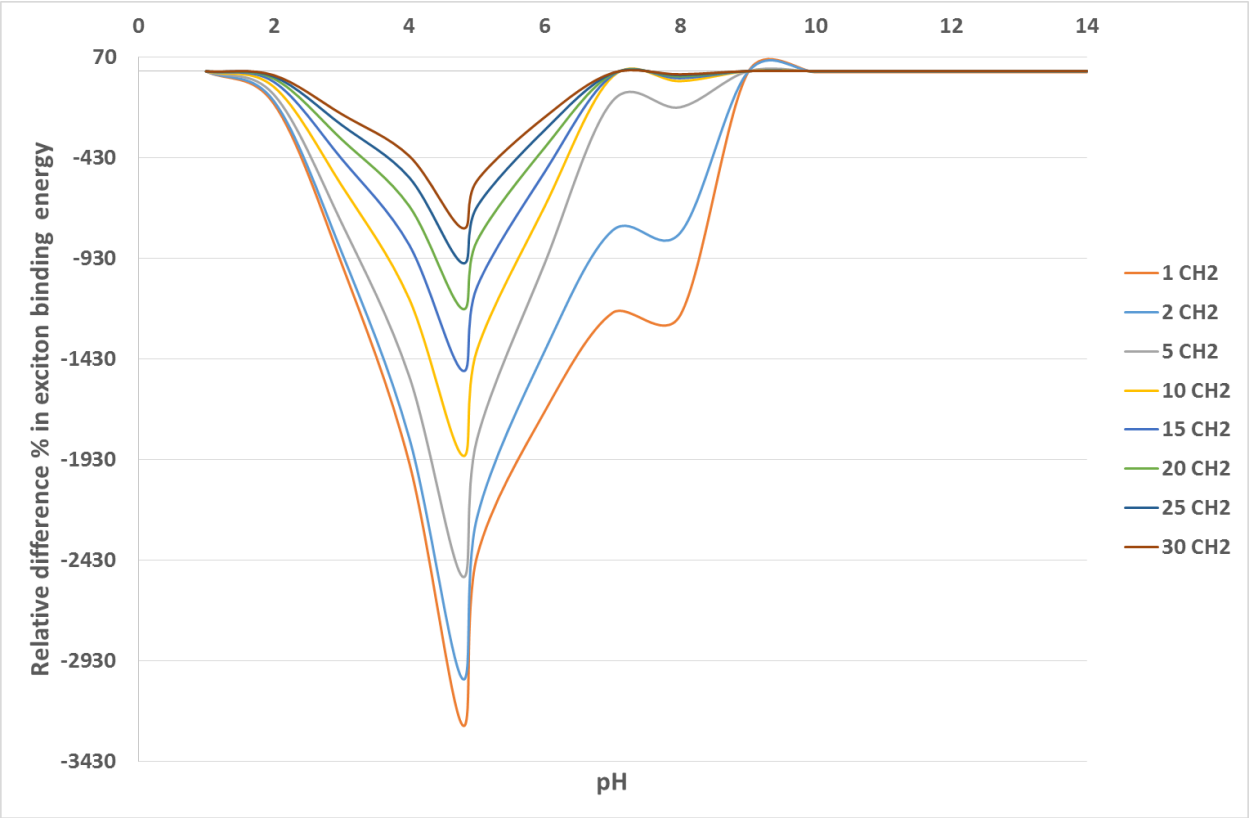

Figure 4.5: Relative difference percentage of exciton binding energy for the 9 nm CdSe quantum dot with ligands from 1-30 CH_2 units and pH 1-14.

not all) of the charges are zero. In the case of the high pH, the majority (if not all) of the charges are negative. This may lead to a homogeneous electric field. As ligand charges are removed randomly, there is a greater possibility for asymmetric in the charges to develop which may lead to inhomogeneous electric field. In this inhomogeneous electric field, both the electron and the hole may localized in very different spatial locations which would leads to a spatial separation of the electron and hole. This spatial separation lowers the exciton binding energy.

4.5 Conclusion

The relationship between the quantum dots and the ligands that passivate the surface is a complex and multifaceted subject. In this work, the relationship between the length of a charged ligand and the exciton binding energy was studied. In isolation from other parameters, the effect of the length of the ligand was studied. It was found that shorter ligands have a greater effect on exciton binding energy than longer ligands. The effect of the environmental pH was also studied. It was found that the maximum decrease in the exciton binding energy occurred when near $\mathrm{pH} = \mathrm{p}K_\mathrm{a}$. This is likely due to the increased inhomogeneity of the electric field that occurs when 50% of the charges have become neutral. Both the low pH and high pH lead to a fairly homogeneous electric field inside the quantum dot.

Ligands on quantum dots play an important role in determining the optical and electronic properties of the systems. However, to what extent each of the many properties (length, charge, functional group type, etc) of the ligand impacts the properties of the system to the largest degree. In experimental systems, it is difficult or impossible to isolate one facet of the multifaceted ligands. In this work, ligand length and charge density were separated from the other variables in the ligand.

This separation may provide a useful insight into nature of the ligand in quantum dot systems. This insight may give further coarse and fine control of the optical and electronic properties of the already versatile quantum dot systems.

Chapter 5: Conclusions

In this work, the effects of electric fields on nanoparticles, the quantum-confined Stark effect, were studied for quantum dot systems. In each of the chapters, different aspects of the optical and electronic properties of nanoparticle systems were developed.

In chapter 2, the electron-hole cumulant was used to define an electron-hole correlation length. The electron-hole correlation length is a useful quantity that measures the length at which the correlation effects become minimal. This quantity was determined in a series of CdSe quantum dots with diameters between 1.25 nm and 20 nm. The electron-hole correlation length was also used to calculate parameters in the explicit correlation operator without performing energy minimizations. This construction of the explicit correlation operator has the potential to greatly improve the computational efficiency of the explicitly correlated methods.

In chapter 3, the effect of homogeneous electric fields on the optical and electronic properties of GaAs parabolic quantum dots. It was found that the electron-hole recombination probability was more influenced than the exciton binding energy. In order to gain the most accurate description of the system, the variational polaron transformation was developed for electron-hole systems.

In chapter 4, the effect of ligand length and environmental pH on the optical and electronic properties of CdSe parabolic quantum dots were determined. It was found that the length of the ligand has a great impact on the exciton binding energy, with shorter ligands causing a greater re-

duction in the exciton binding energy. The change in pH showed the greatest reduction in exciton binding energy when the pH = pK_a. The exciton binding energy behavior is likely tied to the inhomogeneity of electric field as charges are randomly neutralized on the ligands as the environmental pH changes.

5.1 Potential avenues for future work

There are several avenues for future work. The use of the electron-hole correlation length for the construction explicitly correlated operators has only been demonstrated for one system. In the future, this method may become the primary method for either the initial determination of the geminal parameters or as a initial screening for the potential sets of geminal parameters for energy minimization.

The study of the effect of electric fields is a very interesting avenue. Many of the aspects of the ligands can be studied and the effects in isolation are still relatively unknown. By studying various systems, the parameters necessary for customization of the optical and electronic properties will be better understood. Also, one potential project is the effect of a time-dependent electric field. It is of great interest to observe what happens the electric field changes and to see how the system reacts.

Appendices

Chapter A: Derivation of r_{eh}^2

A.1 Introduction

We wish to calculate $\langle r_{\mathrm{eh}}^2 \rangle$ where $\mathbf{r}_{\mathrm{eh}} = \mathbf{r}_{\mathrm{e}} - \mathbf{r}_{\mathrm{h}}$. We begin by

$$\begin{aligned}\langle \Psi(\mathbf{r}_{\mathrm{e}}, \mathbf{r}_{\mathrm{h}}) | r_{\mathrm{eh}}^2 | \Psi(\mathbf{r}_{\mathrm{e}}, \mathbf{r}_{\mathrm{h}}) \rangle &= \langle \Psi(\mathbf{r}_{\mathrm{e}}, \mathbf{r}_{\mathrm{h}}) | (x_{\mathrm{e}} - x_{\mathrm{h}})^2 | \Psi(\mathbf{r}_{\mathrm{e}}, \mathbf{r}_{\mathrm{h}}) \rangle \\ &+ \langle \Psi(\mathbf{r}_{\mathrm{e}}, \mathbf{r}_{\mathrm{h}}) | (y_{\mathrm{e}} - y_{\mathrm{h}})^2 | \Psi(\mathbf{r}_{\mathrm{e}}, \mathbf{r}_{\mathrm{h}}) \rangle \\ &+ \langle \Psi(\mathbf{r}_{\mathrm{e}}, \mathbf{r}_{\mathrm{h}}) | (z_{\mathrm{e}} - z_{\mathrm{h}})^2 | \Psi(\mathbf{r}_{\mathrm{e}}, \mathbf{r}_{\mathrm{h}}) \rangle \end{aligned} \tag{A.1}$$

We develop only the x-term here, since the integrals will be of the same form for each coordinate The first term on the right hand side of Eq. (A.1) is

$$\begin{aligned}\langle \Psi(\mathbf{r}_{\mathrm{e}}, \mathbf{r}_{\mathrm{h}}) | (x_{\mathrm{e}} - x_{\mathrm{h}})^2 | \Psi(\mathbf{r}_{\mathrm{e}}, \mathbf{r}_{\mathrm{h}}) \rangle &= \langle \Psi(\mathbf{r}_{\mathrm{e}}, \mathbf{r}_{\mathrm{h}}) | x_{\mathrm{e}}^2 | \Psi(\mathbf{r}_{\mathrm{e}}, \mathbf{r}_{\mathrm{h}}) \rangle \\ &- 2 \langle \Psi(\mathbf{r}_{\mathrm{e}}, \mathbf{r}_{\mathrm{h}}) | x_{\mathrm{e}} x_{\mathrm{h}} | \Psi(\mathbf{r}_{\mathrm{e}}, \mathbf{r}_{\mathrm{h}}) \rangle \\ &+ \langle \Psi(\mathbf{r}_{\mathrm{e}}, \mathbf{r}_{\mathrm{h}}) | x_{\mathrm{h}}^2 | \Psi(\mathbf{r}_{\mathrm{e}}, \mathbf{r}_{\mathrm{h}}) \rangle \end{aligned} \tag{A.2}$$

A.2 Centered at Zero

If the wavefunction can be seperated as $\Psi(\mathbf{r}_\mathrm{e},\mathbf{r}_\mathrm{h}) = \psi_x(x_\mathrm{e},x_\mathrm{h})\psi_y(y_\mathrm{e},y_\mathrm{h})\psi_z(z_\mathrm{e},z_\mathrm{h})$ and we use a wavefunction $\psi_x(x_\mathrm{e},x_\mathrm{h}) = \phi_x^\mathrm{e}(n_x,\alpha_x)\phi_x^\mathrm{h}(m_x,\beta_x)$, which has been centered at zero.

Then, Eq. (A.2) becomes

$$\begin{aligned}\langle\psi_\mathrm{x}(x_\mathrm{h},x_\mathrm{h})|(x_\mathrm{e}-x_\mathrm{h})^2|\psi_\mathrm{x}(x_\mathrm{e},x_\mathrm{h})\rangle = \langle\phi_x^\mathrm{e}(n_x,\alpha_x)\phi_x^\mathrm{h}(m_x,\beta_x)|\phi_x^\mathrm{e}(n_x+2,\alpha_x)\phi_x^\mathrm{h}(m_x,\beta_x)\rangle \\ -2\langle\phi_x^\mathrm{e}(n_x,\alpha_x)\phi_x^\mathrm{h}(m_x,\beta_x)|\phi_x^\mathrm{e}(n_x+1,\alpha_x)\phi_x^\mathrm{h}(m_x,\beta_x+1)\rangle \\ +\langle\phi_x^\mathrm{e}(n_x,\alpha_x)\phi_x^\mathrm{h}(m_x,\beta_x)|\phi_x^\mathrm{e}(n_x,\alpha_x)\phi_x^\mathrm{h}(m_x+2,\beta_x)\rangle \end{aligned} \tag{A.3}$$

A.3 Generalized Function

A general way to express the wavefunction is

$$\Psi(\mathbf{r}_\mathrm{e},\mathbf{r}_\mathrm{h}) = \phi_\mathrm{e}(\mathbf{r}_\mathrm{e})\phi_\mathrm{h}(\mathbf{r}_\mathrm{h}) \tag{A.4}$$

Each $\phi_\mathrm{e}(\mathbf{r}_\mathrm{e})$ is

$$\phi_\mathrm{e}(\mathbf{r}_\mathrm{e}) = \phi_x^\mathrm{e}(n_x,\alpha_x,A_x)\phi_y^\mathrm{e}(n_y,\alpha_x,A_x)\phi_z^\mathrm{e}(n_z,\alpha_z,A_z), \tag{A.5}$$

where A_x is the x-center (and so on).

We need only derive the expression for one coordinate, which will be x to find the form for

all three components. we will now calculate

$$\langle \phi_x^{\mathrm{e}}(n_x,\alpha_x,A_x)\phi_x^{\mathrm{h}}(m_x,\beta_x,B_x)|(x_{\mathrm{e}}-x_{\mathrm{h}})^2|\phi_x^{\mathrm{e}}(n_x,\alpha_x,A_x)\phi_x^{\mathrm{h}}(m_x,\beta_x,B_x)\rangle \tag{A.6}$$

For which, we need to express $(x_{\mathrm{e}}-x_{\mathrm{h}})^2$ as

$$\begin{aligned}(x_{\mathrm{e}}-x_{\mathrm{h}})^2 &= [(x_{\mathrm{e}}-A_x+A_x)-(x_{\mathrm{h}}-B_x+B_x)]^2\\ &= [(x_{\mathrm{e}}-A_x)-(x_{\mathrm{h}}-B_Y)+(A_x+B_X)]^2\\ &= [(x_{\mathrm{e}}-A_x)-(x_{\mathrm{h}}-B_x)]^2+(A_x-B_y)^2+2(A_x-B_x)[(x_{\mathrm{e}}-A_x)-(x_{\mathrm{h}}-B_x)]\\ &= (x_{\mathrm{e}}-A_x)^2+(x_{\mathrm{h}}-B_x)^2-2(x_{\mathrm{e}}-A_x)(x_{\mathrm{h}}-B_x)+(A_x-B_x)^2\\ &+2(A_x-B_x)[(x_{\mathrm{e}}-A_x)-(x_{\mathrm{h}}-B_x)]\end{aligned} \tag{A.7}$$

Eq. (A.6) is now represented, using Eq. (A.7), as

$$\begin{aligned}&\langle \phi_x^{\mathrm{e}}(n_x,\alpha_x,A_x)\phi_x^{\mathrm{h}}(m_x,\beta_x,B_x)|(x_{\mathrm{e}}-x_{\mathrm{h}})^2|\phi_x^{\mathrm{e}\prime}(n_x,\alpha_x,A_x)\phi_x^{\mathrm{h}\prime}(m_x,\beta_x,B_x)\rangle =\\ &\langle \phi_x^{\mathrm{e}}(n_x,\alpha_x,A_x)\phi_x^{\mathrm{h}}(m_x,\beta_x,B_x)|\phi_x^{\mathrm{e}\prime}(n_x+2,\alpha_x,A_x)\phi_x^{\mathrm{h}\prime}(m_x,\beta_x,B_x)\rangle\\ &+\langle \phi_x^{\mathrm{e}}(n_x,\alpha_x,A_x)\phi_x^{\mathrm{h}}(m_x,\beta_x,B_x)|\phi_x^{\mathrm{e}\prime}(n_x,\alpha_x,A_x)\phi_x^{\mathrm{h}\prime}(m_x+2,\beta_x,B_x)\rangle\\ &-2\langle \phi_x^{\mathrm{e}}(n_x,\alpha_x,A_x)\phi_x^{\mathrm{h}}(m_x,\beta_x,B_x)|\phi_x^{\mathrm{e}\prime}(n_x+1,\alpha_x,A_x)\phi_x^{\mathrm{h}\prime}(m_x+1,\beta_x,B_x)\rangle\\ &+(A_x-B_x)^2\langle \phi_x^{\mathrm{e}}(n_x,\alpha_x,A_x)\phi_x^{\mathrm{h}}(m_x,\beta_x,B_x)|\phi_x^{\mathrm{e}\prime}(n_x,\alpha_x,A_x)\phi_x^{\mathrm{h}\prime}(m_x,\beta_x,B_x)\rangle\\ &+2(A_x-B_x)\langle \phi_x^{\mathrm{e}}(n_x,\alpha_x,A_x)\phi_x^{\mathrm{h}}(m_x,\beta_x,B_x)|\phi_x^{\mathrm{e}\prime}(n_x+1,\alpha_x,A_x)\phi_x^{\mathrm{h}\prime}(m_x,\beta_x,B_x)\rangle\\ &-2(A_x-B_x)\langle \phi_x^{\mathrm{e}}(n_x,\alpha_x,A_x)\phi_x^{\mathrm{h}}(m_x,\beta_x,B_x)|\phi_x^{\mathrm{e}\prime}(n_x,\alpha_x,A_x)\phi_x^{\mathrm{h}\prime}(m_x+1,\beta_x,B_x)\rangle\end{aligned} \tag{A.8}$$

As a check, we set $A_x = B_x = 0$ to find (omitting the center coordinates for emphasis)

$$\begin{aligned}
&\langle \phi_x^{\mathrm{e}}(n_x,\alpha_x)\phi_x^{\mathrm{h}}(m_x,\beta_x)|(x_{\mathrm{e}}-x_{\mathrm{h}})^2|\phi_x^{\mathrm{e}}(n_x,\alpha_x)\phi_x^{\mathrm{h}}(m_x,\beta_x)\rangle = \\
&\langle \phi_x^{\mathrm{e}}(n_x+1,\alpha_x)\phi_x^{\mathrm{h}}(m_x,\beta_x)|\phi_x^{\mathrm{e}}(n_x+1,\alpha_x)\phi_x^{\mathrm{h}}(m_x,\beta_x)\rangle \\
&+\langle \phi_x^{\mathrm{e}}(n_x,\alpha_x)\phi_x^{\mathrm{h}}(m_x+1,\beta_x)|\phi_x^{\mathrm{e}}(n_x,\alpha_x)\phi_x^{\mathrm{h}}(m_x+1,\beta_x)\rangle
\end{aligned} \tag{A.9}$$

which is equal to Eq. (A.3).

Bibliography

[1] Y.-B. Yu, S.-N. Zhu, and K.-X. Guo, "Exciton effects on the nonlinear optical rectification in one-dimensional quantum dots," Physics Letters A **335**, 175 – 181 (2005).

[2] W. Xie, "Effect of an electric field and nonlinear optical rectification of confined excitons in quantum dots," Physica Status Solidi B **246**, 2257–2262 (2009).

[3] C. Cohen-Tannoudji, B. Diu, and F. Laloe, *Quantum Mechanics* (Wiley-VCH Verlag GmbH, 2006).

[4] R. Shankar, *Principles of Quantum Mechanics*, 2nd ed. (Springer London, Limited, 2012).

[5] D. Griffiths, *Introduction to Quantum Mechanics* (Pearson Education, Limited, 2013).

[6] A. Szabo and N. Ostlund, *Modern Quantum Chemistry: Introduction to Advanced Electronic Structure Theory*, Dover Books on Chemistry (Dover Publications, 2012).

[7] L. Piela, "Ideas of quantum chemistry," (Elsevier Science, 2006) Chap. 1, pp. 1–54.

[8] E. Schrödinger, "An undulatory theory of the mechanics of atoms and molecules," Phys. Rev. **28**, 1049–1070 (1926).

[9] F. Pilar, *Elementary Quantum Chemistry*, Dover Books on Chemistry Series (Dover Publications, 2001).

[10] A. Szabo and N. Ostlund, "Modern quantum chemistry: Introduction to advanced electronic structure theory," (Dover Publications, 2012) Chap. 2, pp. 39–107.

[11] L. Piela, *Ideas of Quantum Chemistry* (Elsevier Science, 2006).

[12] J. Leszczynski, *Handbook of Computational Chemistry*, Springer reference (Springer, 2012).

[13] D. McQuarrie, *Quantum Chemistry* (University Science Books, 2008).

[14] D. Cook, *Handbook of Computational Quantum Chemistry*, Dover Books on Chemistry (Dover Publications, 2012).

[15] C. Cramer, *Essentials of Computational Chemistry: Theories and Models* (Wiley, 2005).

[16] E. Lewars, *Computational Chemistry: Introduction to the Theory and Applications of Molecular and Quantum Mechanics* (Springer, 2010).

[17] T. Helgaker, P. Jorgensen, and J. Olsen, *Molecular Electronic-Structure Theory* (Wiley, 2013).

[18] A. Szabo and N. Ostlund, "Modern quantum chemistry: Introduction to advanced electronic structure theory," (Dover Publications, 2012) Chap. 3, pp. 108–229.

[19] L. He and W. Xie, "Effects of an electric field on the confined hydrogen impurity states in a spherical parabolic quantum dot," Superlattices and Microstructures **47**, 266 – 273 (2010).

[20] T. Kato, "On the eigenfunctions of many-particle systems in quantum mechanics," Communications on Pure and Applied Mathematics **10**, 151–177 (1957).

[21] B. di Bartolo, "Optical properties of excited states in solids," (Springer US, 2012) Chap. 1, pp. 1–72.

[22] M. Olivucci, *Computational Photochemistry*, Theoretical and Computational Chemistry (Elsevier Science, 2005).

[23] H. Nakatsuji, "Cluster expansion of the wavefunction. electron correlations in ground and excited states by {SAC} (symmetry-adapted-cluster) and {SAC} {CI} theories," Chemical Physics Letters **67**, 329 – 333 (1979).

[24] H. Nakatsuji, "Cluster expansion of the wavefunction. calculation of electron correlations in ground and excited states by {SAC} and {SAC} {CI} theories," Chemical Physics Letters **67**, 334 – 342 (1979).

[25] A. I. Krylov, "Equation-of-motion coupled-cluster methods for open-shell and electronically excited species: The hitchhiker's guide to fock space," Annual Review of Physical Chemistry **59**, 433–462 (2008), pMID: 18173379, http://dx.doi.org/10.1146/annurev.physchem.59.032607.093602 .

[26] O. Christiansen, H. Koch, and P. Jrgensen, "The second-order approximate coupled cluster singles and doubles model {CC2}," Chemical Physics Letters **243**, 409 – 418 (1995).

[27] A. P. Alivisatos, "Semiconductor clusters, nanocrystals, and quantum dots," Science New Series, **271**, 933–937 (1996).

[28] W. C. Chan, D. J. Maxwell, X. Gao, R. E. Bailey, M. Han, and S. Nie, "Luminescent quantum dots for multiplexed biological detection and imaging," Current Opinion in Biotechnology **13**, 40 – 46 (2002).

[29] A. Zhu, J. Wang, Y. Du, D. Zhao, and Q. Gao, "Effects of Zn impurities on the electronic properties of Pr doped CaTiO 3," Physica B **407**, 849–854 (2012).

[30] Y. Ghosh, B. Mangum, J. Casson, D. Williams, H. Htoon, and J. Hollingsworth, "New insights into the complexities of shell growth and the strong influence of particle volume in nonblinking "giant" core/shell nanocrystal quantum dots," Journal of the American Chemical Society **134**, 9634–9643 (2012).

[31] W. Bae, L. Padilha, Y.-S. Park, H. McDaniel, I. Robel, J. Pietryga, and V. Klimov, "Controlled alloying of the core-shell interface in cdse/cds quantum dots for suppression of auger recombination," ACS Nano **7**, 3411–3419 (2013).

[32] Z. Lin, A. Franceschetti, and M. Lusk, "Size dependence of the multiple exciton generation rate in cdse quantum dots," ACS Nano **5**, 2503–2511 (2011).

[33] R. Alam, D. Fontaine, B. Branchini, and M. Maye, "Designing quantum rods for optimized energy transfer with firefly luciferase enzymes," Nano Letters **12**, 3251–3256 (2012).

[34] H. Han, G. Di Francesco, and M. Maye, "Size control and photophysical properties of quantum dots prepared via a novel tunable hydrothermal route," Journal of Physical Chemistry C **114**, 19270–19277 (2010).

[35] W. J. Parak, L. Manna, F. C. Simmel, D. Gerion, and P. Alivisatos, "Nanoparticles: From theoy to application," (Wiley, 2004) Chap. Quantum Dots, pp. 4–49.

[36] C. Burda, X. Chen, R. Narayanan, and M. A. El-Sayed, "Chemistry and properties of nanocrystals of different shapes," Chemical Reviews **105**, 1025–1102 (2005).

[37] A. Schliwa, M. Winkelnkemper, and D. Bimberg, "Impact of size, shape, and composition on piezoelectric effects and electronic properties of in (ga) asgaas quantum dots," Physical Review B - Condensed Matter and Materials Physics **76**, 205324 (2007).

[38] P. Reiss, M. Protire, and L. Li, "Core/shell semiconductor nanocrystals," Small **5**, 154–168 (2009).

[39] K. Park, Z. Deutsch, J. Li, D. Oron, and S. Weiss, "Single molecule quantum-confined stark effect measurements of semiconductor nanoparticles at room temperature," ACS Nano **6**, 10013–10023 (2012).

[40] C. J. Blanton, C. Brenon, and A. Chakraborty, "Development of polaron-transformed explicitly correlated full configuration interaction method for investigation of quantum-confined Stark effect in GaAs quantum dots," J. Chem. Phys. **138**, 054114 (2013).

[41] J. Teubert, S. Koslowski, S. Lippert, M. Schfer, J. Wallys, G. Dimitrakopulos, T. Kehagias, P. Komninou, A. Das, E. Monroy, and M. Eickhoff, "Ingan/gan quantum dots as optical probes for the electric field at the gan/electrolyte interface," Journal of Applied Physics **114**, 074313 (2013).

[42] Z. Li and W. Liu, "Theoretical and numerical assessments of spin-flip time-dependent density functional theory," J. Chem. Phys. **136**, 024107 (2012).

[43] N. Yaacobi-Gross, M. Soreni-Harari, M. Zimin, S. Kababya, A. Schmidt, and N. Tessler, "Molecular control of quantum-dot internal electric field and its application to cdse-based solar cells," Nature Materials **10**, 974–979 (2011).

[44] F. Liu, E. Proynov, J. G. Yu, T. R. Furlani, and J. Kong, "Comparison of the performance of exact-exchange-based density functional methods," J. Chem. Phys. **137**, 114104 (2012).

[45] M. Green, "The nature of quantum dot capping ligands," Journal of Materials Chemistry **20**, 5797–5809 (2010).

[46] F. Aldeek, L. Balan, J. Lambert, and R. Schneider, "The influence of capping thioalkyl acid on the growth and photoluminescence efficiency of cdte and cdse quantum dots," Nanotechnology **19**, 475401 (2008).

[47] Y. Gao, M. Aerts, C. Sandeep, E. Talgorn, T. Savenije, S. Kinge, L. Siebbeles, and A. Houtepen, "Photoconductivity of pbse quantum-dot solids: Dependence on ligand anchor group and length," ACS Nano **6**, 9606–9614 (2012).

[48] T. Inerbaev, A. Masunov, S. Khondaker, A. Dobrinescu, A.-V. Plamad, and Y. Kawazoe, "Quantum chemistry of quantum dots: Effects of ligands and oxidation," Journal of Chemical Physics **131**, 044106 (2009).

[49] A. Munro and D. Ginger, "Photoluminescence quenching of single cdse nanocrystals by ligand adsorption," Nano Letters **8**, 2585–2590 (2008).

[50] M. Nirmal, B. Dabbousi, M. Bawendi, J. Macklin, J. Trautman, T. Harris, and L. Brus, "Fluorescence intermittency in single cadmium selenide nanocrystals," Nature **383**, 802–804 (1996).

[51] L.-s. Li, J. Hu, W. Yang, and A. P. Alivisatos, "Band gap variation of size- and shape-controlled colloidal cdse quantum rods," Nano Letters **1**, 349–351 (2001).

[52] D. Katz, T. Wizansky, O. Millo, E. Rothenberg, T. Mokari, and U. Banin, "Size-dependent tunneling and optical spectroscopy of cdse quantum rods," Phys. Rev. Lett. **89**, 086801 (2002).

[53] W. E. Buhro and V. L. Colvin, "Semiconductor nanocrystals: Shape matters," Nat Mater **2**, 138–139 (2003).

[54] X. Peng, L. Manna, W. Yang, J. Wickham, E. Scher, A. Kadavanich, and A. P. Alivisatos, "Shape control of cdse nanocrystals," Nature **404**, 59–61 (2000).

[55] K.-T. Yong, Y. Sahoo, K. R. Choudhury, M. T. Swihart, J. R. Minter, and P. N. Prasad, "Shape control of pbse nanocrystals using noble metal seed particles," Nano Letters **6**, 709–714 (2006).

[56] Z. A. Peng and X. Peng, "Mechanisms of the shape evolution of cdse nanocrystals," Journal of the American Chemical Society **123**, 1389–1395 (2001).

[57] T. Mokari, E. Rothenberg, I. Popov, R. Costi, and U. Banin, "Selective growth of metal tips onto semiconductor quantum rods and tetrapods," Science **304**, 1787–1790 (2004).

[58] S. Kudera, L. Carbone, M. F. Casula, R. Cingolani, A. Falqui, E. Snoeck, W. J. Parak, and L. Manna, "Selective growth of pbse on one or both tips of colloidal semiconductor nanorods," Nano Letters **5**, 445–449 (2005).

[59] M. Grundmann, R. Heitz, N. Ledentsov, O. Stier, D. Bimberg, V. Ustinov, P. Kop'ev, Z. Alferov, S. Ruvimov, P. Werner, U. Gsele, and J. Heydenreich, "Electronic structure and energy relaxation in strained inas/gaas quantum pyramids," Superlattices and Microstructures **19**, 81 – 95 (1996).

[60] D. Bimberg, N. N. Ledentsov, M. Grundmann, N. Kirstaedter, O. G. Schmidt, M. H. Mao, V. M. Ustinov, A. Y. Egorov, A. E. Zhukov, P. S. Kopev, Z. I. Alferov, S. S. Ruvimov, U. Gsele, and J. Heydenreich, "Inas-gaas quantum dots: From growth to lasers," physica status solidi (b) **194**, 159–173 (1996).

[61] D. Lu, J. Ahn, S. Freisem, D. Gazula, and D. G. Deppe, "Lens-shaped all-epitaxial quantum dot microcavity," Applied Physics Letters **87**, 163105 (2005).

[62] H. Drexler, D. Leonard, W. Hansen, J. P. Kotthaus, and P. M. Petroff, "Spectroscopy of quantum levels in charge-tunable ingaas quantum dots," Phys. Rev. Lett. **73**, 2252–2255 (1994).

[63] S. S. Nath, D. Chakdar, G. Gope, J. Kakati, B. Kalita, A. Talukdar, and D. K. Avasthi, "Green luminescence of zns and zns:cu quantum dots embedded in zeolite matrix," Journal of Applied Physics **105**, 094305 (2009).

[64] S. Kako, M. Holmes, S. Sergent, M. Brger, D. J. As, and Y. Arakawa, "Single-photon emission from cubic gan quantum dots," Applied Physics Letters **104**, 011101 (2014).

[65] R. Khordad, G. Rezaei, B. Vaseghi, F. Taghizadeh, and H. Kenary, "Study of optical properties in a cubic quantum dot," Optical and Quantum Electronics **42**, 587–600 (2011).

[66] M. R. McPhail and E. A. Weiss, "Role of organosulfur compounds in the growth and final surface chemistry of pbs quantum dots," Chemistry of Materials **26**, 3377–3384 (2014).

[67] R. A. Bley, S. M. Kauzlarich, J. E. Davis, and H. W. H. Lee, "Characterization of silicon nanoparticles prepared from porous silicon," Chemistry of Materials **8**, 1881–1888 (1996).

[68] R. K. Baldwin, K. A. Pettigrew, E. Ratai, M. P. Augustine, and S. M. Kauzlarich, "Solution reduction synthesis of surface stabilized silicon nanoparticles," Chem. Commun. , 1822–1823 (2002).

[69] Z. Kang, C. H. A. Tsang, N.-B. Wong, Z. Zhang, and S.-T. Lee, "Silicon quantum dots:a general photocatalyst for reduction, decomposition, and selective oxidation reactions," Journal of the American Chemical Society **129**, 12090–12091 (2007), pMID: 17880086.

[70] J. R. Heath, J. J. Shiang, and A. P. Alivisatos, "Germanium quantum dots: Optical properties and synthesis," The Journal of Chemical Physics **101**, 1607–1615 (1994).

[71] B. R. Taylor, S. M. Kauzlarich, G. R. Delgado, and H. W. H. Lee, "Solution synthesis and characterization of quantum confined ge nanoparticles," Chemistry of Materials **11**, 2493–2500 (1999).

[72] N. Zaitseva, Z. R. Dai, C. D. Grant, J. Harper, and C. Saw, "Germanium nanocrystals synthesized in high-boiling-point organic solvents," Chemistry of Materials **19**, 5174–5178 (2007).

[73] C. B. Murray, D. J. Norris, and M. G. Bawendi, "Synthesis and characterization of nearly monodisperse cde (e = sulfur, selenium, tellurium) semiconductor nanocrystallites," Journal of the American Chemical Society **115**, 8706–8715 (1993).

[74] S. Dolai, A. Dass, and R. Sardar, "Photophysical and redox properties of molecule-like cdse nanoclusters," Langmuir **29**, 6187–6193 (2013).

[75] S. Dolai, P. R. Nimmala, M. Mandal, B. B. Muhoberac, K. Dria, A. Dass, and R. Sardar, "Isolation of bright blue light-emitting cdse nanocrystals with 6.5 kda core in gram scale: High photoluminescence efficiency controlled by surface ligand chemistry," Chemistry of Materials **26**, 1278–1285 (2014).

[76] J. C. Newton, K. Ramasamy, M. Mandal, G. K. Joshi, A. Kumbhar, and R. Sardar, "Low-temperature synthesis of magic-sized cdse nanoclusters: Influence of ligands on nanocluster growth and photophysical properties," The Journal of Physical Chemistry C **116**, 4380–4389 (2012).

[77] J. Joo, H. B. Na, T. Yu, J. H. Yu, Y. W. Kim, F. Wu, J. Z. Zhang, and T. Hyeon, "Generalized and facile synthesis of semiconducting metal sulfide nanocrystals," Journal of the American Chemical Society **125**, 11100–11105 (2003).

[78] W.-T. Sun, A. Yu, H.-Y. Pan, X.-F. Gao, Q. Chen, and L.-M. Peng, "Cds quantum dots sensitized tio2 nanotube-array photoelectrodes," Journal of the American Chemical Society **130**, 1124–1125 (2008).

[79] J. Ouyang, J. Kuijper, S. Brot, D. Kingston, X. Wu, D. Leek, M. Hu, J. Ripmeester, and K. Yu, "Photoluminescent colloidal cds nanocrystals with high quality via noninjection one-pot synthesis in 1-octadecene," Journal of Physical Chemistry C **113**, 7579–7593 (2009).

[80] L. E. Shea-Rohwer, J. E. Martin, X. Cai, and D. F. Kelley, "Red-emitting quantum dots for solid-state lighting," ECS J. Solid State Sci. Technol. **2**, R3112–R3118 (2013).

[81] J. M. An, A. Franceschetti, and A. Zunger, "The excitonic exchange splitting and radiative lifetime in pbse quantum dots," Nano Lett. **7**, 2129–2135 (2007).

[82] B. Ullrich, H. Xi, and J. S. Wang, "Photoinduced band filling in strongly confined colloidal pbs quantum dots," Journal of Applied Physics **115**, 233503 (2014).

[83] D. Gammon, E. S. Snow, B. V. Shanabrook, D. S. Katzer, and D. Park, "Fine structure splitting in the optical spectra of single gaas quantum dots," Phys. Rev. Lett. **76**, 3005–3008 (1996).

[84] A. A. Guzelian, J. E. B. Katari, A. V. Kadavanich, U. Banin, K. Hamad, E. Juban, A. P. Alivisatos, R. H. Wolters, C. C. Arnold, and J. R. Heath, "Synthesis of size-selected, surface-passivated inp nanocrystals," The Journal of Physical Chemistry **100**, 7212–7219 (1996).

[85] Z. Li, L. Yu, Y. Liu, and S. Sun, "Cds/cdse quantum dots co-sensitized tio2 nanowire/nanotube solar cells with enhanced efficiency," Electrochimica Acta **129**, 379 – 388 (2014).

[86] M. Tomasulo, I. Yildiz, S. Kaanumalle, and F. Raymo, "ph-sensitive ligand for luminescent quantum dots," Langmuir **22**, 10284–10290 (2006).

[87] M. Tomasulo, I. Yildiz, and F. Raymo, "ph-sensitive quantum dots," Journal of Physical Chemistry B **110**, 3853–3855 (2006).

[88] K. Robinson, "Quantum dot coating improves specificity of tumor targeting and imaging," Biophotonics International **11**, 52–53 (2004).

[89] S.-S. Yang, C.-L. Ren, Z.-Y. Zhang, J.-J. Hao, Q. Hu, and X.-G. Chen, "Aqueous synthesis of cdte/cdse core/shell quantum dots as ph-sensitive fluorescence probe for the determination of ascorbic acid," Journal of Fluorescence **21**, 1123–1129 (2011).

[90] V. Albert, S. Ivanov, S. Tretiak, and S. Kilina, "Electronic structure of ligated cdse clusters: Dependence on dft methodology," Journal of Physical Chemistry C **115**, 15793–15800 (2011).

[91] K. Seeger, "Semiconductor physics: An introduction," (U.S. Government Printing Office, 2004) Chap. 11.5, pp. 340–344.

[92] P. Yu and M. Cardona, "Fundamentals of semiconductors: Physics and materials properties," (Springer, 2010) Chap. 6.6.3, pp. 322–329.

[93] D. A. B. Miller, D. S. Chemla, T. C. Damen, A. C. Gossard, W. Wiegmann, T. H. Wood, and C. A. Burrus, "Band-edge electroabsorption in quantum well structures: The quantum-confined stark effect," Phys. Rev. Lett. **53**, 2173–2176 (1984).

[94] D. A. B. Miller, D. S. Chemla, T. C. Damen, A. C. Gossard, W. Wiegmann, T. H. Wood, and C. A. Burrus, "Electric field dependence of optical absorption near the band gap of quantum-well structures," Phys. Rev. B **32**, 1043–1060 (1985).

[95] V. Perebeinos and P. Avouris, "Exciton ionization, franzkeldysh, and stark effects in carbon nanotubes," Nano Letters **7**, 609–613 (2007), pMID: 17261074.

[96] D. Bimberg, M. Stubenrauch, G. Stracke, H. Schmeckebier, and D. Arsenijevic, "Quantum-dot based distributed feedback lasers and electro-absorption modulators for datacom applications," in *Transparent Optical Networks (ICTON), 2012 14th International Conference on* (2012) pp. 1–4.

[97] N. Yaacobi-Gross, N. Garphunkin, O. Solomeshch, A. Vaneski, A. S. Susha, A. L. Rogach, and N. Tessler, "Combining ligand-induced quantum-confined stark effect with type ii heterojunction bilayer structure in cdte and cdse nanocrystal-based solar cells," ACS Nano **6**, 3128–3133 (2012).

[98] S. De, A. Layek, S. Bhattacharya, D. Kumar Das, A. Kadir, A. Bhattacharya, S. Dhar, and A. Chowdhury, "Quantum-confined stark effect in localized luminescent centers within ingan/gan quantum-well based light emitting diodes," Applied Physics Letters **101**, 121919 (2012).

[99] D. Li, J. Zhang, Q. Zhang, and Q. Xiong, "Electric-field-dependent photoconductivity in cds nanowires and nanobelts: Exciton ionization, franzkeldysh, and stark effects," Nano Letters **12**, 2993–2999 (2012).

[100] M. Ghali, K. Ohtani, Y. Ohno, and H. Ohno, "Generation and control of polarization-entangled photons from gaas island quantum dots by an electric field," Nat Commun **3**, 661 (2012).

[101] V. G. Talalaev, J. W. Tomm, A. S. Sokolov, I. V. Shtrom, B. V. Novikov, A. T. Winzer, R. Goldhahn, G. Gobsch, N. D. Zakharov, P. Werner, U. Gsele, G. E. Cirlin, A. A. Tonkikh, V. M. Ustinov, and G. G. Tarasov, "Tuning of the interdot resonance in stacked inas quantum dot arrays by an external electric field," Journal of Applied Physics **100**, 083704 (2006).

[102] Y. Jin and X. Gao, "Plasmonic fluorescent quantum dots," Nat Nano **4**, 571–576 (2009).

[103] F. Erogbogbo, X. Liu, J. L. May, A. Narain, P. Gladding, M. T. Swihart, and P. N. Prasad, "Plasmonic gold and luminescent silicon nanoplatforms for multimode imaging of cancer cells," Integr. Biol. **5**, 144–150 (2013).

[104] J.-W. Liaw and C.-L. Liu, "Plasmonic effect of nanoshelled nanocavity on encapsulated emitter's spontaneous emission," Journal of Quantitative Spectroscopy and Radiative Transfer **112**, 2480 – 2485 (2011).

[105] S. Jin, E. DeMarco, M. J. Pellin, O. K. Farha, G. P. Wiederrecht, and J. T. Hupp, "Distance-engineered plasmon-enhanced light harvesting in cdse quantum dots," The Journal of Physical Chemistry Letters **4**, 3527–3533 (2013), http://pubs.acs.org/doi/pdf/10.1021/jz401801v .

[106] R. West and S. M. Sadeghi, "Enhancement of energy transfer between quantum dots: The impact of metallic nanoparticle sizes," The Journal of Physical Chemistry C **116**, 20496–20503 (2012), http://pubs.acs.org/doi/pdf/10.1021/jp305910j .

[107] S. Jaziri, "Effects of electric and magnetic fields on excitons in quantum dots," Solid State Communications **91**, 171 – 175 (1994).

[108] K. Kowalik, O. Krebs, A. Lematre, S. Laurent, P. Senellart, P. Voisin, and J. A. Gaj, "Influence of an in-plane electric field on exciton fine structure in inas-gaas self-assembled quantum dots," Applied Physics Letters **86**, 041907 (2005).

[109] W. Xie and Q. Xie, "Electric field effects of hydrogenic impurity states in a disc-like quantum dot," Physica B: Condensed Matter **404**, 1625 – 1628 (2009).

[110] L. Lu and W. Xie, "Electric field effects on the intersubband optical absorptions and refractive index in double-electron quantum dots," Physica Scripta **84**, 025703 (2011).

[111] T. Chen, W. Xie, and S. Liang, "The nonlinear optical rectification of an ellipsoidal quantum dot with impurity in the presence of an electric field," Physica E: Low-dimensional Systems and Nanostructures **44**, 786 – 790 (2012).

[112] D. M.-T. Kuo and Y.-C. Chang, "Electron tunneling rate in quantum dots under a uniform electric field," Phys. Rev. B **61**, 11051–11056 (2000).

[113] C. Dane, H. Akbas, S. Minez, and A. Guleroglu, "Electric field effect in a gaas/alas spherical quantum dot," Physica E: Low-dimensional Systems and Nanostructures **41**, 278 – 281 (2008).

[114] M. G. Barseghyan, A. A. Kirakosyan, and C. A. Duque, "Donor-impurity related binding energy and photoinization cross-section in quantum dots: electric and magnetic fields and hydrostatic pressure effects," The European Physical Journal B **72**, 521–529 (2009).

[115] C. M. Duque, M. G. Barseghyan, and C. A. Duque, "Donor impurity in vertically-coupled quantum-dots under hydrostatic pressure and applied electric field," The European Physical Journal B **73**, 309–319 (2010).

[116] C. Dane, H. Akbas, S. Minez, and A. Guleroglu, "Simultaneous effects of electric and magnetic fields in a gaas/alas spherical quantum dot with a hydrogenic impurity," Physica E: Low-dimensional Systems and Nanostructures **42**, 1901 – 1904 (2010).

[117] M. Kirak, S. Ylmaz, M. ahin, and M. Gencaslan, "The electric field effects on the binding energies and the nonlinear optical properties of a donor impurity in a spherical quantum dot," Journal of Applied Physics **109**, 094309 (2011).

[118] R. E. Acosta, A. Zapata, C. Duque, and M. Mora-Ramos, "Electric field effects on excitons in cylindrical quantum dots with asymmetric axial potential. influence on the nonlinear optical properties," Physica E: Low-dimensional Systems and Nanostructures **44**, 1936 – 1944 (2012).

[119] L. He, G. Bester, and A. Zunger, "Singlet-triplet splitting, correlation, and entanglement of two electrons in quantum dot molecules," Phys. Rev. B **72**, 195307 (2005).

[120] B. Szafran, E. Barczyk, F. M. Peeters, and S. Bednarek, "Exciton spectra in vertical stacks of triple and quadruple quantum dots in an electric field," Phys. Rev. B **77**, 115441 (2008).

[121] M. E. Reimer, M. Korkusiński, D. Dalacu, J. Lefebvre, J. Lapointe, P. J. Poole, G. C. Aers, W. R. McKinnon, P. Hawrylak, and R. L. Williams, "Prepositioned single quantum dot in a lateral electric field," Phys. Rev. B **78**, 195301 (2008).

[122] M. Korkusinski, M. E. Reimer, R. L. Williams, and P. Hawrylak, "Engineering photon cascades from multiexciton complexes in a self-assembled quantum dot by a lateral electric field," Phys. Rev. B **79**, 035309 (2009).

[123] A. Kwasniowski and J. Adamowski, "Exchange interaction tuned by electric field in quantum dots," physica status solidi (c) **6**, 821–824 (2009).

[124] W. J. Pasek and B. Szafran, "Negative trion emission spectrum in stacked quantum dots: External electric field and valence band mixing," Phys. Rev. B **85**, 085301 (2012).

[125] J.-W. Luo, R. Singh, A. Zunger, and G. Bester, "Influence of the atomic-scale structure on the exciton fine-structure splitting in ingaas and gaas quantum dots in a vertical electric field," Phys. Rev. B **86**, 161302 (2012).

[126] M. Braskan, M. Lindberg, D. Sundholm, and J. Olsen, "Full configuration interaction calculations of electron-hole correlation effects in strain-induced quantum dots," Physica Status Solidi B **224**, 775–779 (2001).

[127] M. Braskén, M. Lindberg, D. Sundholm, and J. Olsen, "Full configuration interaction calculations of electron-hole correlation effects in strain-induced quantum dots," Phys. Rev. B **61**, 7652–7655 (2000).

[128] S. Corni, M. Brasken, M. Lindberg, J. Olsen, and D. Sundholm, "Electron-hole recombination density matrices obtained from large configuration-interaction expansions," Phys. Rev. B **67**, 853141–853147 (2003).

[129] O. Lehtonen, D. Sundholm, and T. Vanska, "Computational studies of semiconductor quantum dots," Phys. Chem. Chem. Phys. **10**, 4535–4550 (2008).

[130] N. C. Greenham, X. Peng, and A. P. Alivisatos, "Charge separation and transport in conjugated-polymer/semiconductor-nanocrystal composites studied by photoluminescence quenching and photoconductivity," Phys. Rev. B **54**, 17628–17637 (1996).

[131] A. Kongkanand, K. Tvrdy, K. Takechi, M. Kuno, and P. V. Kamat, "Quantum dot solar cells. tuning photoresponse through size and shape control of cdsetio2 architecture," Journal of the American Chemical Society **130**, 4007–4015 (2008).

[132] T. López-Luke, A. Wolcott, L.-p. Xu, S. Chen, Z. Wen, J. Li, E. De La Rosa, and J. Z. Zhang, "Nitrogen-doped and cdse quantum-dot-sensitized nanocrystalline tio2 films for solar energy conversion applications," The Journal of Physical Chemistry C **112**, 1282–1292 (2008).

[133] P. V. Kamat, "Quantum dot solar cells. semiconductor nanocrystals as light harvesters," J. Phys. Chem. C **112**, 18737–18753 (2008).

[134] K. W. Johnston, A. G. Pattantyus-Abraham, J. P. Clifford, S. H. Myrskog, D. D. MacNeil, L. Levina, and E. H. Sargent, "Schottky-quantum dot photovoltaics for efficient infrared power conversion," Applied Physics Letters **92**, 151115 (2008).

[135] J. P. Clifford, K. W. Johnston, L. Levina, and E. H. Sargent, "Schottky barriers to colloidal quantum dot films," Applied Physics Letters **91**, 253117 (2007).

[136] E. J. D. Klem, H. Shukla, S. Hinds, D. D. MacNeil, L. Levina, and E. H. Sargent, "Impact of dithiol treatment and air annealing on the conductivity, mobility, and hole density in pbs colloidal quantum dot solids," Applied Physics Letters **92**, 212105 (2008).

[137] G. I. Koleilat, L. Levina, H. Shukla, S. H. Myrskog, S. Hinds, A. G. Pattantyus-Abraham, and E. H. Sargent, "Efficient, stable infrared photovoltaics based on solution-cast colloidal quantum dots," ACS Nano **2**, 833–840 (2008).

[138] H.-Y. Si, Z.-H. Sun, and H.-L. Zhang, "Photoelectrochemical response from cdse-sensitized anodic oxidation tio2 nanotubes," Colloids and Surfaces A: Physicochemical and Engineering Aspects **313-314**, 604 – 607 (2008), nanoscience and Nanotechnology.

[139] R. Plass, S. Pelet, J. Krueger, M. Grätzel, and U. Bach, "Quantum dot sensitization of organic-inorganic hybrid solar cells," The Journal of Physical Chemistry B **106**, 7578–7580 (2002).

[140] A. Zaban, O. I. Mii, B. A. Gregg, and A. J. Nozik, "Photosensitization of nanoporous tio2 electrodes with inp quantum dots," Langmuir **14**, 3153–3156 (1998).

[141] P. Yu, K. Zhu, A. G. Norman, S. Ferrere, A. J. Frank, and A. J. Nozik, "Nanocrystalline tio2 solar cells sensitized with inas quantum dots," The Journal of Physical Chemistry B **110**, 25451–25454 (2006), pMID: 17165992.

[142] V. I. Klimov, A. A. Mikhailovsky, S. Xu, A. Malko, J. A. Hollingsworth, C. A. Leatherdale, H.-J. Eisler, and M. G. Bawendi, "Optical gain and stimulated emission in nanocrystal quantum dots," Science **290**, 314–317 (2000).

[143] C. Foucher, B. Guilhabert, N. Laurand, and M. D. Dawson, "Wavelength-tunable colloidal quantum dot laser on ultra-thin flexible glass," Appl. Phys. Lett. **104**, 141108 (2014).

[144] Y. Wu and L. V. Asryan, "Direct and indirect capture of carriers into the lasing ground state and the light-current characteristic of quantum dot lasers," J. Appl. Phys. **115**, 103105 (2014).

[145] Y. Wang, V. D. Ta, Y. Gao, T. C. He, R. Chen, E. Mutlugun, H. V. Demir, and H. D. Sun, "Stimulated emission and lasing from cdse/cds/zns core-multi-shell quantum dots by simultaneous three-photon absorption," Adv. Mat. **26**, 2954–2961 (2014).

[146] P. O. Anikeeva, J. E. Halpert, M. G. Bawendi, and V. Bulovc, "Electroluminescence from a mixed red-green-blue colloidal quantum dot monolayer," Nano Lett. **7**, 2196–2200 (2007).

[147] E. Jang, S. Jun, H. Jang, J. Lim, B. Kim, and Y. Kim, "White-light-emitting diodes with quantum dot color converters for display backlights," Advanced Materials **22**, 3076–3080 (2010).

[148] I. S. Sohn, S. Unithrattil, and W. B. Im, "Stacked quantum dot embedded silica film on a phosphor plate for superior performance of white light-emitting diodes," ACS Applied Materials & Interfaces **6**, 5744–5748 (2014).

[149] H. Labiadh, T. Chaabane, L. Balan, N. Becheik, S. Corbel, G. Medjahdi, and R. Schneider, "Preparation of cu-doped zns qds/tio2 nanocomposites with high photocatalytic activity," Applied Catalysis B: Environmental **144**, 29–35 (2013).

[150] H. Yan, J. Yang, G. Ma, G. Wu, X. Zong, Z. Lei, J. Shi, and C. Li, "Visible-light-driven hydrogen production with extremely high quantum efficiency on ptpds/cds photocatalyst," Journal of Catalysis **266**, 165 – 168 (2009).

[151] G.-S. Li, D.-Q. Zhang, and J. C. Yu, "A new visible-light photocatalyst: Cds quantum dots embedded mesoporous tio2," Environmental Science & Technology **43**, 7079–7085 (2009).

[152] U. Soni, P. Tripathy, and S. Sapra, "Photocatalysis from fluorescence-quenched cdse/au nanoheterostructures: A size-dependent study," The Journal of Physical Chemistry Letters **5**, 1909–1916 (2014).

[153] V. Singh, I. J. C. Beltran, J. C. Ribot, and P. Nagpal, "Photocatalysis deconstructed: Design of a new selective catalyst for artificial photosynthesis," Nano Letters **14**, 597–603 (2014).

[154] A. A. Mansur, H. S. Mansur, F. P. Ramanery, L. C. Oliveira, and P. P. Souza, ""green" colloidal zns quantum dots/chitosan nano-photocatalysts for advanced oxidation processes: Study of the photodegradation of organic dye pollutants," Applied Catalysis B: Environmental **158159**, 269 – 279 (2014).

[155] H. Li, R. Liu, S. Lian, Y. Liu, H. Huang, and Z. Kang, "Near-infrared light controlled photocatalytic activity of carbon quantum dots for highly selective oxidation reaction," Nanoscale **5**, 3289–3297 (2013).

[156] A. Pourahmad, "Photocatalytic activity of quantum dots incorporated in molecular sieves for generation of hydrogen," Spectrochimica Acta Part A: Molecular and Biomolecular Spectroscopy **94**, 18 – 22 (2012).

[157] M. A. Holmes, T. K. Townsend, and F. E. Osterloh, "Quantum confinement controlled photocatalytic water splitting by suspended cdse nanocrystals," Chem. Commun. **48**, 371–373 (2012).

[158] Z. Chen and D. Wu, "Colloidal znse quantum dot as ph probes for study of enzyme reaction kinetics by fluorescence spectroscopic technique," Colloids and Surfaces A: Physicochemical and Engineering Aspects **414**, 174–179 (2012).

[159] D. Wu and Z. Chen, "Zns quantum dots as ph probes for study of enzyme reaction kinetics," Enzyme and Microbial Technology **51**, 47–52 (2012).

[160] Z. Deng, Y. Zhang, J. Yue, F. Tang, and Q. Wei, "Green and orange cdte quantum dots as effective ph-sensitive fluorescent probes for dual simultaneous and independent detection of viruses," Journal of Physical Chemistry B **111**, 12024–12031 (2007).

[161] D. Yu, Z. Wang, Y. Liu, L. Jin, Y. Cheng, J. Zhou, and S. Cao, "Quantum dot-based ph probe for quick study of enzyme reaction kinetics," Enzyme and Microbial Technology **41**, 127–132 (2007).

[162] A. Gupta, "Nanomedicine approaches in vascular disease: A review," Nanomedicine: Nanotechnology, Biology, and Medicine **7**, 763–779 (2011).

[163] N. Erathodiyil and J. Ying, "Functionalization of inorganic nanoparticles for bioimaging applications," Accounts of Chemical Research **44**, 925–935 (2011).

[164] S. Nune, P. Gunda, P. Thallapally, Y.-Y. Lin, M. Laird Forrest, and C. Berkland, "Nanoparticles for biomedical imaging," Expert Opinion on Drug Delivery **6**, 1175–1194 (2009).

[165] T. Asefa, C. Duncan, and K. Sharma, "Recent advances in nanostructured chemosensors and biosensors," Analyst **134**, 1980–1990 (2009).

[166] M. Frasco and N. Chaniotakis, "Semiconductor quantum dots in chemical sensors and biosensors," Sensors **9**, 7266–7286 (2009).

[167] W. Yu, "Semiconductor quantum dots: Synthesis and water-solubilization for biomedical applications," Expert Opinion on Biological Therapy **8**, 1571–1581 (2008).

[168] A. Quarta, R. Di Corato, L. Manna, A. Ragusa, and T. Pellegrino, "Fluorescent-magnetic hybrid nanostructures: Preparation, properties, and applications in biology," IEEE Transactions on Nanobioscience **6**, 298–308 (2007).

[169] S. Nie, Y. Xing, G. Kim, and J. Simons, "Nanotechnology applications in cancer," Annual Review of Biomedical Engineering **9**, 257–288 (2007).

[170] X. Gao and S. Dave, "Quantum dots for cancer molecular imaging," Advances in Experimental Medicine and Biology **620**, 58–73 (2007).

[171] B. Ballou, "Quantum dot surfaces for use in vivo and in vitro," Current Topics in Developmental Biology **70**, 103–120 (2005).

[172] I. Medintz, H. Uyeda, E. Goldman, and H. Mattoussi, "Quantum dot bioconjugates for imaging, labelling and sensing," Nature Materials **4**, 435–446 (2005).

[173] R. Bailey, A. Smith, and S. Nie, "Quantum dots in biology and medicine," Physica E: Low-Dimensional Systems and Nanostructures **25**, 1–12 (2004).

[174] J. Huang, T. Leshuk, and F. Gu, "Emerging nanomaterials for targeting subcellular organelles," Nano Today **6**, 478–492 (2011).

[175] J. Lovriá, H. Bazzi, Y. Cuie, G. Fortin, F. Winnik, and D. Maysinger, "Differences in subcellular distribution and toxicity of green and red emitting cdte quantum dots," Journal of Molecular Medicine **83**, 377–385 (2005).

[176] S. Selvan, P. K. Patra, C. Y. Ang, and J. Y. Ying, "Synthesis of silica-coated semiconductor and magnetic quantum dots and their use in the imaging of live cells," Angewandte Chemie International Edition **46**, 2448–2452 (2007).

[177] K.-T. Yong, H. Ding, I. Roy, W.-C. Law, E. J. Bergey, A. Maitra, and P. N. Prasad, "Imaging pancreatic cancer using bioconjugated inp quantum dots," ACS Nano **3**, 502–510 (2009).

[178] X. Yang, Y. Zhuo, S. Zhu, Y. Luo, Y. Feng, and Y. Dou, "Novel and green synthesis of high-fluorescent carbon dots originated from honey for sensing and imaging," Biosensors and Bioelectronics **60**, 292 – 298 (2014).

[179] P. G. Luo, S. Sahu, S.-T. Yang, S. K. Sonkar, J. Wang, H. Wang, G. E. LeCroy, L. Cao, and Y.-P. Sun, "Carbon "quantum" dots for optical bioimaging," J. Mater. Chem. B **1**, 2116–2127 (2013).

[180] H. Zhu, N. Song, and T. Lian, "Wave function engineering for ultrafast charge separation and slow charge recombination in type ii core/shell quantum dots," J. Am. Chem. Soc. **133**, 8762–8771 (2011).

[181] K. Wu, Z. Liu, H. Zhu, and T. Lian, "Exciton annihilation and dissociation dynamics in group iiv cd3p2 quantum dots," The Journal of Physical Chemistry A **117**, 6362–6372 (2013).

[182] M. Grätzel, "Solar energy conversion by dye-sensitized photovoltaic cells," Inorg. Chem. **44**, 6841–6851 (2005).

[183] M. R. Golobostanfard and H. Abdizadeh, "Tandem structured quantum dot/rod sensitized solar cell based onsolvothermal synthesized cdse quantum dots and rods," Journal of Power Sources **256**, 102 – 109 (2014).

[184] S. Mcdonald, G. Konstantatos, S. Zhang, P. Cyr, E. Klem, L. Levina, and E. Sargent, "Solution-processed pbs quantum dot infrared photodetectors and photovoltaics," Nat. Mater. **4**, 138–142 (2005).

[185] T. R. Chetia, D. Barpuzary, and M. Qureshi, "Enhanced photovoltaic performance utilizing effective charge transfers and light scattering effects by the combination of mesoporous, hollow 3d-zno along with 1d-zno in cds quantum dot sensitized solar cells," Phys. Chem. Chem. Phys. **16**, 9625–9633 (2014).

[186] G. Malloci, L. Chiodo, A. Rubio, and A. Mattoni, "Structural and optoelectronic properties of unsaturated zno and zns nanoclusters," J. Phys. Chem. C **116**, 8741–8746 (2012).

[187] A. Castro, J. Werschnik, and E. K. U. Gross, "Controlling the dynamics of many-electron systems from first principles: A combination of optimal control and time-dependent density-functional theory," Phys. Rev. Lett. **109**, 153603 (2012).

[188] C. A. Ullrich and G. Vignale, "Collective charge-density excitations of noncircular quantum dots in a magnetic field," Phys. Rev. B **61**, 2729–2736 (2000).

[189] S. A. Fischer, A. M. Crotty, S. V. Kilina, S. A. Ivanov, and S. Tretiak, "Passivating ligand and solvent contributions to the electronic properties of semiconductor nanocrystals," Nanoscale **4**, 904–914 (2012).

[190] K. Hyeon-Deuk and O. V. Prezhdo, "Multiple exciton generation and recombination dynamics in small si and cdse quantum dots: An ab initio time-domain study," ACS Nano **6**, 1239–1250 (2012).

[191] E. Badaeva, J. W. May, J. Ma, D. R. Gamelin, and X. Li, "Characterization of excited-state magnetic exchange in mn2+-doped zno quantum dots using time-dependent density functional theory," J. Phys. Chem. C **115**, 20986–20991 (2011).

[192] M. L. del Puerto, M. L. Tiago, and J. R. Chelikowsky, "Excitonic effects and optical properties of passivated cdse clusters," Phys. Rev. Lett. **97**, 096401 (2006).

[193] M. C. Troparevsky, L. Kronik, and J. R. Chelikowsky, "Optical properties of cdse quantum dots," J. Chem. Phys. **119**, 2284–2287 (2003).

[194] D. Neuhauser, E. Rabani, and R. Baer, "Expeditious stochastic approach for mp2 energies in large electronic systems," J. Chem. Theory Comput. **9**, 24–27 (2013).

[195] V. Janis and V. Pokorny, "Quantum transport in strongly disordered crystals: Electrical conductivity with large negative vertex corrections," J. Phys: Conf. Ser. **400**, 042023 (2012).

[196] G. Pal, G. Lefkidis, H. C. Schneider, and W. Hübner, "Optical response of small closed-shell sodium clusters," J. Chem. Phys. **133**, 154309 (2010).

[197] G. Pal, Y. Pavlyukh, W. Hübner, and H. C. Schneider, "Optical absorption spectra of finite systems from a conserving Bethe-Salpeter equation approach," Euro. Phys. J. B **79**, 327–334 (2011).

[198] V. Perebeinos, J. Tersoff, and P. Avouris, "Radiative lifetime of excitons in carbon nanotubes," Nano Lett. **5**, 2495–2499 (2005).

[199] P. Puschnig and C. Ambrosch-Draxl, "Optical absorption spectra of semiconductors and insulators including electron-hole correlations: An ab initio study within the LAPW method," Phys. Rev. B **66**, 1651051–1651059 (2002).

[200] M. Rohlfing and S. G. Louie, "Electron-hole excitations in semiconductors and insulators," Phys. Rev. Lett. **81**, 2312–2315 (1998).

[201] Y.-F. Jiang, N.-P. Wang, and M. Rohlfing, "Quasiparticle band structure and optical spectrum of libr," Euro. Phys. J. B **86**, 1–6 (2013).

[202] Y. Ping, D. Rocca, D. Lu, and G. Galli, "¡i¿ab initio¡/i¿ calculations of absorption spectra of semiconducting nanowires within many-body perturbation theory," Phys. Rev. B **85**, 035316 (2012).

[203] M. Rohlfing and S. G. Louie, "Electron-hole excitations and optical spectra from first principles," Phys. Rev. B **62**, 4927–4944 (2000).

[204] M. Brasken, S. Corni, M. Lindberg, J. Olsen, and D. Sundholm, "Full configuration interaction studies of phonon and photon transition rates in semiconductor quantum dots," Mole. Phys. **100**, 911–918 (2002).

[205] S. Corni, M. Brasken, M. Lindberg, J. Olsen, and D. Sundholm, "Stabilization energies of charged multiexciton complexes calculated at configuration interaction level," Physica E **18**, 436–442 (2003).

[206] Y. Z. Hu, M. Lindberg, and S. W. Koch, "Theory of optically excited intrinsic semiconductor quantum dots," Phys. Rev. B **42**, 1713–1723 (1990).

[207] A. Franceschetti and A. Zunger, "Exciton dissociation and interdot transport in cdse quantum-dot molecules," Phys. Rev. B **63**, 153304 (2001).

[208] E. Rabani, B. Hetnyi, B. J. Berne, and L. E. Brus, "Electronic properties of cdse nanocrystals in the absence and presence of a dielectric medium," J. Chem. Phys. **110**, 5355–5369 (1999).

[209] D. Farmanzadeh and L. Tabari, "An ab initio study of the ground and excited states of mercaptoacetic acid-capped silicon quantum dots," Monatsh. Chem. **144**, 1281–1286 (2013).

[210] J. Shumway, "Quantum Monte Carlo simulation of exciton-exciton scattering in a GaAs/AlGaAs quantum well," Physica E **32**, 273–276 (2006).

[211] J. Shumway and D. M. Ceperley, "Quantum Monte Carlo simulations of exciton condensates," Solid State Commun. **134**, 19–22 (2005).

[212] X. Zhu, M. S. Hybertsen, and P. B. Littlewood, "Electron-hole system revisited: A variational quantum Monte Carlo study," Phys. Rev. B **54**, 13575–13580 (1996).

[213] M. Harowitz, D. Shin, and J. Shumway, "Path-integral quantum Monte Carlo techniques for self-assembled quantum dots," J. Low Temp. Phys. **140**, 211–226 (2005).

[214] M. Harowitz and J. Shumway, "Path integral simulations of charged multiexcitons in InGaAs/GaAs quantum dots," in *PHYSICS OF SEMICONDUCTORS: 27th International Conference on the Physics of Semiconductors, ICPS-27*, Vol. 772 (2005) pp. 697–698.

[215] J. M. Elward and A. Chakraborty, "Effect of dot size on exciton binding energy and electron-hole recombination probability in CdSe quantum dots," J. Chem. Theory Comput. **9**, 4351–4359 (2013).

[216] J. M. Elward, J. Hoffman, and A. Chakraborty, "Investigation of electron-hole correlation using explicitly correlated configuration interaction method," Chem. Phys. Lett. **535**, 182–186 (2012).

[217] J. M. Elward, J. Hoja, and A. Chakraborty, "Variational solution of the congruently transformed Hamiltonian for many-electron systems using a full-configuration-interaction calculation," Phys. Rev. A **86**, 062504 (2012).

[218] J. M. Elward, B. Thallinger, and A. Chakraborty, "Calculation of electron-hole recombination probability using explicitly correlated Hartree-Fock method," J. Chem. Phys. **136**, 124105 (2012).

[219] L. M. Sander, H. B. Shore, and L. J. Sham, "Surface structure of electron-hole droplets," Phys. Rev. Lett. **31**, 533–536 (1973).

[220] S. G. Brush, "History of the Lenz-Ising model," Rev. Mod. Phys. **39**, 883–893 (1967).

[221] A. A. Middleton and D. S. Fisher, "Three-dimensional random-field ising magnet: Interfaces, scaling, and the nature of states," Phys. Rev. B **65**, 134411 (2002).

[222] A. A. Middleton and N. S. Wingreen, "Collective transport in arrays of small metallic dots," Phys. Rev. Lett. **71**, 3198–3201 (1993).

[223] C. K. Thomas and A. A. Middleton, "Exact algorithm for sampling the two-dimensional ising spin glass," Phys. Rev. E **80**, 046708 (2009).

[224] C. Domb and G. S. Joyce, "Cluster expansion for a polymer chain," J. Phys. C: Solid State Phys. **5**, 956–976 (1972).

[225] P. D. Gujrati, "A binary mixture of monodisperse polymers of fixed architectures, and the critical and the theta states," J. Chem. Phys. **108**, 5104–5121 (1998).

[226] J. L. Spouge, "Exact solutions for diffusion-reaction processes in one dimension: II. Spatial distributions," J. Phys. A: Math. Gen. **21**, 4183–4199 (1988).

[227] A. Vilenkin, "The theory of melting in heteropolymers. I. Random chains," Journal of Statistical Physics **19**, 391–404 (1978).

[228] L. Luer, S. Hoseinkhani, D. Polli, J. Crochet, T. Hertel, and G. Lanzani, "Size and mobility of excitons in (6, 5) carbonnanotubes," Nat. Phys. **5**, 54–58 (2009).

[229] S. W. Koch, W. Hoyer, M. Kira, and V. S. Filinov, "Exciton ionization in semiconductors," Phys. Status Solidi B **238**, 404–410 (2003).

[230] P. Corfdir, B. Van Hattem, E. Uccelli, S. Conesa-Boj, P. Lefebvre, A. Fontcuberta I Morral, and R. T. Phillips, "Three-dimensional magneto-photoluminescence as a probe of the electronic properties of crystal-phase quantum disks in GaAs nanowires," Nano Lett. **13**, 5303–5310 (2013).

[231] E. I. Proynov and D. R. Salahub, "Simple but efficient correlation functional from a model pair-correlation function," Phys. Rev. B **49**, 7874–7886 (1994).

[232] E. I. Proynov, A. Vela, and D. R. Salahub, "Gradient-free exchange-correlation functional beyond the local-spin-density approximation," Phys. Rev. A **50**, 3766–3774 (1994).

[233] E. I. Proynov, A. Vela, and D. R. Salahub, "Nonlocal correlation functional involving the Laplacian of the density," Chem. Phys. Lett. **230**, 419–428 (1994).

[234] E. I. Proynov, A. Vela, and D. R. Salahub, "Nonlocal correlation functional involving the Laplacian of the density (Chem. Phys. Letters 230 (1994) 419) (PII:0009-2614(94)01189-3)," Chem. Phys. Lett. **234**, 462 (1995).

[235] D. A. Mazziotti, "Quantum chemistry without wave functions: Two-electron reduced density matrices," Acc. Chem. Res. **39**, 207–215 (2006).

[236] D. Mazziotti, "Chapter 3: Variational two-electron reduced-density-matrix theory," Adv. Chem. Phys. **134**, 21–59 (2007).

[237] D. Mazziotti, "Two-electron reduced density matrix as the basic variable in many-electron quantum chemistry and physics," Chem. Rev. **112**, 244–262 (2012).

[238] D. Rohr, J. Toulouse, and K. Pernal, "Combining density-functional theory and density-matrix-functional theory," Phys. Rev. A **82**, 052502 (2010).

[239] D. Rohr and K. Pernal, "Open-shell reduced density matrix functional theory," J. Chem. Phys. **135**, 074104 (2011).

[240] A. Rajam, I. Raczkowska, and N. Maitra, "Semiclassical electron correlation in density-matrix time propagation," Phys. Rev. Lett. **105**, 113002 (2010).

[241] P. Elliott and N. Maitra, "Electron correlation via frozen gaussian dynamics," J. Chem. Phys. **135**, 104110 (2011).

[242] K. Chatterjee and K. Pernal, "Excitation energies from extended random phase approximation employed with approximate one- and two-electron reduced density matrices," J. Chem. Phys. **137**, 204109 (2012).

[243] P. Joergensen, *Second Quantization-Based Methods in Quantum Chemistry* (Elsevier Science, 2012).

[244] W. Nolting and W. D. Brewer, *Fundamentals of Many-body Physics: Principles and Methods* (Springer, 2009).

[245] G. C. Wick, "The evaluation of the collision matrix," Phys. Rev. **80**, 268–272 (1950).

[246] W. Kutzelnigg and D. Mukherjee, "Normal order and extended wick theorem for a multiconfiguration reference wave function," The Journal of Chemical Physics **107**, 432–449 (1997).

[247] R. Parr and W. Yang, *Density-Functional Theory of Atoms and Molecules*, International Series of Monographs on Chemistry (Oxford University Press, USA, 1994).

[248] W. McComb, *Renormalization Methods: A Guide For Beginners* (OUP Oxford, 2007).

[249] R. Mattuck, *A Guide to Feynman Diagrams in the Many-Body Problem*, Dover Books on Physics (Dover Publications, 2012).

[250] A. Fetter and J. Walecka, *Quantum Theory of Many-particle Systems*, Dover Books on Physics (Dover Publications, 2003).

[251] T. D. Crawford and H. F. Schaefer, "An introduction to coupled cluster theory for computational chemists," in *Reviews in Computational Chemistry* (John Wiley & Sons, Inc., 2007) pp. 33–136.

[252] E. A. Burovski, A. S. Mishchenko, N. V. Prokof'ev, and B. V. Svistunov, "Diagrammatic quantum monte carlo for two-body problems: Applied to excitons," Phys. Rev. Lett. **87**, 186402 (2001).

[253] M. Wimmer, S. V. Nair, and J. Shumway, "Biexciton recombination rates in self-assembled quantum dots," Phys. Rev. B **73**, 165305 (2006).

[254] U. Woggon, *Optical Properties of Semiconductor Quantum Dots*, Springer Tracts in Modern Physics (Springer Berlin Heidelberg, 2013).

[255] S. Corni, M. Braskén, M. Lindberg, J. Olsen, and D. Sundholm, "Size dependence of the electron-hole recombination rates in semiconductor quantum dots," Phys. Rev. B **67**, 453131–453139 (2003).

[256] T. Vanska, M. Lindberg, J. Olsen, and D. Sundholm, "Computational methods for studies of multiexciton complexes," Physica Status Solidi B **243**, 4035–4045 (2006).

[257] T. Vänskä and D. Sundholm, "Interpretation of the photoluminescence spectrum of double quantum rings," Phys. Rev. B **82**, 085306 (2010).

[258] D. Sundholm and T. Vanska, "Computational methods for studies of semiconductor quantum dots and rings," Annu. Rep. Prog. Chem., Sect. C: Phys. Chem. **108**, 96–125 (2012).

[259] S. Francoeur and S. Marcet, "Effects of symmetry-breaking perturbations on excitonic states bound to systems of reduced symmetry," Journal of Applied Physics **108**, 043710 (2010).

[260] O. Takagi and T. Saso, "Magnetic field effects on transport properties of a quantum dot studied by modified perturbation theory," Journal of the Physical Society of Japan **68**, 1997–2005 (1999).

[261] G. Onida and A. Rubio, "Electronic excitations: density-functional versus many-body Green's-function approaches," Reviews of Modern Physics **74**, 601–659 (2002).

[262] S. Suhai, "Green's-function study of optical properties of polymers: Charge-transfer exciton spectra of polydiacetylenes," Physical Review B **29**, 4570 (1984).

[263] Y. Ma, M. Rohlfing, and C. Molteni, "Modeling the Excited States of Biological Chromophores within Many-Body Green's Function Theory," Journal of Chemical Theory and Computation **6**, 257–265 (2010).

[264] A. Cancio and Y. Chang, "Quantum Monte Carlo studies of binding energy and radiative lifetime of bound excitons in direct-gap semiconductors," Physical Review B **47**, 13246 (1993).

[265] E. Wang, Y. Zhou, C. Ting, J. Zhang, T. Pang, and C. Chen, "Excitons in spatially separated electronhole systems: A quantum Monte Carlo study," Journal of applied physics **78**, 7099–7102 (1995).

[266] Y. Takahashi, "Monte Carlo simulations of the spatial transport of excitons in a quantum well structure." Physical review. B, Condensed matter **53**, 7322–7333 (1996).

[267] J. Shumway and D. M. Ceperley, "Quantum Monte Carlo treatment of elastic exciton-exciton scattering," Phys. Rev. B **63**, 1652091–1652097 (2001).

[268] J. G. Pedersen, L. Zhang, M. J. Gilbert, and J. Shumway, "A path integral study of the role of correlation in exchange coupling of spins in double quantum dots and optical lattices," Journal of Physics: Condensed Matter **22**, 145301 (2010).

[269] P. Laufer and J. Krieger, "Test of density-functional approximations in an exactly soluble model," Physical Review A **33**, 1480 (1986).

[270] W. Que, "Excitons in quantum dots with parabolic confinement," Phys. Rev. B **45**, 11036–11041 (1992).

[271] W. Que, "Excitons in quantum dots with parabolic confinement," Physical Review B **45**, 11036 (1992).

[272] M. Taut, "Two electrons in an external oscillator potential: Particular analytic solutions of a Coulomb correlation problem," Physical Review A **48**, 3561–3566 (1993).

[273] S. Kais, D. R. Herschbach, N. C. Handy, C. W. Murray, and G. J. Laming, "Density functionals and dimensional renormalization for an exactly solvable model," The Journal of Chemical Physics **99**, 417 (1993).

[274] C. Filippi, C. Umrigar, and M. Taut, "Comparison of exact and approximate density functionals for an exactly soluble model," The Journal of chemical physics **100**, 1290 (1994).

[275] Z. Qian and V. Sahni, "Physics of transformation from Schrodinger theory to Kohn-Sham density-functional theory: Applications to an exactly solvable model," Physical Review A **57**, 2527–2538 (1998).

[276] M. Taut, A. Ernst, and H. Eschrig, "Two electrons in an external oscillator potential: exact solution versus one-particle approximations," Journal of Physics B: Atomic, Molecular and Optical Physics **31**, 2689 (1998).

[277] J. Karwowski and L. Cyrnek, "A class of exactly solvable Schrödinger equations," Collection of Czechoslovak Chemical Communications **70**, 864–880 (2005).

[278] P. Ramvall, S. Tanaka, S. Nomura, P. Riblet, and Y. Aoyagi, "Observation of confinement-dependent exciton binding energy of gan quantum dots," Applied Physics Letters **73**, 1104–1106 (1998).

[279] M. Bayer, S. Walck, T. Reinecke, and A. Forchel, "Exciton binding energies and diamagnetic shifts in semiconductor quantum wires and quantum dots," Physical Review B - Condensed Matter and Materials Physics **57**, 6584–6591 (1998).

[280] R. G. Parr and W. Yang, *Density-functional theory of atoms and molecules*, Vol. 16 (Oxford university press, 1989) pp. 32–35.

[281] T. Juhasz and D. Mazziotti, "The cumulant two-particle reduced density matrix as a measure of electron correlation and entanglement," J. Chem. Phys. **125**, 174105 (2006).

[282] A. J. Coleman, "Density matrices in the quantum theory of matter: Energy, intracules and extracules," Int. J. Quantum Chem. **1**, 457–464 (1967).

[283] J. Ugalde, C. Sarasola, L. Domnguez, and R. Bovd, "The evaluation of electronic extracule and intracule densities and related probability functions in terms of gaussian basis functions," J. Math. Chem. **6**, 51–61 (1991).

[284] T. Koga and H. Matsuyama, "Electronic extracule moments of atoms in position and momentum spaces," J. Chem. Phys. **108**, 3424–3430 (1998).

[285] P. Gill, A. Lee, N. Nair, and R. Adamson, "Insights from coulomb and exchange intracules," THEOCHEM **506**, 303–312 (2000).

[286] P. Gill, D. O'Neill, and N. Besley, "Two-electron distribution functions and intracules," Theor. Chem. Acc. **109**, 241–250 (2003).

[287] N. Besley, D. O'Neill, and P. Gill, "Computation of molecular hartree-fock wigner intracules," J. Chem. Phys. **118**, 2033–2038 (2003).

[288] P. Gill, D. Crittenden, D. O'Neill, and N. Besley, "A family of intracules, a conjecture and the electron correlation problem," Phys. Chem. Chem. Phys. **8**, 15–25 (2006).

[289] M. G. Bayne, J. Drogo, and A. Chakraborty, "Infinite-order diagrammatic summation approach to the explicitly correlated congruent transformed hamiltonian," Phys. Rev. A **89**, 032515 (2014).

[290] M. El-Said, "The ground-state energy of an exciton in a parabolic quantum dot," Semicond. Sci. Technol. **9**, 272 (1994).

[291] A. Nenashev, S. Baranovskii, M. Wiemer, F. Jansson, R. Osterbacka, A. Dvurechenskii, and F. Gebhard, "Theory of exciton dissociation at the interface between a conjugated polymer and an electron acceptor," Phys. Rev. B **84**, 035210 (2011).

[292] A. Poszwa, "Relativistic electron confined by isotropic parabolic potential," Phys. Rev. A **82**, 052110 (2010).

[293] V. Halonen, T. Chakraborty, and P. Pietilinen, "Excitons in a parabolic quantum dot in magnetic fields," Phys. Rev. B **45**, 5980–5985 (1992).

[294] J. Song and S. Ulloa, "Magnetic field effects on quantum ring excitons," Phys. Rev. B **63**, 1253021–1253029 (2001).

[295] M. Taut, P. MacHon, and H. Eschrig, "Violation of noninteracting v -representability of the exact solutions of the schrödinger equation for a two-electron quantum dot in a homogeneous magnetic field," Phys. Rev. A **80**, 022517 (2009).

[296] A. Kolovsky, F. Grusdt, and M. Fleischhauer, "Quantum particle in a parabolic lattice in the presence of a gauge field," Phys. Rev. A **89**, 033607 (2014).

[297] A. Trojnar, E. Kadantsev, M. Korkusiski, and P. Hawrylak, "Theory of fine structure of correlated exciton states in self-assembled semiconductor quantum dots in a magnetic field," Phys. Rev. B **84**, 245314 (2011).

[298] L. Fernandez, Y.ndez-Menchero and H. Summers, "Stark effect in neutral hydrogen by direct integration of the hamiltonian in parabolic coordinates," Phys. Rev. A **88**, 022509 (2013).

[299] Y. Fernandez, M. Vasilevskiy, C. Trallero-Giner, and A. Kavokin, "Condensed exciton polaritons in a two-dimensional trap: Elementary excitations and shaping by a gaussian pump beam," Phys. Rev. B **87**, 195441 (2013).

[300] A. Rey, G. Pupillo, C. Clark, and C. Williams, "Ultracold atoms confined in an optical lattice plus parabolic potential: A closed-form approach," Phys. Rev. A **72**, 033616 (2005).

[301] S.-S. Kim, S.-K. Hong, and K.-H. Yeon, "Linear optical properties of the semiconductor quantum shell," Phys. Rev. B **76**, 115322 (2007).

[302] G. Rezaei, B. Vaseghi, and M. Sadri, "External electric field effect on the optical rectification coefficient of an exciton in a spherical parabolic quantum dot," Physica B **406**, 4596 – 4599 (2011).

[303] W. Liu, D. Neshev, A. Miroshnichenko, I. Shadrivov, and Y. Kivshar, "Bouncing plasmonic waves in half-parabolic potentials," Phys. Rev. A **84**, 063805 (2011).

[304] S. Blundell and K. Joshi, "Precise correlation energies in small parabolic quantum dots from configuration interaction," Phys. Rev. B **81**, 115323 (2010).

[305] Y. Zhao, P.-F. Loos, and P. Gill, "Correlation energy of anisotropic quantum dots," Phys. Rev. A **84**, 032513 (2011).

[306] K. Teichmann, M. Wenderoth, H. Prser, K. Pierz, H. Schumacher, and R. Ulbrich, "Harmonic oscillator wave functions of a self-assembled inas quantum dot measured by scanning tunneling microscopy," Nano Lett. **13**, 3571–3575 (2013).

[307] A. Morales, N. Raigoza, C. Duque, and L. Oliveira, "Effects of growth-direction electric and magnetic fields on excitons in gaas- ga1-x alx as coupled double quantum wells," Phys. Rev. B **77**, 113309 (2008).

[308] F. Nammas, A. Sandouqa, H. Ghassib, and M. Al-Sugheir, "Thermodynamic properties of two-dimensional few-electrons quantum dot using the static fluctuation approximation (sfa)," Physica B **406**, 4671 – 4677 (2011).

[309] L.-W. Wang and A. Zunger, "Pseudopotential calculations of nanoscale cdse quantum dots," Phys. Rev. B **53**, 9579–9582 (1996).

[310] S. F. Boys, "Electronic wave functions. i. a general method of calculation for the stationary states of any molecular system," Proc. R. Soc. London, Ser. A **200**, 542–554 (1950).

[311] K. Singer, "The use of gaussian (exponential quadratic) wave functions in molecular problems. i. general formulae for the evaluation of integrals," Proc. R. Soc. London, Ser. A **258**, 412–420 (1960).

[312] B. J. Persson and P. R. Taylor, "Accurate quantum-chemical calculations: The use of gaussian-type geminal functions in the treatment of electron correlation," J. Chem. Phys. **105**, 5915–5926 (1996).

[313] B. J. Persson and P. R. Taylor, "Molecular integrals over gaussian-type geminal basis functions," Theor. Chem. Acc. **97**, 240–250 (1997).

[314] D. Prendergast, M. Nolan, C. Filippi, S. Fahy, and J. C. Greer, "Impact of electron-electron cusp on configuration interaction energies," The Journal of Chemical Physics **115**, 1626–1634 (2001).

[315] C. Hättig, W. Klopper, A. Khn, and D. P. Tew, "Explicitly correlated electrons in molecules," Chemical Reviews **112**, 4–74 (2012).

[316] L. Kong, F. A. Bischoff, and E. F. Valeev, "Explicitly correlated r12/f12 methods for electronic structure," Chemical Reviews **112**, 75–107 (2012).

[317] S. A. Varganov and T. J. Martãnez, "Variational geminal-augmented multireference self-consistent field theory: Two-electron systems," The Journal of Chemical Physics **132**, 054103 (2010).

[318] R. A. Harris and R. Silbey, "Variational calculation of the tunneling system interacting with a heat bath. ii. dynamics of an asymmetric tunneling system," The Journal of Chemical Physics **83**, 1069–1074 (1985).

[319] U. Weiss, "Quantum dissipative systems," (World Scientific, 2008) Chap. 3.2, pp. 31–38.

[320] R. Silbey and R. A. Harris, "Variational calculation of the dynamics of a two level system interacting with a bath," The Journal of Chemical Physics **80**, 2615–2617 (1984).

[321] R. Silbey and R. A. Harris, "Tunneling of molecules in low-temperature media: an elementary description," The Journal of Physical Chemistry **93**, 7062–7071 (1989).

[322] J. P. Perdew, M. Ernzerhof, K. Burke, and A. Savin, "On-top pair-density interpretation of spin density functional theory, with applications to magnetism," International Journal of Quantum Chemistry **61**, 197–205 (1997).

[323] K. Burke, J. P. Perdew, and M. Ernzerhof, "Why semilocal functionals work: Accuracy of the on-top pair density and importance of system averaging," The Journal of Chemical Physics **109**, 3760–3771 (1998).

[324] J. Gräenstein, A. M. Hjerpe, E. Kraka, and D. Cremer, "An accurate description of the bergman reaction using restricted and unrestricted dft: Stability test, spin density, and on-top pair density," The Journal of Physical Chemistry A **104**, 1748–1761 (2000).

[325] R. Takeda, S. Yamanaka, and K. Yamaguchi, "Approximate on-top pair density into one-body functions for cas-dft," International Journal of Quantum Chemistry **96**, 463–473 (2004).

[326] S. Gusarov, P. A. Malmqvist, and R. Lindh, "Using on-top pair density for construction of correlation functionals for multideterminant wave functions," Mol. Phys. **102**, 2207–2216 (2004).

[327] U. Weiss, "Quantum dissipative systems," (World Scientific, 2008) Chap. 18.1, pp. 261–269.

[328] A. A. Frost, "Floating spherical gaussian orbital model of molecular structure. i. computational procedure. lih as an example," The Journal of Chemical Physics **47**, 3707–3713 (1967).

[329] A. A. Frost, "Floating spherical gaussian orbital model of molecular structure. ii. one- and two-electron pair systems," The Journal of Chemical Physics **47**, 3714–3716 (1967).

[330] A. A. Frost, "A floating spherical gaussian orbital model of molecular structure. iii. first-row atom hydrides," The Journal of Physical Chemistry **72**, 1289–1293 (1968).

[331] F. M. Peeters, "Magneto-optics in parabolic quantum dots," Phys. Rev. B **42**, 1486–1487 (1990).

[332] Jaziri, S., Bastard, G., and Bennaceur, R., "Stark effect in parabolic quantum dot," Le Journal de Physique IV **03**, C5–367–C5–372 (1993).

[333] R. Rinaldi, P. V. Giugno, R. Cingolani, H. Lipsanen, M. Sopanen, J. Tulkki, and J. Ahopelto, "Zeeman effect in parabolic quantum dots," Phys. Rev. Lett. **77**, 342–345 (1996).

[334] A. F. Terzis and S. Baskoutas, "Binding energy of donor states in a gaas quantum dot: effect of electric and magnetic field," Journal of Physics: Conference Series **10**, 77 (2005).

[335] A. Kar and C. Bose, "Ground state energy in a spherical gaas-(al,ga)as quantum dot with parabolic confinement," Ind. J. Phys. **80**, 357 (2006).

[336] S. Stobbe, T. W. Schlereth, S. Höfling, A. Forchel, J. M. Hvam, and P. Lodahl, "Large quantum dots with small oscillator strength," Phys. Rev. B **82**, 233302 (2010).

[337] M. Karimi and G. Rezaei, "Effects of external electric and magnetic fields on the linear and nonlinear intersubband optical properties of finite semi-parabolic quantum dots," Physica B: Condensed Matter **406**, 4423 – 4428 (2011).

[338] J. S. Weiner, D. A. B. Miller, and D. S. Chemla, "Quadratic electro-optic effect due to the quantum-confined stark effect in quantum wells," Applied Physics Letters **50**, 842–844 (1987).

[339] J. W. Robinson, J. H. Rice, K. H. Lee, J. H. Na, R. A. Taylor, D. G. Hasko, R. A. Oliver, M. J. Kappers, C. J. Humphreys, and G. A. D. Briggs, "Quantum-confined stark effect in a single ingan quantum dot under a lateral electric field," Applied Physics Letters **86**, 213103 (2005).

[340] D. Peng, B. Zhao, A. J. Cohen, X. Hu, and W. Yang, "Optimized effective potential for calculations with orbital-free potential functionals," Mol. Phys. **110**, 925–934 (2012).

[341] T. H. Yu, W. G. Liu, Y. Sha, B. V. Merinov, P. Shirvanian, and W. A. Goddard, "The effect of different environments on Nafion degradation: Quantum mechanics study," J. Membr. Sci. **437**, 276–285 (2013).

[342] K. Rajeshwar, N. De Tacconi, and C. Chenthamarakshan, "Semiconductor-based composite materials: Preparation, properties, and performance," Chemistry of Materials **13**, 2765–2782 (2001).

[343] I. Y. Zhang and X. Xu, "Doubly hybrid density functional for accurate description of thermochemistry, thermochemical kinetics and nonbonded interactions," Int. Rev. Phys. Chem. **30**, 115–160 (2011).

[344] R. Freeman and I. Willner, "Optical molecular sensing with semiconductor quantum dots (qds)," Chemical Society Reviews **41**, 4067–4085 (2012).

[345] B. Dabbousi, J. Rodriguez-Viejo, F. Mikulec, J. Heine, H. Mattoussi, R. Ober, K. Jensen, and M. Bawendi, "(cdse)zns core-shell quantum dots: Synthesis and characterization of a size series of highly luminescent nanocrystallites," Journal of Physical Chemistry B **101**, 9463–9475 (1997).

[346] W. Kwon, S. Do, D. Won, and S.-W. Rhee, "Carbon quantum dot-based field-effect transistors and their ligand length-dependent carrier mobility," ACS Applied Materials and Interfaces **5**, 822–827 (2013).

[347] K.-G. Ma, J.-Y. Bai, T. Fang, and H.-Q. Guo, "Effect of the structure of isomers of mercaptovaleric acid on optical properties of cdte quantum dots," Nano **8**, 1350049 (2013).

Index

Christopher Blanton

3243 Center Church Rd
Mullins, SC 29574
☎ (843) 289-1632
✉ christopher.blanton@gmail.com

Education

2014 **Ph.D.**, *Syracuse University*, Syracuse, NY.
Chemistry

2011 **M.Ph.**, *Syracuse University*, Syracuse, NY.
Chemistry

2004 **B.Sc.**, *Francis Marion University*, Florence, SC.
Chemistry/Mathematics

Teaching Experience

- Consistently exceptional evaluations in multiple disciplines.
- Courses taught:

General Chemistry Recitation
Reinforced chemical concepts by a combination of lecture and discussion periods with small (30 student enrollment) sections. Responsible for teaching lectures when the primary lecturer was unavailable.

Physical Science Laboratory
Responsible for facilitating the learning of non-major students through introductory chemical and physical concepts. Guided the students through experiments that were design to intrigue and capture the student interests in likely only physical science class.

Organic Chemistry Laboratory
Supervised undergraduates in organic chemistry laboratories. Experiments included thin-layer chromatography, column chromatography, acquisition and interpretation of IR and NMR spectra, synthesis of several materials, and many more standard organic experiments. Evaluated students through verbal, written, and observed performance.

Physical Chemistry Laboratory
Supervised multiple students in the performance of experiments. Prepared all aspects of the experiments. Evaluated the students through verbal, written, and observed feedback.

Research Experience

Computational studies of quantum dots: Under Prof. Arindam Chakraborty, studied the effects of size, shape, ligands, pH, and external electric fields on the optical and electronic properties of semiconductor quantum dots. Development of new theoretical methods to explore said systems. Implementation of both original and known methods in high performance computing systems.

Development of methods for explicit correlation: Under Prof. Arindam Chakraborty, developed methods for studying and incorporating explicit correlation into mutlicomponent systems.

Mentoring Experience

- Successfully mentored a high school student, resulting in the publication of a research paper and successful regional science fair award.
- Mentored several undergraduates. Lead these students through all aspects of work in theoretical and computational chemistry at the research level. Guided these students through the use of cutting edge custom computational chemistry software programs.

Research Interests

Computational and Theoretical Chemistry

Development and application of multicomponent methods to excited electronic system. Study of semiconductors under the influence of external fields. Application of multiscale methods to the study of complex computational problems, such as surface-passivated quantum dots.

Chemical Education

Interfacing understanding of macroscopic and microscopic concepts in chemistry and physics. Effective use of computers in chemical learning environments. Interfacing laboratory experiences with theoretical explorations in undergraduate science learning. Incorporating technology in the learning of chemistry at all levels.

Professional Societies

- American Chemical Society
- American Physical Society

Awards and Scholarships

- Analytical Chemistry Award (Francis Marion University 2003)
- Chemistry Major Award (Francis Marion University 2003)
- South Carolina Section of the American Chemical Society Outstanding Chemistry Major Award (2003)

Publications

Christopher J. Blanton, Christopher Brenon, and Arindam Chakraborty. Development of polaron-transformed explicitly correlated full configuration interaction method for investigation of quantum-confined Stark effect in GaAs quantum dots. *The Journal of Chemical Physics*, 138(5):054114, 2013.

Christopher J. Blanton and Arindam Chakraborty. Determination of electron-hole correlation length in cdse quantum dots using an explicitly correlated two-particle cumulant. *J. Chem. Phys. (Submitted)*, 2014.

Christopher J. Blanton and Arindam Chakraborty. Influence of environment acidity on optical and electronic properties of quantum dots. *In preparation*, 2014.

Christopher J. Blanton and Arindam Chakraborty. Influence of the length of linking ligands on the optical and electronic properties of CdSe quantum dot. *In preparation*, 2014.